Holistic synthesis of iron-based metal-organic frameworks using unconventional metal feedstock and polyethylene terephthalate derived organic linkers

.....

by

Nqobile Themba Mthembu

.....

Submitted in fulfilment of the requirements for the degree

Master of Science (Chemistry)

UNIVERSITEIT VAN PRETORIA
UNIVERSITY OF PRETORIA
YUNIBESITHI YA PRETORIA

In the Faculty of Natural & Agricultural Sciences

University of Pretoria

Republic of South Africa, Pretoria

Supervisor: **Dr. Nicholas M. Musyoka**

Co-Supervisor: **Prof. Henrietta W. Langmi**

December 2022

Declaration

I, Ngobile Themba Mthembu declare that the thesis/dissertation, which I hereby submit for the degree Master of science (Chemistry) at the University of Pretoria, is my own work and has not previously been submitted by me for a degree at this or any other tertiary institution.

SIGNATURE:

DATE: 14 December 2022

Acknowledgements

Firstly, I would like to thank God, the almighty king for aiding in the success of this project. I would like to extend my gratitude to my supervisor, Dr N. Musyoka for the guidance and advices received during this journey that has led to such a fruitful outcome. I am deeply grateful to Professor H. Langmi for availing herself to assist and provide wisdom whenever I required it and ensured the success of this project. Not forgetting Dr X. Dyosiba for consistently being there and always ready to lend a helping hand wherever she could, I have learned quite a lot from you in this short space of time that I have known you. I would like to thank the HySA team as well for being so generous in sharing and assisting whenever I required it, you guys were a home away from home and made the burden of being so far away from home easier to bear.

Lastly, I would like to extend my sincere gratitude to the council for scientific and industrial research (CSIR), Department of science and innovation (DSI) and Future Leaders Africa Independent Research (FLAIR) for financial support as well as the University of Pretoria (UP) for extending their resources such that this study was a success.

Dedication

I humbly dedicate this dissertation to my mother, Thabisile Mthembu and I am truly grateful to her for always being a supportive structure I required at the time and continuously ready to assist where she could. I am truly grateful to all my siblings (Wanda, Spiphamandla, Nomcebo, Khethokuhle and Nelisiwe Mthembu) for the love and support received during my studies, for always being so optimistic even when I felt despaired.

I also dedicate this to my two kids, Azanda and Basanda Mthembu and I would like to thank them for forever being by my side, understanding, loving and always putting a smile on mommy's face even when circumstances were not favourable to them. Not forgetting the support and words of encouragements from my nephews and nieces (Mitchelle, Nolwandle, Sanelisiwe, Nkanyezi, Siyanda, Anele, Liyakhanya, Sibulelo and Ziyanda Mthembu) I have truly been blessed to have each and every one of you present in my life and I do not take that for granted.

Table of Contents

List of figures i

List of Tables iv

List of equations v

Nomenclature vi

Abstract viii

Achievements during the Master's study: x

Chapter 1 1

1. Introduction 1

1.1 Background and motivation 1

1.1.1 Metal-organic frameworks 3

1.1.2 Hydrogen storage 4

1.2 Problem statement 5

1.3 Motivation 6

1.4 Research objectives 7

1.5 Hypothesis 8

1.6 Thesis layout 8

Chapter 2 9

2. Literature review 9

2.1 Chapter outline 9

2.2 Metal-organic frameworks (MOFs) 9

2.2.1 MOF synthesis 14

2.2.2 Applications of MOFs 17

2.2.3 MIL series of MOFs 19

2.2.4 Limitations of MOFs 26

2.2.5 Waste to MOFs 26

2.3 Chapter summary 30
Chapter 3 32
3. Experimental 32
3.1 Chapter outline 32
3.2 Synthesis of MIL MOFs 32
3.2.1 Materials and reagents 33
3.2.2 Depolymerization of Poly ethylene (PET) waste bottles 34
3.2.3 Extraction of Fe metal from AMD 34
3.2.4 Synthesis of Fe-MOFs 34
3.3 Characterization 36
3.3.1 Inductively coupled plasma- optical emission spectroscopy (ICP-OES) 36
3.3.2 Thermogravimetric analysis (TGA) 36
3.3.3 Powder X-ray diffraction (PXRD) 37
3.3.4 Fourier transform infrared spectroscopy (FTIR) 38
3.3.5 Scanning electron microscopy (SEM) 39
3.3.6 Adsorption-desorption studies- Brunauer-Emmett-Teller (BET) theory 40
3.3.7 X-ray spectroscopy (XPS) 43
3.4 Chapter summary 44
Chapter 4 45
4. Results and discussion: Fe-MIL-101 45
4.1 Chapter outline 45
4.2 Chapter summary 70
Chapter 5 71
5. Results and discussion: Fe-MIL-88B 71
5.1 Chapter outline 71
5.2 Chapter summary 95

Chapter 6.....97

6. Conclusions.....97

6.1 Future work.....98

References.....99

Supplementary data.....122

Appendix I- Fe precipitates.....122

Appendix II-MIL-101.....124

Appendix III- MIL-88B.....127

List of figures

Chapter 1-3

Figure 1: Simplified diagram of the current approaches in H_2 storage technology. Taken from reference 33. 4

Figure 2: Schematic diagram displaying the four generations of MOFs. The picture was taken from reference 55. 10

Figure 3: Ball and stick simulation of the crystal structure of MOF-5. Picture is taken from reference 66. 12

Figure 4: Schematic diagram displaying the bridging angles in a ZIF structure and a zeolite. Diagram reproduced from reference 69. 12

Figure 5: Schematic diagram showing the formation of ZIF-8 structure highlighting the SOD topology. Picture taken from https://crystallography365.wordpress.com/ on the 08/12/21 13

Figure 6: Schematic diagram for the synthesis of MOFs via conventional synthesis methods. Image reproduced from reference 78. 14

Figure 7: Simulation of a) MIL-53 and b) MIL-88 structures in their larger-pore dehydrated form. Taken from reference 60 and 61, respectively. 20

Figure 8: MIL-101 **s**tructure showing hexagonal and pentagonal windows. Picture reproduced from reference 130. 22

Figure 9: Schematic diagram summarising the entire process leading up to the synthesis of waste-derived Fe-MIL-101 and Fe-MIL-88B MOFs. 33

Figure 10: Schematic representation of the Bragg's law concept. Taken from reference 200. 38

Figure 11: Working principles of the Fourier-Transform Infrared spectroscopy. Reproduced from reference 203. 39

Figure 12: Schematic representation of Scanning Electron Microscopy (SEM). Image reproduced from reference 205. 39

Figure 13: Schematic representation of the electron beam interacting with the specimen. Image reproduced from reference 205. 40

Figure 14: Adsorption Isotherms for gas as per the IUPAC classification. Reproduced from reference 207. 42

Figure 15: Representation of the photoelectric effect. Image reproduced from https://theory.labster.com/photoelectric-effect/, accessed on the 06/12/2022 43

Chapter 4

Figure 1: XPS spectra for AMD-Fe precipitates where a) and b) are survey spectra; c) and d) are Fe2p spectra for rAMD-Fe and $_{OHo}$AMD-Fe, respectively. 52
Figure 2: a) XRD pattern and b) FTIR spectra for AMD-Fe precipitates. 53
Figure 3: a) XRD pattern and b) FTIR spectra for commercial and PET derived BDC. 54
Figure 4: Showing XRD pattern and FTIR spectra for Fe-MIL-101 samples prepared using (a and b) Chloride (c and d) Nitrate precursors. 56
Figure 5: SEM images for Fe-MIL-101 MOFs where a) Fe-MIL-101(Cl)$_{pet}$ b) $_{OHo}$AMD-Fe-MIL-101(Cl) c) $_{OH}$oAMD-Fe-MIL-101(NO_3)$_{pet}$ d) rAMD-Fe-MIL-101(NO_3)$_{pet}$. 57
Figure 6: TGA profiles for the prepared Fe-MIL-101 samples using a) Chloride and b) Nitrate precursors. 59
Figure 7: Hydrogen adsorption isotherms of rAMD-Fe-MIL-101(NO_3)$_{pet}$.....62

Chapter 5

Figure 1: XPS spectra for AMD-Fe precipitates where a) and b) are broad spectra; c) and d) are Fe2p spectra for rAMD-Fe and $_{OHo}$AMD-Fe, respectively. 80
Figure 2: a) XRD and b) FTIR spectra for AMD-Fe precipitates.....81
Figure 3: XRD and b) FTIR spectra for commercial BDC vs PET-derived BDC. 82
Figure 4: XRD patterns (a and b) and FTIR) spectra (c and d) for Fe-MIL-88B samples. 84
Figure 5: SEM images of a) Fe-MIL-88B(Cl) b) $_{OHo}$AMD-Fe-MIL-88B(Cl) c) $_{OHo}$AMD-Fe-MIL-88B (Cl)$_{pet}$ d) rAMD-Fe-MIL-88B (Cl)$_{pet}$ materials prepared from the chloride precursors. 85
Figure 6: SEM images of a) MIL-88B(NO_3)pet b) MIL-88B-$_{OHo}$AMD-Fe(NO_3) c) MIL-88B-rAMD-Fe(NO_3) d) MIL-88B-rAMD-Fe(NO_3)$_{pet}$ materials prepared from the nitrate precursors. 86
Figure 7: TGA profiles for MIL-88B samples prepared from a) Chloride and b) Nitrate precursors. 87
Figure 8: Hydrogen adsorption isotherm of rAMD-Fe-MIL-88B(NO_3). 90

Supplementary data

Figure S1: a) O1s scan b) C1s scan c) S2p scan and d) N1s scan for rAMD-Fe. 122

Figure S2: a) O1s scan b) C1s scan and c) S2p scan for $_{OHo}$AMD-Fe precipitate. 123
Figure S3: Nitrogen adsorption/desorption isotherms for Fe-MIL-101 materials. 124
Figure S4: Pore size distribution (PSD) for Fe-MIL-101 materials. 125
Figure S5: SEM images for a) Fe-MIL-101(Cl) b) OHoAMD-Fe-MIL-101(Cl)$_{pet}$ c) rAMD-Fe-MIL-101(Cl) and d) rAMD-Fe-MIL-101(Cl)$_{pet}$. 125
Figure S6: SEM images for a) Fe-MIL-101(NO_3) b) Fe-MIL-101(NO_3)$_{pet}$ c) rAMD-Fe-MIL-101 (NO_3) d) $_{OHo}$AMD-Fe-MIL-101(NO_3).....126
Figure S7: Nitrogen adsorption/desorption isotherms for Fe-MIL-88B materials. 127
Figure S8: Pore size distribution (PSD) for Fe-MIL-88B materials. 127
Figure S9: SEM images for a) Fe-MIL-88B(Cl)$_{pet}$ and b) $_{OHo}$AMD-Fe-MIL-88B(Cl). 128
Figure S10: SEM images for a) Fe-MIL-88B(NO_3)$_{pet}$ and b) rAMD-Fe-MIL-88B (NO_3)$_{pet}$. 128

List of Tables

Chapter 4

Table 1: Summary table for BET surface areas and pore volumes obtained for MIL-101 samples. 60

Chapter 5

Table 1: Concentration levels in AMD treated differently for the extraction of Fe. 78

Table 2: Showing surface areas and pore volumes of prepared Fe-MIL-88B materials. 88

Supplementary data

Table S1: ICP-OES measured elemental concentrations from raw AMD and after the extraction of Fe using NaOH with and without the use of an oxidant (H_2O_2).....122

Table S2: Summary table for BET surface areas and pore volumes obtained for MIL-101 samples. 124

List of equations

Oxidation of pyrite (2.2.1).....29

Conversion of Fe^{2+} to Fe^{3+} (2.2.2) 29

Hydrolysis of Fe^{3+} (2.2.3).....29

Bragg's equation (3.3.1).....37

BET equation (3.3.2).....42

Energy conservation equation (3.3.3).....43

Nomenclature

ACs- activated carbons

ACFs- Activated carbon fibres

ACMs- Activated carbon monoliths

AMD- Acid mine drainage

BDC- 1,4-benzyl-dicarboxylic acid

BET- Brunauer-emmett-teller

CUS- coordinative unsaturated sites

DCPD- dicyclopentadiene

DDSs- drug delivery systems

DMF- *N,N*-dimethylformamide

DMSO- Dimethyl sulfoxide

DOX- doxorubicin

EG- ethylene glycol

FTIR- Fourier Transform InfraRed spectroscopy

HKUST- Hong Kong University of Science and Technology

ICP-OES- Inductively Coupled Plasma-Optical Emission Spectroscopy

Im- Imidazolate

IRMOFs- Isoreticular metal–organic frameworks

IUPAC- international union of pure and applied chemistry

MCR- multi-component reaction

MIL- Materials Institute Lavoisier

IMC- imidacloprid

MOFs- Metal-organic frameworks

MW- microwave

PACs- powdered activated carbons

PANI- polyaniline

PCP- porous coordinated polymers

PET- polyethylene terephthalate

PV- Pore volume

PXRD- Powder X-ray diffraction

rGO- reduced graphene oxide

SA- Surface area

SBU- Secondary building units

SEM- Scanning Electron microscopy

SOD- sodalite

TGA- Thermal gravimetric analysis

UiO- Universiteit i Oslo

XPS- X-ray spectroscopy

ZIFs- zeolitic imidazolate frameworks

3D- three-dimensional

Abstract

The high costs associated with the synthesis of Metal-organic frameworks (MOFs) owing to the expensive raw materials have significantly attributed to the lack of large-scale production of MOFs regardless of their appealing qualities. The synthesis of MOFs from polyethylene terephthalate (PET) waste source for organic linker and other metal sources has recently been reported as an alternative way to lower the costs of the synthesis process of MOFs thus enabling their industrialization. Though other metal sources used as metal precursors for MOF synthesis had been reported, this study focuses on the use of AMD as well as PET waste precursors to successfully synthesize MOFs of two different morphologies but in the same class. In this work, Fe-MIL-101 and Fe-MIL-88B were successfully synthesized using acid mine drainage (AMD) wastewater as the source for the Iron (Fe) metal as well as BDC derived from waste PET bottles. Two extraction methods (A. oxidation & precipitation with air; B. oxidation with Hydrogen peroxide & precipitation with NaOH) were explored for the extraction of Fe in the AMD thus yielding Fe of different phases / species. The synthesis procedure follows a widely reported solvothermal route and the waste-derived MOFs are compared to MOFs synthesized from commercial precursors.

Fe-MIL-101 synthesized via the solvothermal route from waste precursor sources displayed similar properties to those synthesized from commercial grade precursors. Octahedral morphologies were observed on SEM imaging however, materials prepared from AMD-derived Fe dissolved in HCl displayed mixed morphologies of Fe-MIL-88B and Fe-MIL-101 as well as broken Fe-MIL-88 structures. XRD and FTIR exhibited characteristic diffraction peaks as well as vibrations and stretching bends that confirmed the coordination of BDC to the metal centre, respectively. $_{OHo}$AMD-Fe-MIL-101(Cl)$_{pet}$ exhibited the lowest textural properties of 52.5 m^2/g and 0.0623 cm^3/g, however, all Fe-MIL-101 materials displayed type I N_2 isotherms with surface areas within the range of 501-2052 m^2/g and pore size distribution in the micro- and mesoporous range. Fe-MIL-101 samples prepared from waste Fe displayed decreased surface areas and pore volumes compared to Fe-MIL-101 prepared from commercial precursors. All prepared materials proved to be thermally stable up to temperatures above 300 °C, typical of Fe-MIL-101 and further confirming the successful preparations of Fe-MIL-101 from both commercial and waste-derived precursors. Hydrogen adsorption studies on the Fe-MIL-101 material yielded 1.18 wt% at 1 bar and 77 K which is

comparable to the values previously reported in literature relative to the surface area obtained.

Waste derived Fe-MIL-88B displayed similar morphologies, crystal phases as well as vibrations and stretching bands when compared to those prepared from commercial precursors. Most Fe-MIL-88B MOFs showed a type I N_2 isotherm however, waste-derived Fe-MIL-88B had enhanced surface areas when compared to those prepared from commercial grade precursors with surface areas significantly below 100 m_2/g. The pore size distribution mostly lied in the meso-porous range with some in the macro-porous range for most Fe-MIL-88B MOFs. The use of AMD as a source for Fe yielded Fe-MIL-88B MOFs with high thermal stabilities surpassing Fe-MIL-88B prepared from commercial precursors. Hydrogen adsorption studies conducted at 77 K and 1 bar showed that waste derived Fe-MIL-88B MOFs were good candidates since a value of 0.81 wt% found to be consistent with the previously reported data for M-MIL-88B MOFs to date.

This study has therefore, successfully demonstrated that a holistic strategy that utilizes two waste starting materials (AMD and waste PET) can be used to produce Fe-based MOFs of comparable properties as those obtained when commercial feedstock is used. This strategy contributes to lowering of costs associated with the production of MOFs and thus advancing them towards commercialization.

Achievements during the Master's study:

- **Oral presentation**
  1. Nqobile Mthembu, Xoliswa Dyosiba, Nicholas M. Musyoka and Henrietta W. Langmi. Holistic synthesis of low-cost Fe-based MOFs using unconventional metal feedstock and PET-derived organic linkers, 3rd International Workshop for Porous Materials and their Applications (IWPMA-2021), Virtual, 27-28 July 2021

- Two **articles** are to be submitted for **journal publications**:
  1. Nqobile Mthembu, Xoliswa Dyosiba, Nicholas M. Musyoka and Henrietta W. Langmi. Holistic strategy for the synthesis of Fe-based MOFs using Fe obtained from AMD and PET waste
  2. Nqobile Mthembu, Xoliswa Dyosiba, Nicholas M. Musyoka and Henrietta W. Langmi. The use of complete waste-derived metal and organic ligand precursors for the holistic synthesis of Fe-MIL-88B via the solvothermal route

Chapter 1

1. Introduction

1.1 Background and motivation

Porous materials are identified as materials comprising cavities of various shapes and sizes, and they have been of great interest in a variety of research fields. Porous materials play a significant role in the modern science field as they have found use in numerous applications, however, their use dates back to ancient times as far as the BC era.[1] This is due to their attractive properties such as high surface areas, large pore volume, and specific surface chemistry. Porous materials can be of inorganic, organic or inorganic-organic nature with tuneable pore sizes and pore walls.[2-3] Porous materials can be classified as low porosity, medium porosity, or high porosity materials based on the number of pores they have. Materials with low and medium porosity generally have closed pores whereas materials with high porosity consist of either two- or three-dimensional array of pores that are interconnected thus creating an open structure. The IUPAC classifies porous materials into three groups, based on the pore sizes contained within the material; i) microporous materials have <2 nm pores, ii) mesoporous materials consist of pores between 2-50 nm and lastly, iii) macroporous materials are mainly composed of large pores >50 nm.[4]

These materials have a wide range of applications which include catalysis, medicine, biology, sensors, energy storage and conversion.[5] The performance of a porous material in a specified application is directly affected by the pore volume, shape and size distribution of the pores. Porous materials with evenly distributed nanosized pores of uniform shape and volume, possess superior properties thus aiding in their utilization in gas-related applications. Previous studies have shown that porous materials exhibit improved thermal properties such as higher convective heat transfer coefficients and higher thermal conductivity and can therefore be used in solar energy storage applications. Highly porous materials such as zeolites, metallic foams and alumina have high structural rigidity and low weight, and thus make suitable candidates in adsorption applications.

Zeolites, carbon materials, silica gel, mesoporous alumina, porous organic materials and metal organic frameworks (MOFs) are the most popular porous materials that have been

reported for energy and environmental applications.[6-7] The purification of gases using porous materials has been applied industrially owing to their good permeability, reactive pore walls and ability to trap solid particulates. The conventional use of porous materials including activated carbon and zeolites as sorbent materials has been employed in various industrial applications such as filtration, separation, purification, cooling and drying. The microstructure and polarity of zeolite structures is suitable for gas separation applications by means of molecular size exclusion and coulombic interactions (thermodynamic selectivity).[8-9] Owing to these properties, zeolites have been widely used in catalysis, gas purification, hydrocarbon separation and have been evaluated for hydrogen storage. However, the inability to control the zeolite pore structures restricts their efficiency. This is particularly experienced in the separation of gas molecules with high similarities in physical and chemical properties.[10] The presence of water molecules in zeolite structures is also considered a major drawback.[11]

Some of the advantages imposed by activated carbons (ACs) over zeolites include cost-efficiency, hydro-stability, and low heat of adsorption requiring less energy for regeneration.[12] ACs are the most common carbon materials with amphoteric properties and are widely used in various applications stemming mainly from their large micropore and mesopore volumes which then result in high surface areas. This large surface area together with high surface reactivity has seen the diverse use of ACs in applications such as air and water purification, adsorption, catalysis and energy storage.[13] The application of mesoporous silica for gas separation is owing to their high (thermal, chemical and mechanical) stabilities, low-cost, flexibility for surface functionalization and a 3D structure with interconnected pores that mitigates transport issues with diffusion. Mesoporous silica has been demonstrated as a good support for separation membranes and therefore offer selectivity over other gases such as CH_4 and N_2.[14-15] Modified silica materials have been reported to perform better than unmodified ones as they tend to increase surface reactivity with the gas molecules for improved selectivity.[16]

The storage of hydrogen in porous materials through physisoprtion is being considered as one of the solutions to the hydrogen economy challenges due to the large specific surface areas that they possess.[17] Another advantage of using porous materials for the storage of hydrogen is due to the weak Van der Waal bonds between molecular hydrogen and the

material thus allowing for use of low temperatures and pressures to achieve significant hydrogen storage capacities. Hydrogen storage has been widely reported for materials such as zeolites, carbon materials and metal organic frameworks (MOFs) with proven recyclability and hydrogen-storage capacity as well as rapid hydrogen desorption.[18] Studies on various types of zeolites for H_2 adsorption have been conducted and found that their H_2 capacities are dependent on the framework structure, composition as well as the acidic-basic nature of the zeolites.[19-21] Carbon materials and MOFs have reported the highest hydrogen storage capacities (8-10 wt%) at -196 °C, however, carbon materials suffer from low density and require dopants to enhance heat conductivity to achieve high H_2 capacities.[22-23] The major advantage of MOFs over other porous materials is the formation of unsaturated metal centers (UMCs) upon removal of coordinated solvent molecules through vacuum drying.[24-25] Further details on MOFs and H_2 storage studies will be discussed in the following subsections.

1.1.1 Metal-organic frameworks

Metal-organic frameworks were discovered over two decades ago and have contributed significantly into the research of porous materials, and thus became the fastest growing chemistry research field. Numerous novel structures have been synthesized over the years with surface areas reaching as far as 10 000 m^2/g, far exceeding those obtained for traditional porous materials such as zeolites and carbon materials.[26-27] MOFs have found application in a variety of fields such as catalysis, gas separation, biomedicine and more especially in hydrogen storage. This is owing to their extraordinary properties such as high surface areas and porosity, ease of functionalization and tuneability as well as their diversity in topology. Several methods have been explored for the synthesis of MOFs with the hydrothermal and solvothermal routes being the traditional ones owing to their simplicity. The long reaction times, high energy demands, use of large amounts of solvents and expensive raw materials for MOF synthesis have hindered large scale production of MOFs and has led to research steered towards greener approaches.[28]

The use of cheaper and lower-grade waste materials as precursors for the synthesis of MOFs has been reported; this includes the breaking down of polyethylene terephthalate (PET) to its components of which terephthalic acid is then used as a linker in the synthesis of MOFs. Various waste metal sources have been used for metal extraction such that they are

recovered and used as alternative metal precursors in a number of syntheses, including MOFs.[29-30] This greatly reduces the costs associated with the production of MOFs whilst abating environmental pollution thus paving way for their industrial application. MOFs have proved to possess a significant potential for use in hydrogen storage owing to their reversible and high-rate hydrogen adsorption process.[31]

1.1.2 Hydrogen storage

The use of Hydrogen (H_2) as fuel eliminates the dependency on coal and oil for the generation of power. H_2 is a non-polluting energy carrier with the potential to reduce environmental impacts arising from the use of fossil fuels such as carbon emissions.[32] H_2 is the most abundant element in the universe but because it is not present in great quantities on earth, the H_2 used for fuel is produced from other sources such as natural gas reforming, coal and biomass gasification, water electrolysis and other renewable energy resources. H_2 acts as a chemical energy carrier that can be used to store, move, and deliver energy. Figure 1 provides a simplified summary diagram of the current approaches used to store hydrogen. H_2 can be stored either physically or chemically such that it is stored in either a gaseous state, liquid or chemically bonded to the surface of an adsorbent. The storage of H_2 in a gaseous state is a commonly used method that typically entails the use of high pressure tanks, whereas storing it in liquid form necessitates the application of cryogenic temperatures to prevent vaporization thus requires effective thermal insulation to prevent losses.[33]

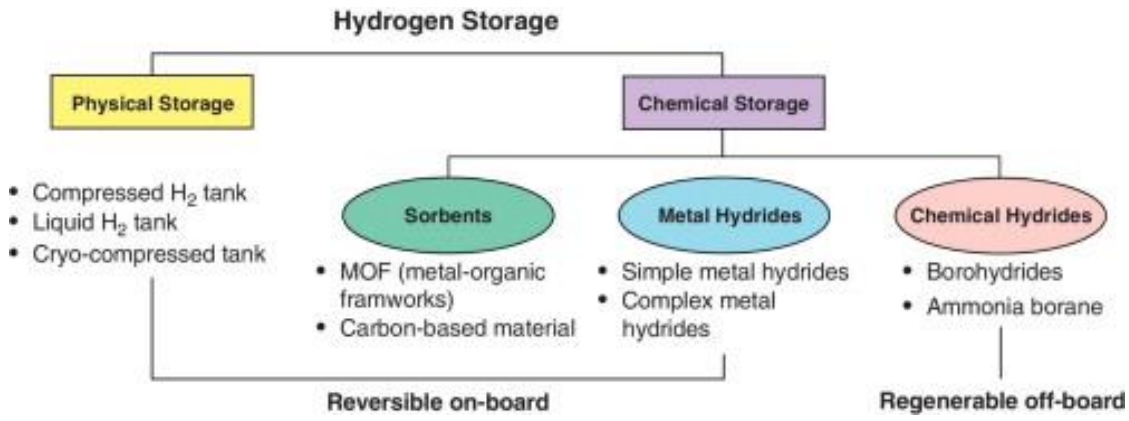

Figure 1: Simplified diagram of the current approaches in H_2 storage technology. Taken from reference 33.

The use of hydrogen physisorption on porous materials serves as a potential to overcome the current challenges such that storage of large amounts of hydrogen at near-ambient temperatures and reasonable pressures is achieved.[34] The physisorption process is simple and easy to handle, it is a reversible process owing to the low binding energy compared to chemisorption, and fast adsorption-desorption kinetics are achieved. H_2 molecules are attached to the surface of the porous material via the weak van der Waal forces, the adsorption capacity of the material is therefore dependent on the surface area, pore volume, working temperature and pressure.[35-36] MOFs are regarded as one of the most promising candidates for H_2 storage owing to their enormous surface areas of over 4 000 m^2/g. Numerous reports of porous MOFs have been published following H_2 studies on MOF-5 in 2003. One of the advantages of MOFs is that the framework topology, pore size, and surface area can be easily tuned to increase H_2 storage capacities.[37]

1.2 Problem statement

The development of green approaches towards the preparation of MOFs has been of great significance recently, with the desperation to put their unique and extraordinary properties to use having grown exponentially over the past decade. Industrial application of MOFs has been hindered by several factors which include the use of large amounts of harmful solvents (i.e dimethyl formaldehyde (DMF) and dimethyl sulfoxide (DMSO), long reaction hours with high temperatures required for MOF synthesis thus consuming large amounts of energy, as well as the high costs associated with the starting materials thus rendering industrial production not economically feasible. Attempts to address these shortcomings have been reported, such as the exploration of green solvents as a replacement for the toxic solvents traditionally used for the synthesis of MOFs. Solvent-free methods (e.g. mechanochemical method) have also been explored as a way to completely eliminate solvents, thus eliminating the danger and costs associated with their use.

The key focus, however, has been the synthesis of MOFs from waste materials by recycling landfill waste materials such as waste PET bottles for the extraction of terephthalic acid (BDC), an organic linker. Recycling of PET waste has proven to be costly with low-value end-products and as a result, the degrading of PET to its monomers to be re-used in other reactions has been proven to be a viable option. The extraction of metals from wastewaters has offered a promising solution for a cheaper inorganic feedstock with a variety of metals

available which can be used towards the synthesis of MOFs. Acid mine drainage (AMD) is a potential alternative for the extraction of metals to be utilized in the synthesis of MOFs whilst abating pollution and lessening the expenses associated with MOF synthesis.[38-40] The synthesis of MOFs using the iron metal recycled from the acid mine drainage potentially introduces a drastic decrease in the production costs of MOFs whilst eliminating mining waste, thus allowing for environmental and biological sustainability. To our knowledge, the use of metals extracted from AMD for MOF synthesis has not been reported yet.

1.3 Motivation

The study undertaken aims to provide a holistic approach to the synthesis of Fe-based MOFs from waste derived precursors as means to reduce costs associated with MOFs synthesis. This study sets the groundwork for the synthesis procedure of MOFs from AMD and PET-derived precursors and outlines areas of improvement through characterization using various analytical techniques. This project investigated the synthesis of the Fe-based MIL MOFs (Fe-MIL-88B and Fe-MIL-101) from AMD-derived Fe (using two different methods) and PET-derived BDC as an organic linker, thereby offering somewhat green approach to the synthesis of Fe-MOFs.[41] A comparison is provided for Fe-MIL-101 and Fe-MIL-88B prepared from commercial grade precursors following the same synthesis approach. Further comparisons are conducted where either the metal precursor or linker is replaced by a waste-derived material to assess the effect of waste-derived precursors on the structural and textural properties of Fe-MIL-101 and Fe-MIL-88B. Hydrogen adsorption capacities for the synthesized materials are then determined to assess storage capacities of the synthesized Fe-MOFs.

1.4 Research objectives

The main aim of the project was to synthesize Fe-based MOFs using unconventional feedstocks (i.e. waste PET and AMD). The project evaluated the best method for Fe precipitation from AMD and then studied the effect of using Fe derived from the AMD and PET-derived BDC linker on the integrity of the MOF.

The following objectives are set:

- To synthesize MIL-101 and MIL-88B from commercial precursors, such that commercial Fe chloride and nitrate are individually combined with the commercial grade BDC.
- To synthesize MIL-101 and MIL-88B from the two commercial Fe sources (chloride and nitrate) by replacing commercial grade BDC with PET-derived BDC as the organic linker.
- To precipitate the Fe from the AMD using three methods and thoroughly characterize the precipitates to determine the chemical nature of the precipitated iron.
- To synthesize MIL-101 and MIL-88B using the resultant complexes from the digestion of the Fe source by replacing the commercial Fe source and commercial grade BDC kept as the linker.
- To also synthesize Fe-MOFs from complete waste precursors, where the AMD acid digested Fe precipitates (individually) are combined with PET-derived BDC under similar conditions.
- To then fully characterize all the synthesized MOFs and compare them to their counterparts synthesized from commercial high purity precursors.

1.5 Hypothesis

- Waste-derived MOFs are to have similar chemical and physical properties as the one derived from commercial precursors.
- Waste-derived MOFs are to have decreased BET surface areas owing to the impurities being deposited into the pores thus hindering gas from accessing the pores.
- MOFs derived from waste Fe precursors are expected to have enhanced thermal stabilities and lower weight losses because of the presence of Fe in a pure state and not in a hydrate form.

1.6 Thesis layout

Chapter 1 presents an overview of the research topic. In this chapter, the study is introduced and the background story is well stated. The problem statement and significance of the study is outlined and research objectives are identified.

Chapter 2 reviews the existing literature relating to the current research topic to identify key approaches and strategies to successfully synthesize Fe-based MOFs from two waste sources.

Chapter 3 carefully outlines the research methodology used such that the study is a success. This chapter presents the practical aspect of this study, stating the synthesis method as well as the characterization techniques used in the identification of the synthesized MOFs.

Chapter 4 presents results obtained from the characterization techniques as well as hydrogen adsorption studies for the Fe-MIL-101 synthesized from complete commercial precursors, semi-commercial/semi-waste precursors and complete waste precursors.

Chapter 5 presents the findings for the Fe-MIL-88B synthesized from complete commercial precursors, semi-commercial/semi-waste precursors and complete waste precursors.

Chapter 6 provides the summary of findings from chapter 4 and 5, outlines the pros and cons of the study as well as suggestions as to how they can be mitigated for future purposes.

Chapter 2

2. Literature review

2.1 Chapter outline

Various metal-organic frameworks (MOFs) morphologies have been reported over the 20 years since their discovery. MOFs have attracted much attention from various fields for various applications such as catalysis/photocatalysis, biosensors, gas separation and hydrogen storage. The synthesis method is the crucial aspect in tailoring MOFs such that they possess the desired properties, however, several synthesis methods have been reported so far. These include conventional (solvothermal or hydrothermal), microwave-assisted, mechanical, sonochemical and ultrasonic synthesis methods with each of these methods presenting advantages and disadvantages. Several MOF structures have been reported, MIL MOFs have recently taken centre stage due to their high chemical stability and can be prepared from non-toxic metals, such as Ca, Mg, Fe, etc,. Fe-based MIL MOFs are biocompatible thus can be used in medicinal applications, such as drug delivery, without causing bodily harm. Previous research has demonstrated superior hydrogen storage in Fe-based MIL MOFs owing to their increased metal-ligand interactions and number of active sites. This chapter introduces MOFs and discusses relevant literature on the synthesis and applications of MOFs. It further places emphasis on MIL series of MOFs.

2.2 Metal-organic frameworks (MOFs)

Metal-organic frameworks (MOFs) are a fairly new class of porous materials that have recently gained much traction owing to their unique properties that allow for a variety of applications in the field of science. MOFs are a class of crystalline hybrid network supramolecular solid materials resulting from self-assembled organic linkers and metal ions, also referred to as porous coordinated polymers (PCPs).[42] MOFs have a wide range of applications such as gas separation and storage, optical, chemical sensing, catalysis, biomedicine, and as supercapacitors.[43] However, they are classically known for their application as microporous materials for storage of gases such as CH_4, H_2 and CO_2.[44-46] The tuneable nature of MOFs allows for a wide range of pore sizes, from the microporous to the mesoporous by adjusting the length of the linkers as well as the functionalization of organic linker with chemical groups for improved gas uptake.[47]

The ease with which the metal SBUs and organic linkers can be varied to create open crystalline frameworks with permanent porosity has resulted in the development of thousands of compounds to-date.[27] MOFs can either be rigid or flexible, this is determined by the structural conformation and how it responds to external stimuli.[48-49] MOFs of different network morphologies have been realized with the careful selection of synthetic conditions and chemical composition. This has allowed for the production of tailored MOF materials suitable for a specific application.[50-52] Several structures have been synthesized in the past, such as i) octahedron- consisting of six (6) points of connection, ii) trigonal- the coordination number, coordination geometry of the metal ions, and the nature of the functional groups dictate the definitive MOF structure.[53]

Kitawa and Kondo classified MOFs primarily into three (3) generations[54]; the first (1st) generation are the types of MOFs that are designed based on molecular architecture such that they consist of the metal cluster and organic moieties. These types of MOFs collapse on the removal of guest molecules and are rendered nonporous.[55] The second (2nd) generation MOFs are derived from the 1st generation by manipulation of chemical modifications however, they consist of framework rigidity thus retain permanent porosity on removal of guest molecules. The third (3rd) generation MOFs are built from biomolecules with dynamic and flexible structures upon guest molecule inclusion and removal, thus they adapt to external stimuli without collapsing.[56] Their spatial and electronic structures can be modified thus accomplishing magnetic, dielectric, and oxidation–reduction properties.[57] Figure 2 is a schematic representation of MOF generations clearly showing their structural differences.

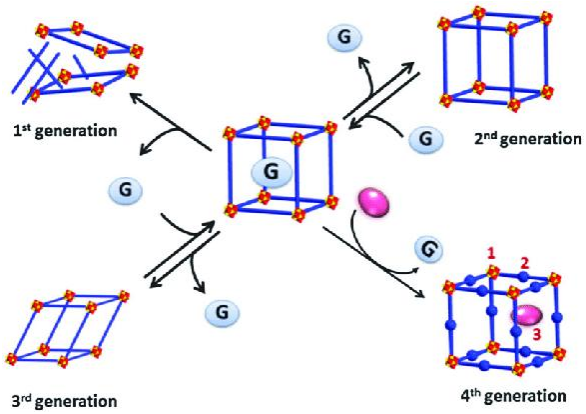

Figure 2: Schematic diagram displaying the four generations of MOFs. The picture was taken from reference 55.

Lastly, the fourth (4^{th}) generation of MOFs was recently defined by Liu *et al*. as porous materials with modifiable pore size and chemistry through post-synthetic modification. This class of MOFs retain their morphology and structural integrity with the ability to adapt pore size and pore chemistry to accommodate different guest species.[58] 3^{rd} and 4^{th} generation MOFs have hundreds of highly porous structures with different open-space channels and therefore have massive potential for use in gas separation due to their extremely high selectivity, high storage capacities, and catalysis functions.[59-61]

The stability of MOFs is defined as the ability of MOFs to maintain their structural intactness when subjected to different conditions such as high temperatures (thermal stability), mechanical forces (mechanical stability) and chemical environments (chemical stability). The stability of MOFs is governed by, amongst others, oxidation state and ionic radius of the metal ion, metal-ligand coordination geometry, as well as the hydrophobicity of the structure.[62] MOFs built from the low-valence cations (divalents or M^{2+}) have proven to be susceptible to chemical instability and hydrolysis as a result of weak metal-ligand bond. The use of metals with high valence, such as trivalent cations (M^{3+}= Fe^{3+}, Cr^{3+}, V^{3+}) or polycations (group V and VI) are preferred as means to produce MOFs with high thermal and chemical stabilities. However, the control of MOF formation then becomes difficult as the high-valence metal cations are highly reactive, therefore, it requires stringent reaction conditions to ensure crystalline MOFs are produced.[63]

The most well-known kinds of MOFs include isoreticular metal–organic frameworks (IRMOFs), zeolitic imidazolate frameworks (ZIFs), HKUST, UiO and MILs. IRMOFs are the type of MOFs consisting of similar structural topology and by the substitution of an organic linker with another or functionalization results in different IRMOFs. These MOFs were first described by Yaghi *et al.* as tetrahedral clusters of Zn_4O connected by dicarboxylate linkers to form a three-dimensional porous cubic framework. IRMOF-1, also known as MOF-5, is the most common representative and base structure of the IRMOFs family, that was first to be synthesized and has widely been studied over the years which has enabled commercialization with applications in various areas.[64-65] Figure 3 is the representation of the MOF-5 unit cell in a two-dimensional view, clearly showing the MOF cavities.[66]

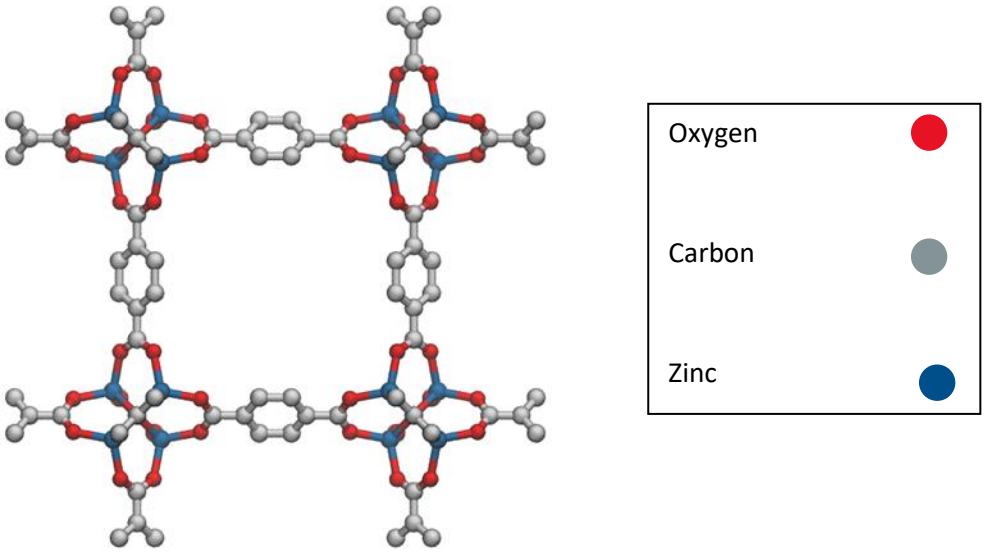

Figure 3: Ball and stick simulation of the crystal structure of MOF-5. Picture is taken from reference 66.

A different subclass of MOFs with zeolite-type morphologies and structures was first published by Yaghi and co-workers in 2010 where they described the synthesis of the twelve-types of zeolitic imidazolate frameworks (ZIFs).[67-68] This is the newest class of MOFs made up of transition metals, such as Zn(II) and Co(II) cations, tetrahedrally-coordinated through the imidazolate (Im) linkers. The bent imidazolate linkers between two metal centres create an angle such that the metal–imidazolate–metal angle is ~145° similar to that of Si-O-Si in aluminosilicate zeolites (see Figure 4).[69]

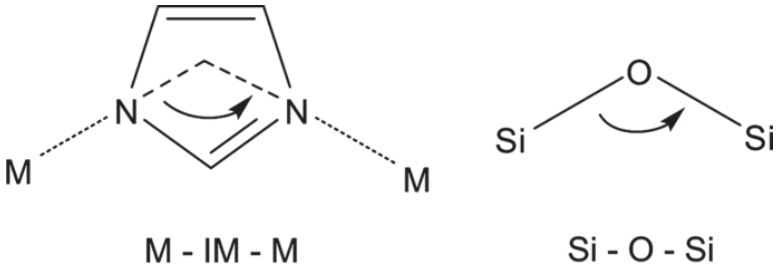

Figure 4: Schematic diagram displaying the bridging angles in a ZIF structure and a zeolite. Diagram reproduced from reference 69.

The use of imidazolate favours the formation of zeolitic tetrahedral topologies. The strong interactions between the metal and the charged imidazolate result in the formation of highly crystalline and porous structures with permanent porosity and high thermal

stabilities. ZIFs tend to possess both MOFs and zeolites characteristics which has enabled them to be explored in numerous applications such as catalysis, gas adsorption and separation.[70-71] The ZIF-8 structure is presented in Figure 5 clearly highlighting the **SOD** topology, large spherical cages and sodalite cages are separated by the six-ring windows of

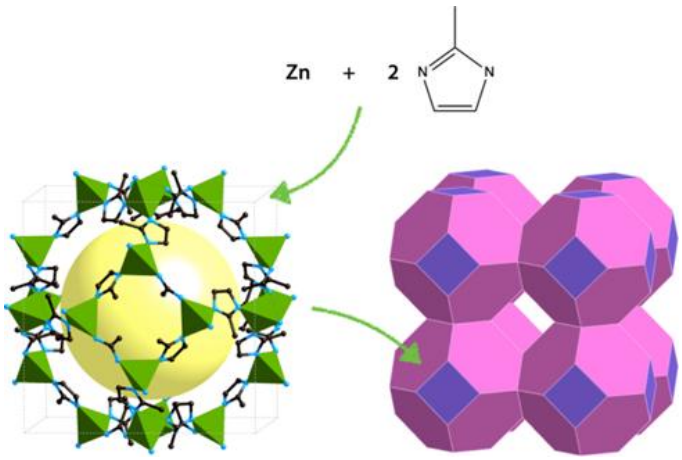

Figure 5: Schematic diagram showing the formation of ZIF-8 structure highlighting the SOD topology. Picture taken from https://crystallography365.wordpress.com/ on the 08/12/21

small openings.

HKUST, UiO and MIL MOFs are named after the institutions or research groups under which they were first synthesized. HKUST stands for the Hong Kong University of Science and Technology where the HKUST-1 (also known as MOF-199) structure was first synthesized from Cu(II), later on the HKUST-1 structure was obtained from other dimeric metals.[72] HKUST-1 structure consists of a pair of metals connected by four (4) benzene tricarboxylate linkers to give a forming face-centred cubic units thus exhibiting high surface area and microporosity.[73] UiO MOFs (UIO = Universiteit i Oslo) are Zr(IV)-based three-dimensional cubic close-packed porous structures consisting of large pores, high surface areas and high structural stabilities. UiO MOFs (UiO-64, -66, -67, -68 and -69) consist of dicarboxylic acid ligands of varying lengths, however, they still maintain the same structure without compromising on the thermal stabilities.[74] Materials Institute Lavoisier (MIL) MOFs will be discussed in details in section 2.2.3 of this chapter.

2.2.1 MOF synthesis

The synthesis of MOFs has been widely achieved through self-assembly of the metal node and organic linker such that 1-, 2- and 3-dimensional defined structures are produced. Various framework morphologies, pore structures and pore sizes can be obtained through the variation of metal centers and organic linkers. The synthesis conditions for MOFs must be such that the kinetics of crystallization are suitable for nucleation and growth of the preferred phase to take place.[75-76] Other factors such as the reaction time, temperature and the nature of solvent are major factors that contribute to the synthesis of MOFs.

2.2.1.1 Conventional synthesis of MOFs

The conventional methods make use of electrical heating to catalyse crystal growth as presented in figure 6. Conventional methods are divided into two categories: solvothermal and hydrothermal methods. With conventional methods, MOFs are synthesized by combining the metal source and organic linker in a closed reaction vessel and heating to temperatures above the boiling point of the solvent for prolonged reaction time under autogenous pressure. The solvothermal synthesis makes use of polar solvents (e.g. *N,N*-dimethylformamide) thus requires lower temperature (50-260 °C), whilst the hydrothermal method uses aqueous solvents or mineralizers as reaction media to dissolve and recrystallize matter relatively indissoluble under typical conditions.[77-78]

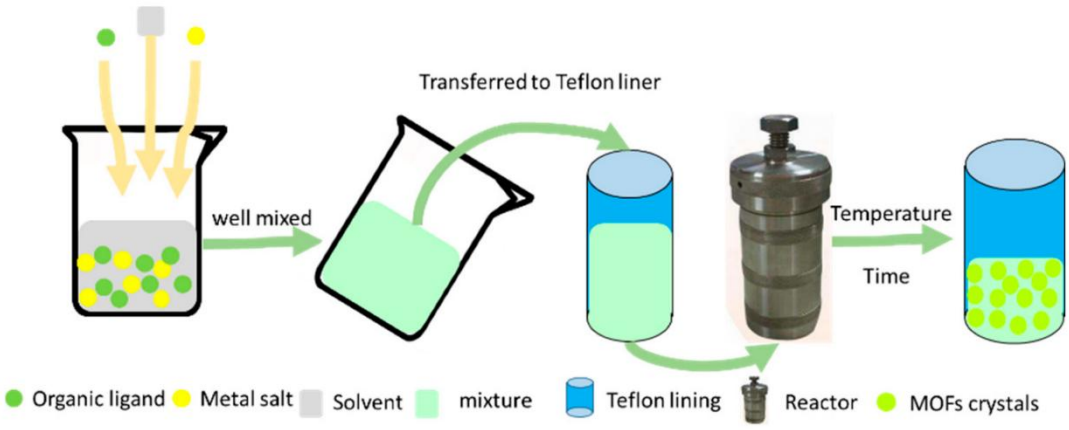

Figure 6: Schematic diagram for the synthesis of MOFs via conventional synthesis methods. Image reproduced from reference 78.

2.2.1.2 Green approach to the synthesis of MOFs

The use of large amounts of solvents, long reaction times and high energy demands with conventional methods propelled the development of new methods to address these limitations. Alternative synthesis methods have been explored recently, including the microwave (MW)-assisted method.[28, 79] The microwave-assisted method makes use of electromagnetic radiation in the microwave region to heat the reaction vessel such that a chemical reaction is initiated. MW irradiation provides sufficient energy for the accelerated synthetic process and therefore leads to dramatic reduction in synthetic time of MOFs to only a few minutes.[80] The fast heating provided by MW energy results in fast growth of crystals which ultimately leads to smaller crystals with ease of morphology control and phase selectivity.[81] This is one of the latest methods considered as a green approach as it provides clean synthesis with the advantage of enhanced reaction rates, higher yields and makes use of less energy and solvent.[82] Other green methods that have been proposed for the synthesis of MOFs include sonochemical, electrochemical and mechanochemical (or ball milling) methods.[83]

Sonochemical synthesis methods entail the use of high intensity ultrasound which makes molecules undergo a chemical reaction for the production of MOF materials without the use of energy, no use of solvents and decreased reaction times.[84] This is a solvent-free synthesis method that results in materials with increased surface areas, homogeneous particle size distribution, improved phase purity and reduced reaction time.[85] The electrochemical synthesis method offers mild reaction conditions, shorter synthesis times and real-time influence of reaction.[86] Synthesis is achieved through direct deposition of MOF thin film with controllable characteristics on a desired substrate and results in homogenous thin films/coatings with tunable thickness and porosity suitable for use in electronic devices.[87-88] Lastly, the mechanochemical synthesis method either completely avoids the use of solvents or uses reduced amounts of solvents, and reduced temperatures, contrary to the conventional methods. This method enables solid phase-reactions without applied heat by milling or grinding solid starting materials.[89] The synthesis of MOFs via the mechanochemical method was first reported in 2006 by Pichon *et al.* and has become a popular method to overcome limitations in large-scale production of MOFs.[90-91]

2.2.1.3 Characterization of MOFs

A number of characterization techniques have been explored for the characterization of porous materials and these techniques have also been adopted for the analysis of MOFs. Owing to their crystalline nature, MOFs are typically characterized by powder x-ray diffraction (PXRD) to determine their crystal phases, phase purity, size of the unit cell and even morphology. The diffraction pattern for porous materials is usually collected over a wide range of 2θ such that large and small unit cell moieties can be detected and analyzed. PXRD is a structural analysis tool that is quite powerful and should not be underestimated as it can provide invaluable structural information about MOFs. The porous nature of MOFs allows for isothermal gas adsorption−desorption analysis to evaluate the pore volume, pore size distribution and surface areas of MOFs. Isothermal gas adsorption−desorption analysis helps determine the amount of a gaseous adsorbate adsorbed and desorbed by an adsorbent at equilibrium over a range of pressures at constant temperature. Nonreactive gases such as Nitrogen (N_2), Hydrogen (H_2) and Carbon dioxide (CO_2), are commonly used at cryogenic temperatures.

Other useful properties for MOFs include their thermal stabilities measured using a thermogravimetric analysis (TGA) technique. This is a destructive technique that measures weight losses of the sample within a temperature range (25-1000 °C). The analysis is done either in an inert environment that is maintained by a continuous flow of nitrogen (N_2) or an oxidizing environment is created by a continuous flow of oxygen (O_2). Weight loss is then expressed in weight % (w/w%) at a specific temperature. Scanning electron microscopy (SEM) is a light scanning technique used for imaging and analysis of surface morphology in solid materials. This technique makes use of a high-energy focused beam of electrons to scan across the surface of the material, several electrons are then scattered to produce an image of the surface.[92-93] Useful information such as size, shape, morphology, and surface composition can is extracted.[94] The Fourier transform infrared (FTIR) and Raman spectroscopy are generally used for functional group identification, these methods are also helpful in identifying adsorbates in the pores of MOFs such as solvents and impurities. A typical FTIR spectrum is recorded between 4000 and 400 cm^{-1} depending on the absorption frequency.[95-96]

2.2.2 Applications of MOFs

Owing to their enormous surface areas, high porosity and tunable nature, MOFs are used in various fields such as catalysis, biomedicine, drug delivery, biosensors, gas separation and storage. Hydrogen (H_2) storage in MOFs has been reported and proven to be viable since MOFs display high H_2 adsorption capacities with reversible capabilities. The most popular applications of MOFs are discussed further in the sections below with the greater focus on the recent advances in hydrogen storage using MOFs (section 2.2.3.3).

2.2.2.1 Gas separation and storage

Amongst applications of MOFs, the separation and storage of gases has been one of the important and crucial applications in the chemical industrial sector. Gas separation refers to the splitting of one or more gas molecules from a mixture to achieve purity or single gas molecules. This can be achieved through the molecular size, dipole moment as well as the electronic charge of the molecules. There are numerous methods that have previously been reported for the separation of gas molecules, including solvent-based separations, cryogenic distillation, membrane and adsorption separation.[97] CO_2 capture, organic vapor removal, and natural gas sweetening are amongst a few technologies in which the gas separation concept has been widely explored.

The search for materials to use in the storage of H_2 has been a major focus over the years as it serves as a greener alternative for use in energy production. The explosive nature of H_2 has driven research into focusing on the development of porous materials with high storage capacities. The application of MOFs as materials for H_2 storage was first reported in 2003 by Rosi *et al.* for MOF-5 and MIL-53 structures.[37, 98] After which, attempts towards the use of MOFs for hydrogen storage attracted worldwide attention with increased focus on exploring various strategies for enhancing hydrogen capacities in porous MOFs at cryogenic temperatures. [47, 99] MOFs generally exhibit superior reversible hydrogen uptake compared to other porous materials thus making them excellent prospects for use in H_2 storage.[100-102]

2.2.2.2 Other applications of MOFs

The high degree of crystallinity of MOFs provides an increased number of active sites thus making them suitable candidates for catalysis/photocatalysis applications. The ease with which the pore size of MOFs can be controlled, and pore walls can be functionalized, puts

MOFs at a greater advantage as heterogeneous catalysts, more especially for organic reactions rather than for bulk chemistry owing to their low thermal stability (<300 °C). The abundance of redox active site and quick mass transfer also make MOFs appealing for electrocatalysis as they offer superior electrocatalytic activity. However, most pristine MOFs have poor conductivity and have therefore been integrated with other functional materials, particularly carbon materials, such that the conductivity and stability of MOFs is improved.[103-104]

MOFs have recently emerged as new candidates for use in selective drug delivery systems (DDSs) as nanocarriers owing to their low cytotoxicity and biodegradability properties. The high surface area, porosities and composition of MOFs offer high loading capacities with efficient drug loading and controlled drug release.[105] Recently, Fe-MOFs have been reported for drug delivery applications, some of these (Fe-MIL-88 and Fe-MIL-53) MOFs offer pore flexibility and can expand or shrink according to the solvent molecular size. However, MOFs such as Fe-MIL-100 and Fe-MIL-101 consist of well-defined, ordered porosity and large pore sizes, thus have proved suitable for drug delivery.[106-107]

Based on the diversity of MOFs properties and working principles, MOFs have been designed such that they are used as magnetic, calorimetric, electrochemical, chemiresistive and photoluminescent sensors.[108] The luminescent properties of MOFs have seen their use as chemo- and biosensors for gases, solvents and explosives gaining much traction as well. Chemical sensing highly relies on surface reactions thus requiring materials with high surface areas and porosity, as a result MOFs have been heavily exploited in this field. The hybrid nature of MOFs allows for structural alteration such that the photoluminescence arises either from the metal centre or the organic ligand. Transition-metal ions and lanthanides exhibit luminescence properties whilst organic linkers with an aromatic ring or free Pi (π) electrons give rise to optical emission or photoluminescence upon excitation.[109-110]

2.2.3 MIL series of MOFs

Materials Institute Lavoisier (MIL) materials are permeable carboxylated metal polymers prepared from various trivalent metal cations and carboxylic acid ligands, and consisting of large pores and high-permanent porosity. MIL MOFs are mainly composed from trivalent metal ions (Cr, Al and Fe) or lanthanides (Eu, Tb and Y) strongly bonded to oxygen-anion terminated linkers, and usually display high chemical stability. The micropore and mesopore structures of MILs can be altered by the manipulation of external factors, which also indicates the flexibility of the MIL structures. MILs MOFs synthesized from non-toxic endogenous cations (Ca, Mg, Fe, Zn, etc.) and naturally occurring derivatives or biomolecules as ligands have also been reported. As a result, nontoxic, and biologically and environmentally compatible MOFs are produced thus making them suitable for medical applications as well as for clean energy and environmental protection. Fe-based MIL MOFs have unique properties such as wide distribution of single iron sites, redox properties, porous structures and large surface areas which make them more superior for different applications.[111-112]

2.2.3.1 Fe-MIL MOFs

The predominance of Fe-MOFs such as MIL-53, MIL-88, MIL-100 and MIL-101, are assigned to the MIL and BioMOF families. Ligands used for the preparation of MIL-88B and MIL-53 are generally the same, however, the molecular structures that result are different. This is solely due to the difference in the nucleation processes that can be manipulated through synthesis conditions. The formation of MIL-88B undertakes a heterogeneous nucleation while MIL-53 forms through a homogenous nucleation. MIL-88B exhibits a three-dimensional cage structure with an **acs** topology whilst MIL-53 structure displays one-dimensional channels (see Figure 7).[107, 113] Apart from being recognized as having a non-toxic nature, MIL-88B has a highly flexible framework, and as such exhibits the 'breathing' effect, thus making it a great candidate for use in a number of applications such as drug delivery, and gas separation and storage.[114] Fe-based MILs have demonstrated enhanced photocatalytic activity owing to their sensitive response to visible light and the small Fe(III) oxo cluster allows for the free electron to exist. To an extent, flexible MOFs are stable in water hence their use in humid and aqueous conditions as adsorbents for the removal of heavy metals and organic pollutants.

A study conducted by Xianghui Li and co-workers discovered that Fe-MIL-101 possessed the highest adsorption and catalytic activity towards the removal of acid orange 7 (AO7). Fe-MIL-88B performed the least amongst all Fe-MILs that were investigated such that the sequence was Fe-MIL-101 > Fe-MIL-100 > Fe-MIL-53 > Fe-MIL-88B.[115] In an investigation conducted by Geng *et al*. where Fe-MIL-101, Fe-MIL-53, Fe-MIL-88B and α-Fe_2O_3 were used for the removal of tetracyline hydrochloride in wastewater using the ultrasound/Fenton system, Fe-MIL-88B exhibited the highest catalytic performance. This was attributed to the highest number of Lewis acid sites present within the Fe-MIL-88B MOF; however, the performance of the catalyst was dependent on the pH, ultrasound speed, H_2O dosage and catalyst concentration.[116] The adsorption of trace arsenate in contaminated water was accomplished by using Fe-MIL-88B as a sorbent material, exhibiting high adsorption capacities at low dosages.[117]

Composites of Fe-MIL-88B have been prepared as means to overcome their shortcomings as photocatalysts since they have a high photogenerated carrier recombination rate and a low efficiency conversion of solar energy. Graphene oxide, carbon nanotubes and carbon quantum dots have been used to address these issues with Fe-MIL-88B. Fe-MIL-88B/graphene oxide composite displayed exceptional photocatalytic performance with a 98% removal efficiency towards the degradation of reactive red dye from aqueous solution.[118] The use of Fe-MIL-88B/CNTs and Fe-MIL-88B/CQDs composites for the degradation of organic pollutants resulted in an improved photocatalytic efficiency.[111, 119]

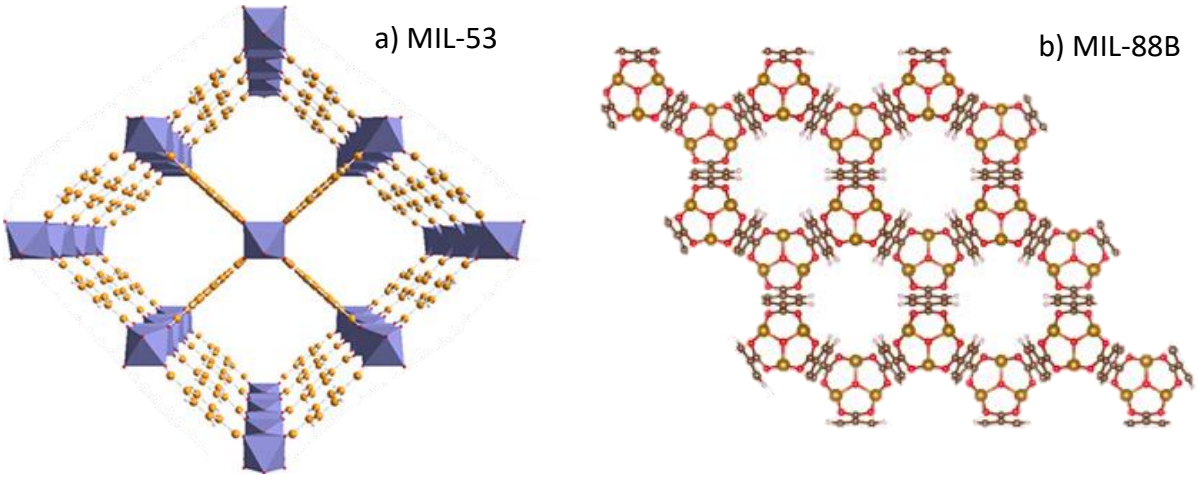

Figure 7: Simulation of a) MIL-53 and b) MIL-88 structures in their larger-pore dehydrated form. Taken from reference 60 and 61, respectively.

The 'breathing' effect is a phenomenon where the pore diameter of the MOF expands or collapses upon interaction with an external stimulus (such as gas molecules, solvents, or pressure) without losing structural integrity. Cameron *et al*. was the first who demonstrated *reversible* swelling behaviour with a $Ni_2(4,4'\text{-bipy})_3(NO_3)_4$ framework using ethanol as a guest molecule.[120-121] Serre *et al*. studied the 'breathing' effect of MIL-88 structures in different solvents which showed that MIL-88 structures are highly selective sorbent materials, and their selectivity is highly reliant on the nature of the organic linker.[122] Horcajada *et al.* further studied the effect of linker modification to the swelling of the Fe-MIL-88B and Fe-Fe-MIL-88D which revealed that the swelling behaviour of these MOFs was drastically affected by steric hindrance and the number of groups per aromatic ring thus leading either to permanent porosity or amplified swelling behaviour.[107, 123] The ability of Fe-MIL-88B pores to expand and shrink in response to external stimuli renders this MOF a suitable candidate for drug delivery and as such, its use has expanded drastically over the years.

For instance, Pham *et al*. studied Fe-MIL-53 and Fe-MIL-88B for in vitro loading and ibuprofen drug release, Fe-MIL-53 demonstrated higher loading capacity of ibuprofen compared to Fe-MIL-88B however, slow drug release was observed with Fe-MIL-88B. The cytotoxicity test revealed that the Fe-MIL-88B particles had no adverse effects on the cell viability for up to 0.1 mg/L at 48 hours.[124] Amine functionalized Fe-MIL-88B nanoscale MOF was used for the encapsulation of methylene blue (a tau aggregate inhibitor) and used as a magnetic resonance contrast material for Alzheimer's disease therapy.[125] Sivakumar *et al*. also carried out a study where Fe-MIL-88B-NH_2 nano MOFs were utilized for the delivery of pH responsive doxorubicin (DOX) anticancer drug. High amounts of DOX were released at an acidic pH while alkali pH saw a decline with amine functional groups providing structural stability and enhanced loading efficiency of DOX.[126]

The adsorptive properties of Fe-MIL-88B have been exploited with hydrocarbons as well, such as alkanes, alcohols and polycyclic aromatic hydrocarbons. Zakariya *et al*. reported the removal of pyrene from wastewater using Fe-MIL-88B and Fe-NH_2-MIL-88B with an efficiency of 99.7 and 96%, respectively. The MOFs were recyclable up to five times with good efficiencies, confirming their stabilities in water.[127]

Ferey *et al*. reported the first Cr(III)-based MIL-101 structure which was used as a bases for the synthesis of Fe-MIL-101 by Bauer *et al.* and Taylor-Pashow *et al.* in 2008 and 2009, respectively. MIL-101 has a rigid zeotype structure of **MTN** topology consisting of two types of mesoporous cages.[128-129] Six linear terephthalic acid (BDC) linkers and four trimeric metal clusters construct a super tetrahedral cage, functioning as edges and vertices, respectively. These super tetrahedra are further connected by their corner sharing vertices of metal clusters to give two types of mesoporous cages with internal free diameters of 29 Å and 34 Å, accessibility is through microporous pentagonal and hexagonal windows of dimensions 1.2 nm and 1.6 nm, respectively (as shown in Fig. 8).[130]

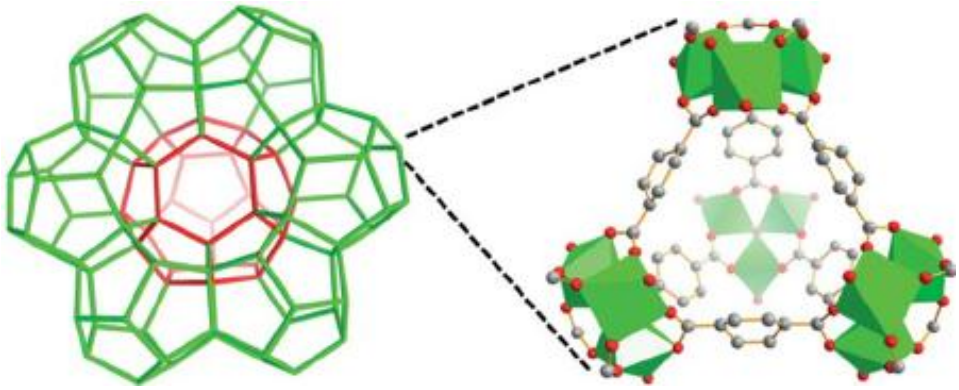

Figure 8: MIL-101 **s**tructure showing hexagonal and pentagonal windows. Picture reproduced from reference 130.

MIL-101 consists of terminal H_2O molecules that can be removed through thermal treatment to yield coordinative unsaturated active sites (CUS) that are desirable for catalysis, as first reported by Hwang *et al*.[131] The MIL-101 structure exhibits a robust nature with superior physicochemical properties when compared to other MOFs. The ability of the MIL-101 to withstand moisture and other chemicals as well as the ease of functional modifications has attracted considerable attention as one of the most promising porous materials for future energy and environmental applications.[132]

The presence of mesoporous and microporous pores has enabled extensive use of MIL-101 in the field of catalysis. Tang and co-workers investigated the use of Fe-MOFs (Fe-MIL-101) as heterogeneous catalysts in a multi-component reaction (MCR) for the synthesis of functionalized pyrroles. The reaction was carried out as a one-pot four-component coupling

reactions (4CRs) of 1,3-dicarbonyl compounds, amines, aldehydes and nitroalkanes. The heterogenous Fe-MIL-101 catalyst displayed high catalytic activity, reaching aniline conversions of 90% in 20 hrs whilst Fe-MIL-88B and Fe-MIL-53 had lower reactivity. The recovered Fe-MIL-101 catalyst could be reused over five cycles with negligible reductions in catalytic activity.[133] A clean and efficient method for the synthesis of Benzoazoles was established by Niknam and colleagues with the use of Cr-based MIL-101 as a heterogeneous catalyst.[134] Kim *et al.* focused on implementing a solvent-free approach for the isomerization of dicyclopentadiene (DCPD) from the endo- to the exo-form with the use of heterogeneous catalysts. Fe and Cr-based MIL-100 and MIL-101 catalysts were investigated with Fe-MIL-101 and Cr-MIL-101 MOFs displaying higher selectivity compared to Fe-MIL-100 and Cr-MIL-100 owing to the high number of acid sites.[135] The use of Fe-MIL-101 for the degradation of organic waste in aqueous solutions has also been investigated by numerous researchers, exhibiting exceptional results when compared to other MOFs.[136]

Different means have been employed to enhance catalytic performance of Fe-MIL-101, including functionalization by adding a reactive group to the organic linker such that MOFs are active and selective solid organocatalysts.[137] An investigation conducted by Barbosa *et al*. on the catalytic performance of Fe-MIL-101 and Fe-NH_2-MIL-101 revealed no difference in their catalytic activities with 100% selectivity towards the ring opening of cyclohexene oxide in the presence of aniline. Cyclic voltammetry studies however, showed a significant improvement of the electrochemical response with Fe-NH_2-MIL-101 compared to Fe-MIL-101.[138] A recent study by Chen *et al.* on the removal of imidacloprid (IMC) from aqueous solution saw Fe-NH_2-MIL-101 possessing a higher adsorption capacity when compared to Fe-NH_2-MIL-88B with a removal ratio of 97 and 93 %, respectively.[139]

Composites are two or more materials combined to address the shortcomings of another, usually consisting of dissimilar properties, such that a desirable material emerges. MOFs have been composited with various materials for improved adsorption and catalytic performance. Zhao *et al*. reported improved photocatalytic performance of Fe-MIL-101/g-C_3N_4 compared to Fe-MIL-101 and g-C_3N_4 for the degradation of bisphenol A and Cr(VI) reduction under visible lights.[140] Multi-walled carbon nanotubes were fabricated onto Fe-MIL-101 for enhanced visible-light photocatalysis of ciprofloxacin in aqueous solution.[141] CNT@Fe-MIL-101 had a lower band gap energy, faster activation and electron transfer were

achieved thus a higher removal rate was observed with improved stability in water compared to Fe-MIL-101. Gündugar and Semerci recently reported Fe-MIL-101 composited with reduced graphene oxide (rGO) and polyaniline (PANI) for enhanced capacitive energy storage properties.[142]

2.2.3.2 Gas storage in MIL MOFs

Gas adsorption is a classical application known for MOFs owing to the rapid adsorption kinetics, superior adsorption characteristic and reversibility as well as high concentrations of active sites (CUS). The MIL-101 structured MOFs particularly became attractive candidates for use in gas storage and hydrocarbon purification as a result of their naturally large surface areas and pore volumes. Lee *et al.* investigated the effect of purification conditions of Cr-MIL-101 on gas storage and C_2 hydrocarbon separation. Cr-MIL-101 obtained through the three-step sequential purification (Cr-MIL-101c) exhibited the highest total hydrogen uptake at 50 bar and 77 K, the highest C_2H_2 storage capacity and higher adsorption capacities of hydrocarbons. The increased number of purification steps removed most of the terephthalic acid in the pores of Cr-MIL-101c thus resulting in higher surface areas and pore volume in comparison to those with one and two-purification steps (Cr-MIL-101a and b).[143]

Cr-MIL-101 synthesized using a solvent-free method at equimolar Cr:BDC, displayed CO_2 adsorption capacity of 18.8 mmol/g at room temperature, a value higher than what had been reported in the literature at the time.[144] The adsorption capacity of CO_2 from a stream of flue gas with trace contaminants using Cr-MIL-101 as an adsorbent was evaluated by Lui *et al.*, and it was shown that the performance of the MOF was minimally impacted and preserved after a 5-cycle regeneration.[145] In a comparative study conducted by Hong *et al.* on the adsorption capacities of CO_2 for Cr-MIL-101 and zeolite 13X monoliths, Cr-MIL-101 monoliths showed a superior CO_2 adsorption performance by 37% and 1.5 times more efficiency than 13X zeolite monoliths.[146] Joshi and co-workers evaluated the efficacy of Zr-UiO-66, Ti-MIL-125, Cr-MIL-101 and their amine-functionalized analogues for the adsorption of hydrogen sulphide (H_2S) in natural gas. Cr-NH_2-MIL-101 had the highest concentration of adsorbed H_2S even in mixtures consisting of CO_2, therefore, amine-functionalized MOFs displayed enhanced H_2S uptake capacities when compared to their respective parent materials.[147]

2.2.3.3 Hydrogen storage in MIL MOFs

In recent years, MOFs have been have been extensively investigated for energy applications, more especially for hydrogen storage. This is mainly due to hydrogen energy serving as one of the most promising alternative for the replacement of non-renewable energy resources and significantly reduces environmental pollution. Hydrogen is an ideal energy carrier that releases water as a main by-product after being combusted. Ren *et al.* investigated the effect of formic acid as a modulator at different concentrations for the synthesis of Cr-MIL-101 to be used for H_2 adsorption. A higher molar ratio of formic acid produced Cr-MIL-101 with better specific surface area and hydrogen storage capacities.[148] Various strategies have also been explored for enhancing binding energies of MOFs towards H_2 and in that way improving their H_2 storage capacities. Metal doped MIL-MOFs and composites have displayed enhanced H_2 adsorption capacities at cryogenic and ambient temperatures, transition metals such as platinum and palladium supported on carbon have been used.

A study by Klyamkin *et al.* investigated H_2 storage in Pt/C doped Cr-MIL-101 at high pressures. Cr-MIL-101 was modified with a Pt supported on carbon black catalyst as a promoter of hydrogen chemisorption.[149] Ghoufi *et al.* conducted a theoretical H_2 adsorption study on Cr-MIL-101 doped with Li^+, Mg^{2+}, Mn^{2+}, and Co^{2+} using the grand canonical Monte Carlo simulations (GCMC) at cryogenic temperature (77 K). The predicted H_2 storage capacity of the cation doped Cr-MIL-101 showed a 10% increase in the amount of adsorbed H_2.[150] Prabhakaran and Deschamps reported the effect of lithium as a dopant in Cr-MIL-101 and Al-MIL-53 MOFS for H_2 adsorption at cryogenic and ambient temperature under high pressure (>100 bar). The study revealed that doping with little amounts of Li (738 and 630 ppm) enhanced H_2 uptake capacity however, excessive concentrations of Li compromise the structure of the framework thus a decrease in hydrogen uptake capacities is observed.[151]

Flexible MOFs such as MIL-53 and MIL-88 tend to have exceptional respiratory effect on gas adsorption and can swell to accommodate gas molecules adsorbed into the pores. In a study conducted by Yurdusen *et al.*, the pore sizes of Fe-MIL-88B crystallites were optimized through the control of Fe:TPA ratio that resulted in an increase in the fraction of ultramicropores which then ultimately enhances H_2 adsorption capacities at 298 K.[152] Fe-MIL-88 series were evaluated for H_2 adsorption capacities by evaluating the H_2 adsorption isotherms at cryogenic and room temperatures as well as at pressures below 100 bar using a

grand canonical Monte Carlo (GCMC) simulations. Fe-MIL-88D exhibited the highest absolute and excess gravimetric H_2 capacities of 5.15 wt% and 4.03 wt% at 77 K, and 0.69 wt% and 0.23 wt% at 298 K, respectively.[114] Huynh *et al.* also investigated H_2 storage in M-MIL-88A substituted with trivalent transition metals in place of Fe. Sc-MIL-88A exhibited the highest gravimetric and highest volumetric uptake H_2 uptake compared to the other M-MIL-88A at cryogenic temperature and ambient temperature.[153]

2.2.4 Limitations of MOFs

The past two decades have been a thrilling journey in the field of porous materials since the discovery of MOFs, which created much excitement as more and more MOF structures were developed with the possibility of being applied in numerous applications. Unfortunately, the commercialization of MOFs proved much harder than anticipated owing to the scalability and costs associated with the synthesis processes.[154] Several factors have limited the industrial production of MOFs, these include the use of large amounts of solvents, intensive energy requirements with longer reaction times and high costs of starting materials.[155] Though a few MOFs are produced industrially, most of them are produced in milligram (mg) scale.[156] This has led to the development of greener synthesis processes with less harsh conditions and that make use of less or no solvents as means to address these issues. The recycling of waste for use as starting materials in replacement of the pure and expensive commercial grade has sparked quite an interest recently as an approach to address the high costs of starting materials.[157] The process of waste removal from the environment and converting it to valuable products is referred to as waste beneficiation.

2.2.5 Waste to MOFs

MOFs play a key role in various fields due to their versatile application capabilities. This has then prompted many researchers to explore much simpler synthesis methods that will consume much less energy, impose low process efficiency, and make use of small amount of raw material.[158] MOFs have been researched widely with numerous structures developed over the years, however, a large portion of MOFs remains at development with no very few of them being produced at industrial scale due to the high costs of the raw materials.[159] The use of waste materials for the synthesis of MOFs could serve as a solution to the production costs and scaling up thus allowing for industrial applications.[160] The recycling of waste to produce value-added products has become a familiar concept more especially in the

chemical industry as a shift towards green chemistry is imperative. Deriving precursors from wastes such as polyethylene (PET) bottles (for organic linker precursor), waste batteries (for metal ions such as Cu, Co and Li), coal fly ash (for extraction of Al) or even waste waters (for metal extraction) are options worth exploring towards reducing costs associated with the synthesis of MOFs.[41, 161-163] The combination of waste PET-derived BDC and AMD-derived Fe metal as precursors in the synthesis of MOFs offers environmental preservation and waste beneficiation. Past research has indicated that the use of low-cost waste-derived precursors does not compromise the integrity of the material and therefore could offer a viable option in abating the high costs associated with the starting materials.[164-165]

2.2.5.1 Polyethylene terephthalate (PET)

Recently, the use of polyethylene terephthalate (PET)-derived terephthalic acid (BDC) as an organic linker for the synthesis of MOFs in replacement of the pure grade commercial BDC has been extensively explored. Polyethylene terephthalate, commonly abbreviated as PET or PETE, is a thermoplastic resin in the polyester family used for the production of food packaging materials, video tapes and x-ray films. Since PET is non-biodegradable polymer, the products from recycled PET are of low value and have adverse effects on the environment due to the presence of contaminants.[41] The innovative use of recycled waste PET for MOF synthesis would contribute to a suitable route for the elimination of PET waste in landfills, assist in decreasing the consumption of fossil fuels and emission of greenhouse gases, as well as preserve the chemical value of polyester while creating a high-value end-use market for PET wastes.[166] Since PET is made from the BDC and ethylene glycol (EG), waste PET bottles have recently been used for the extraction of BDC to use as an organic linker in the synthesis of MOFs.

Quite a few MOFs have to-date been reported to have been synthesized using PET as a source for the organic linker and seem to present similar properties to those synthesized using pure commercial grade precursors.[167] Five nano porous trivalent MOFs were synthesized by Sheng-Han Lo and co-workers using PET-derived BDC as an organic linker instead of terephthalic acid, and all the characterization strongly supported that the synthesized MOFs using PET are similar to those synthesized using commercial grade BDC in literature reports.[168] Similar studies were carried out by Deleu *et al.* where Al-MIL-53 and V-MIL-47 were synthesized, and Ren *et al.* studied the synthesis of a Cr-based MOF. Both

studies investigated the synthesis of MOFs using PET-derived BDC as an organic linker as opposed to the commercial grade BDC. The results were similar to those previously obtained in literature from commercial grade precursors and the Cr-MOF displayed superior textural and hydrogen storage properties.[166, 169]

Dyosiba *et al.* focused on the use of various types of waste PET as sources of BDC linker for the synthesis of the zirconium-based MOF UiO-66(Zr). As expected, textural properties of waste PET-derived UiO-66(Zr) MOFs were analogous with those obtained from MOFs prepared using commercial BDC, however, lower BET surface areas were observed for MOFs synthesized from coloured PET waste bottles owing to the presence of organic dyes that then reside in the pores of the MOF.[159] Eléonore Lagae-Capelle and co-workers reported the combination of PET-derived BDC with Al recovered from Lithium-ion batteries, a Al-MIL-53 prepared had very similar properties to the material formed with pure chemical compounds.[41]

2.2.5.2 Acid mine drainage (AMD)

Metal sources such as spent lithium-ion (Li) batteries and the extraction of heavy metals in wastewaters have been reported in literature such that the synthesis of MOFs is economically viable. [161-162, 170-171] AMD serves as an alternative metal source since it consists of high concentrations of heavy metals, more especially iron (Fe). AMD is a resultant waste from mining processes that is highly acidic, rich in heavy metals and sulfate.[172-173] AMD typically has low pH with high contents of iron metal and a portion of other metals, thus polluting underground and surface water which has devastating effects on biological activities.[174-175] Various technologies have been implemented for the remediation of AMD, though others have no adverse effect on the environment sustainability and are cost-effective, the recycling of metal ions for effective application could be beneficial. Elemental composition of AMD is dependent on the chemistry of the weathered rock and will constitute of many elements, hence AMD can serve as a viable option as a source for metals.[176-177]

The formation of AMD is enabled by the extraction of metal ores or coal which results in sulfide-containing minerals exposed and susceptible to oxidation by air or water. [178]The oxidation of these minerals by water leads to formation of metal sulfates and sulphuric acid (see equation 1). Further oxidation may occur where ferrous sulfate is converted to ferric

sulfate (equation 2), a reaction catalysed by the presence of an acid bacteria known as *acidithiobacillus*. This is the rate-determining reaction and it is pH dependent; in the absence of the bacteria and low pH values, the conversion is relatively slow and increases with increasing pH values. The formed ferric sulfate is dissociated to its ion form due to the acidic nature of water hence the subsequent hydrolysis of the ferric ion therefore, yielding ferric hydroxide ($Fe(OH)_3$) which gives the water its yellow or orange colour (see equation 3). The formed $Fe(OH)_3$ remains in solution under acidic conditions and precipitates out at alkaline conditions.[179-180] AMD occurs through a series of geochemical and microbial reactions as shown in the chemical reactions below:

$$FeS_2 + H_2O + 3\frac{1}{2}O_2 \rightarrow FeSO_4 + H_2SO_4$$ *Oxidation of pyrite* (2.2.1)

$$FeSO_4 \rightarrow Fe_2(SO_4)_3 \rightarrow 2Fe^{3+} + 3SO_4^{2-}$$ *Conversion of Fe^{2+} to Fe^{3+}* (2.2.2)

$$Fe^{3+} + 3H_2O \rightarrow Fe(OH)_3 + 3H^+$$ *Hydrolysis of Fe^{3+}* (2.2.3)

AMD serves as a potential alternative for the extraction of metals to be utilized in the synthesis of MOFs whilst abating pollution and lessening the expenses associated with MOF synthesis. AMD is mostly composed of Fe, Al, Mn, Ca, Na, and Mg in addition to traces of Cu, Co, Zn, Pb, and Ni thus can serve as a viable option as a source for metals.[181] The use of different alkaline reagents has been employed as one of the techniques used for the recovery of metals which yields hydroxides or carbonates.[172, 176-177, 182-184] Seo *et al*. used three neutralizing reagents (NaOH, Na_2CO_3 and $Ca(OH)_2$) for the sequential selective precipitation of Fe, Al and Mn by control of the pH. The study revealed that the type of neutralizing agent had insignificant effect on the precipitation order of the metals, where Fe precipitated out ahead of Al at approximately pH 3.5 and Mn was the last to precipitate out.[185] A yellow pigment (goethite) was successfully prepared from Fe recovered from AMD through selective precipitation. This was achieved by ensuring that metals that might adversely affect the growth of pure goethite are eliminated through purification, alkaline reagent used as well as the separation method employed.[39]

Furthermore, Akinwekomi *et al*. proposed a novel method of beneficiating AMD through the synthesis of valuable minerals with various possible industrial applications. The study indulged in the successful synthesis of high purity goethite, hematite, magnetite, and gypsum through a selective precipitation method of Fe as Fe(III) and Fe(II) species at pH 3.5 and 8.5, respectively.[186] Flores *et al*. reported the use of Iron oxide particles recovered from AMD through a sequential precipitation as low-cost feedstock for the production of geothite, ferrihydrite and magnetite. Thermal treatment of the recovered solids resulted in a suitable catalyst for the removal of azo procion red dye from aqueous solutions.[187]

Plenty of research studies towards the recovery of Fe from AMD to produce valuable materials have proven that the Fe recovered is still highly capable of producing high quality products with properties comparable to those of commercial grade. The use of AMD-derived Fe for the synthesis of Fe-based MOFs has not been reported as yet and by combining the use of waste PET as well as AMD-derived Fe metal, a completely green approach to Fe-MOFs synthesis can be achieved. Previous research has proved that the use of Fe metal for the MOF synthesis offers increased adsorption activity and the higher the valency the more thermally stable the MOF will be owing to increased metal-ligand bond strength.[188] Fe recovery from the AMD also contributes towards waste beneficiating, circular economy and reclaiming of drinking water that will be suitable to aquatic life.[189]

2.3 Chapter summary

Various structures and topologies of MOFs have been developed over the years and have found use in a variety of applications as a result of the unique properties they possess. The synthesis conditions greatly influence MOF topology and are to be taken into consideration during the design of MOFs. MIL-MOFs are a group of innovative crystalline materials consisting of metal ions/units connected through organic linkers with strong covalent bonds. They have found use in various applications such degradation of organic materials in waste waters, catalysis, gas separation and H_2 adsorption. MOFs however, are limited by the use of large solvents and energy requirements during for large scale production. The high cost of the raw materials used in the synthesis of MOFs has been the greatest challenge and as a result, means to reduce these costs include strategies such as waste beneficiation. The recovery of Fe from AMD to use as a metal source and PET as an organic linker could serve as a solution whilst abating pollution. Several studies have been conducted on the use of

waste materials for the synthesis of MOFs that displayed little to no defect in textural and physical properties of MOFs.

Chapter 3

3. Experimental

3.1 Chapter outline

The synthesis of MOFs using the conventional solvothermal synthesis is the most common method owing to their simplicity. Solvothermal synthesis typically offers the solvent as the reaction media but it also partakes in the transportation, and energy dispersion of chemicals. The choice of solvent, reaction conditions and reactants concentrations are some of the attributes to take into consideration when aiming to achieve a certain MOF morphology. This chapter presents the procedures employed for the synthesis of the MIL MOFs and their characterization. Several characterization tools are used to confirm the structure and morphology of the MOFs as well as determine their textural properties. Hydrogen adsorption studies are also carried out on the materials to determine H_2 adsorption capacities at cryogenic temperatures and lower pressure range (<1.2 bar).

3.2 Synthesis of MIL MOFs

The synthesis of Fe-based MOFs followed a 3-step process as presented in Figure 9. The process is separated into three (3) steps; A, B and C. The initial step is the depolymerisation of the PET waste bottles to obtain terephthalic acid, denoted as A.

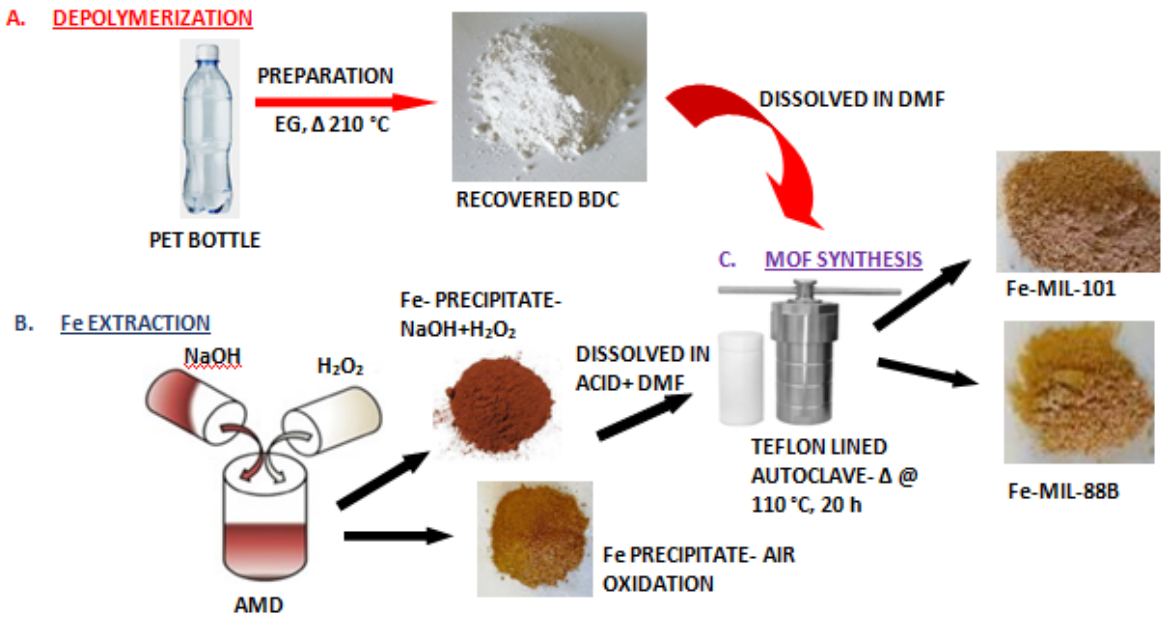

Figure 9: Schematic diagram summarising the entire process leading up to the synthesis of waste-derived Fe-MIL-101 and Fe-MIL-88B MOFs.

The second step (denoted B) is the extraction of Fe from the AMD using three (3) different methods, however, only two are outlined on the diagram since the omitted method also makes use of NaOH but does not make use of H_2O_2. Lastly, Figure 9C is the solvothermal synthesis of Fe-based MIL-MOFs from waste-derived precursors (A and B) and commercial precursors.

3.2.1 Materials and reagents

Iron (III) chloride hexahydrate ($FeCl_3 \cdot 6H_2O$, Sigma Aldrich, 97%), iron (III) nonahydrate ($Fe(NO)_3 \cdot 9H_2O$, Sigma Aldrich, 98%), terephthalic acid (1,4-BDC, Sigma Aldrich, 98%), ethylene glycol ($HOCH_2$-CH_2OH, Sigma Aldrich, 99.8%), *N,N*-dimethylformamide (DMF, Sigma Aldrich, 99.8%), hydrogen peroxide (H_2O_2, 50%), sodium hydroxide (NaOH pellets, Sigma) and ethanol (CH_3CH_2OH, Sigma Aldrich) were used without further modification. Waste PET water bottles were collected from household waste. The caps, rings and labels were removed and then cleaned to avoid contamination. They were cut into small pieces. AMD water was collected from a gold mine in the Gauteng region of the Republic of South Africa (RSA).

3.2.2 Depolymerization of Poly ethylene (PET) waste bottles

The depolymerization of waste PET was carried out in a 500 mL Teflon-lined, high-pressure reactor. 125 g of PET flakes, 125 mL of ethylene glycol (EG) and 300 mL of H_2O were added into the reactor and then gradually heated until a temperature of 210 °C was achieved and maintained for 8 h. Once the reaction time had elapsed, the product was then centrifuged, washed twice with ethanol, and dried at 100 °C for 24 h. Waste-derived BDC was then further used as a precursor in the synthesis of Fe-MOFs.

3.2.3 Extraction of Fe metal from AMD

Fe was precipitated by two methods, first by leaving AMD in open air at room temperature, which resulted in the oxidation of Fe^{2+} to Fe^{3+} which ultimately precipitated out. The precipitate was then filtered under vacuum, washed thoroughly with deionized water and dried at 100 °C overnight. The resultant product was ground to fine powder and labelled rAMD-Fe.

The second method was the selective precipitation of iron by pH control at room temperature using an alkaline reagent as reported by Seo *et al*.[185] In a typical procedure, Fe was first oxidized from Fe^{2+} to Fe^{3+} using 30 % H_2O_2, this solution was then neutralized with 4 M NaOH solution to pH end points of 3.0-3.5. The precipitated product was recovered by filtration under vacuum and dried overnight at 100 °C.[190-191] The dried precipitate was ground to fine powder and labelled $_{OHo}$AMD-Fe. To assess the effectiveness of the oxidation step, raw AMD was neutralized with 4 M NaOH to a pH of 3.0-3.5 and the formed precipitate was washed with distilled water, dried at 100 °C and then labelled $_{OH}$AMD-Fe.

3.2.4 Synthesis of Fe-MOFs

The synthesis of MOFs was carried out using three different Fe metal sources to assess their effects on the morphology and textural properties of the MOFs. The extraction of Fe from the AMD was carried out via two extraction methods, 1) NaOH at pH 3.5 and 2) air injection to obtain $Fe(OH)_3$ and $FeHO_2$, respectively. Two commercial Fe sources were explored ($FeCl_3{\cdot}6H_2O$ and $Fe(NO)_3{\cdot}9H_2O$) thus the two AMD-derived Fe were each dissolved in two acids, HCl and HNO_3, separately. Commercial BDC or PET-derived BDC as an organic linker source was combined with each of the Fe sources in solvothermal synthesis at suitable

conditions to yield either MIL-101 or MIL-88B. Detailed experimental procedures are described below in the next sections.

3.2.4.1 Fe-MIL-101 synthesis

Fe-MIL-101 was synthesized using $FeCl_3 \cdot 6H_2O$ (or $Fe(NO)_3 \cdot 9H_2O$) as a metal source and H_2BDC or PET-BDC as organic linkers. A procedure reported by Kholdeeva *et al.* (2019) was used with minor modifications.[192] In a typical procedure, 5.2 mmol of $FeCl_3 \cdot 6H_2O$ and 2.6 mmol of either H_2BDC or PET-BDC were fully dissolved in 30 mL DMF, transferred to a Teflon lined autoclave and heated at 110 ^{o} C for 20 h. The resultant red precipitate was then centrifuged, followed by washing with DMF and hot ethanol (3 h) twice, respectively.[193] The product was then dried at 80 ^{o} C under vacuum overnight. MOFs prepared from commercial Fe source and commercial grade BDC were labelled as Fe-MIL-101(Cl) and Fe-MIL-101(NO_3) whereas those prepared from PET-derived PET were labelled Fe-MIL-101$(Cl)_{pet}$ and Fe-MIL-101$(NO_3)_{pet}$.

The synthesis of Fe-MIL-101 from rAMD-Fe and $_{OH}$AMD-Fe followed a similar procedure as with the commercial Fe sources. However, 5.2 mmol of rAMD-Fe or $_{OHo}$AMD-Fe were first dissolved in a stoichiometric amount of HCl or HNO_3 with heating at low temperatures (~60 °C) prior to mixing with a solution containing BDC dissolved in DMF. The MOFs synthesized by the dissolution of the precipitates in HCl were labelled as rAMD-Fe-MIL-101(Cl), rAMD-Fe-MIL-101- $(Cl)_{pet}$, $_{OHo}$AMD-Fe-MIL-101(Cl) and $_{OHo}$AMD-Fe-MIL-101$(Cl)_{pet}$. Samples prepared from HNO_3 were labelled as rAMD-Fe-MIL-101(NO_3), rAMD-Fe-MIL-101$(NO_3)_{pet}$, $_{OHo}$AMD-Fe-MIL-101(NO_3) and $_{OHo}$AMD-Fe-MIL-101$(NO_3)_{pet}$.

3.2.4.2 Fe-MIL-88B synthesis

Fe-MIL-88B MOFs were synthesized using a procedure previously reported by Xu et al., (2016). In a typical procedure, 9.06 mmol of the metal source ($FeCl_3 \cdot 6H_2O$ or $Fe(NO_3)_3 \cdot 9H_2O$), 9.06 mmol of the organic linker (H_2BDC or PET-BDC), 0.30 g of NaOH and 4.47 mL of CH_3COOH were all dissolved in 50 ml DMF. The mixture was heated at 110 ^{o} C for 20 h using a teflon-lined stainless-steel bomb in a static oven. The resultant brown-red precipitate was separated from the solvent via centrifugation followed by washing with DMF and hot ethanol (3 h) twice.[193] The product was finally dried at 80 ^{o} C under vacuum overnight. MOFs prepared from commercial Fe and commercial grade BDC were labelled as

Fe-MIL-88B(Cl) and Fe-MIL88B(NO_3) whereas those prepared from PET-derived BDC were labelled Fe-MIL-88B(Cl)$_{pet}$ and Fe-MIL-88B(NO_3)$_{pet}$.

The synthesis of Fe-MIL-88B from rAMD-Fe and $_{OHo}$AMD-Fe followed a similar procedure as with the commercial Fe sources. However, 9.06 mmol of rAMD-Fe or $_{OH}$AMD-Fe was dissolved in a stoichiometric amount of HCl or HNO_3 with heating at low temperatures (~60 °C) prior to mixing with a solution of terephthalic acid dissolved in DMF. The MOFs synthesized by the dissolution of the precipitates in HCl were labelled as rAMD-Fe-MIL-88B(Cl), rAMD-Fe-MIL-88B(Cl)$_{pet}$, $_{OHo}$AMD-Fe-MIL-88B(Cl) and $_{OHo}$AMD-Fe-MIL-88B- (Cl)$_{pet}$. Samples prepared from precipitates digested in HNO_3 were labelled as rAMD-Fe-MIL-88B(NO_3), rAMD-Fe-MIL-101(NO_3)$_{pet}$, $_{OHo}$AMD-Fe-MIL-88B(NO_3) and $_{OHo}$AMD-Fe-MIL-88B(NO_3)$_{pet}$.

3.3 Characterization

Prior to Fe extraction, raw AMD as well as samples of AMD after the extraction of Fe were analyzed for pH and Fe content. The pH meter was first calibrated at pH 4 and 7. The prepared materials were analyzed for various properties with each characterization technique and conditions further explained below:

3.3.1 Inductively coupled plasma- optical emission spectroscopy (ICP-OES)

ICP-OES is a quantitative technique used to determine elemental composition of solution-based samples. This technique makes use of plasma to excite atoms and a spectrometer to quantify the energies given off by the atoms as they exit the excited state. An ICP-OES Perkin Elmer, optima 2100 DV was used to quantify the metal ions present in the AMD samples. Standards of known concentrations were first run to generate a calibration curve prior to running the AMD water samples for quantification of the elements present. To quantify the total metal concentration in the collected AMD sample, the sample was filtered under vacuum to remove any suspended solids that may be present. Metal concentration was also determined in samples after Fe was extracted to determine the efficiency of the extraction methods.

3.3.2 Thermogravimetric analysis (TGA)

TGA is an analytical technique used to establish thermal stabilities of materials as well as the fraction of volatile components by monitoring the weight change that occurs as a sample is

heated at a constant rate to generate a TGA curve (Weight % against temperature). TGA can be run under inert, reductive or oxidative conditions depending on the nature of the sample and information required about that particular material. The environment under which the sample is heated plays a significant role as different environments can affect each material differently.[194] This technique is less expensive, fast, easier, and serves as a valuable tool for understanding nano materials and polymer composition.[195-196] The evaluation of the thermal stabilities of the prepared MOF materials was carried out with the Mettler, Toledo, TGA/SDTA 851e instrument.

3.3.3 Powder X-ray diffraction (PXRD)

PXRD is a technique used for structural analysis of microcrystalline solid materials or powder samples. PXRD gives information about the crystal phases, degree of crystallinity as well as the crystallite size of the material. PXRD is a highly sensitive, non-destructive technique that is fast and reliable, cost-effective with a simple sample preparation. "X-rays are partially scattered by atoms when they strike the surface of a crystal and some pass though the next layer which then causes an overall diffraction pattern. If beams diffracted by two different layers are in phase, constructive interference occurs and the diffraction pattern shows a peak. However, if they are out of phase, destructive interference occurs appear and no peak is observed. Diffraction peaks only occur if it follows Bragg's Law."[197-199] See equation 3.1 and Figure 10 for mathematical and graphical explanation of Bragg's law:[200]

$$n\lambda = 2d \cdot \sin\theta$$ *Bragg's equation* (3.3.1)

Where; n is an integer

λ is the wavelength of the incident X-ray beam

d is the path difference between the atomic layers

and θ is the angle of incidence

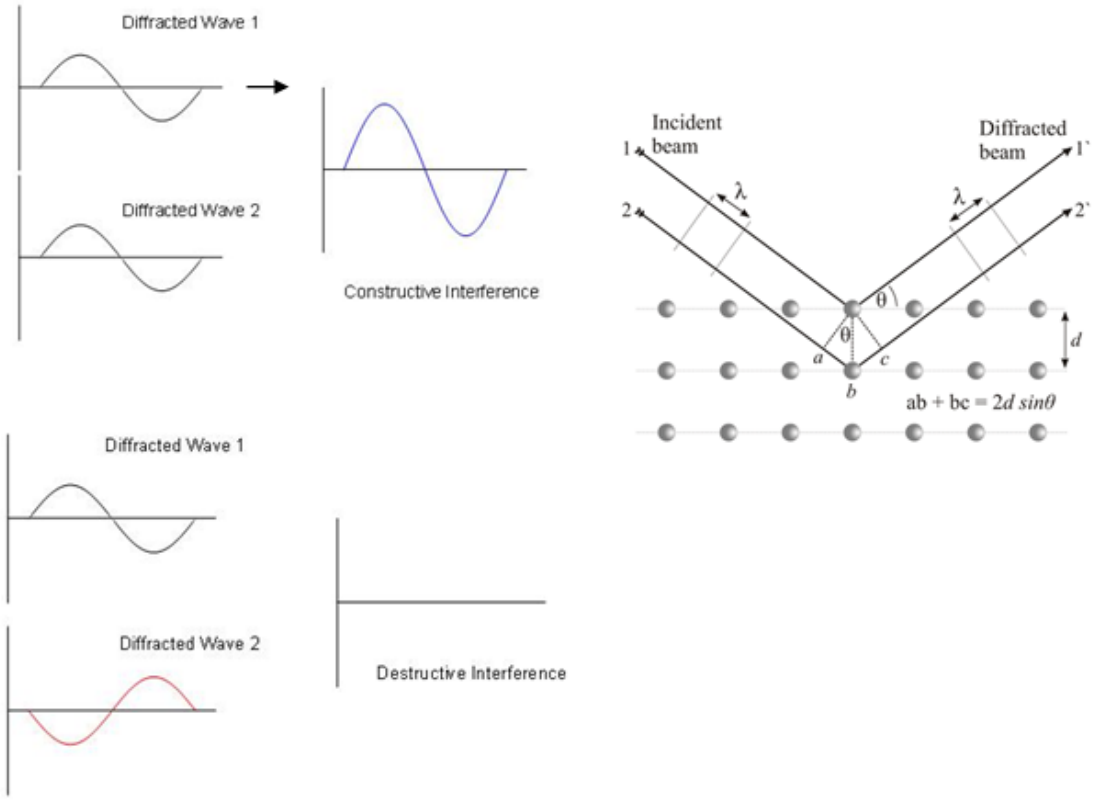

Figure 10: Schematic representation of the Bragg's law concept. Taken from reference 200.

3.3.4 Fourier transform infrared spectroscopy (FTIR)

FTIR was used for structural elucidation by determining the functional groups present in the materials. FTIR is an analytical technique that measures the absorption and emission of infrared radiation over a range of wavelengths. This technique may be applied to solid or liquid samples.[201] In an FTIR, the sample is subjected to a single pulse of radiation with frequencies in a specific range. At particular frequencies (which are characteristic of the sample), the sample will absorb the radiation, resulting in a series of peaks in the spectrum that can be used to identify the sample.[202] Figure 11 gives a summary of the working principle and components of the FTIR instrument.[203] FTIR spectra of the commercial Fe source, Fe precipitates, commercial and PET-derived BDC as well as synthesized MOFs were recorded on a PerkinElmer Spectrum 100 Fourier transform infrared (FTIR) spectrometer, at a range of 4000 to 650 cm^{-1}.

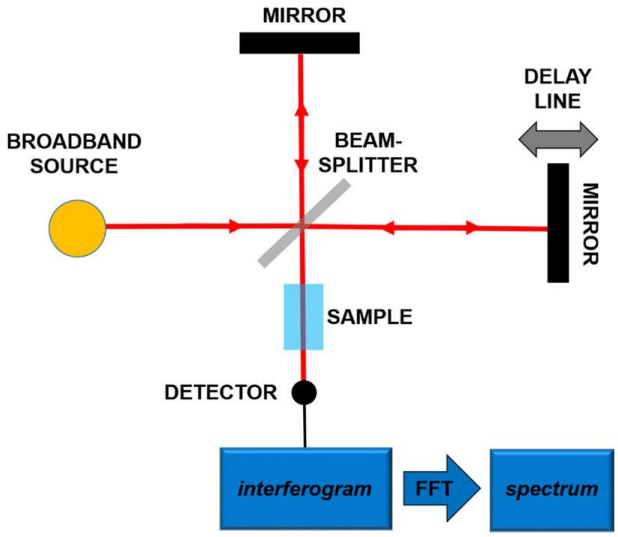

Figure 11: Working principles of the Fourier-Transform Infrared spectroscopy. Reproduced from reference 203.

3.3.5 Scanning electron microscopy (SEM)

SEM is a very powerful analytical technique used to study surface morphologies of a variety of materials to produce high resolution images. The SEM technique makes use a beam of highly charged electrons to scan through the surface of the material to capture information about the crystallite structure, size, and nanoparticle distribution within the materials.[92, 204]

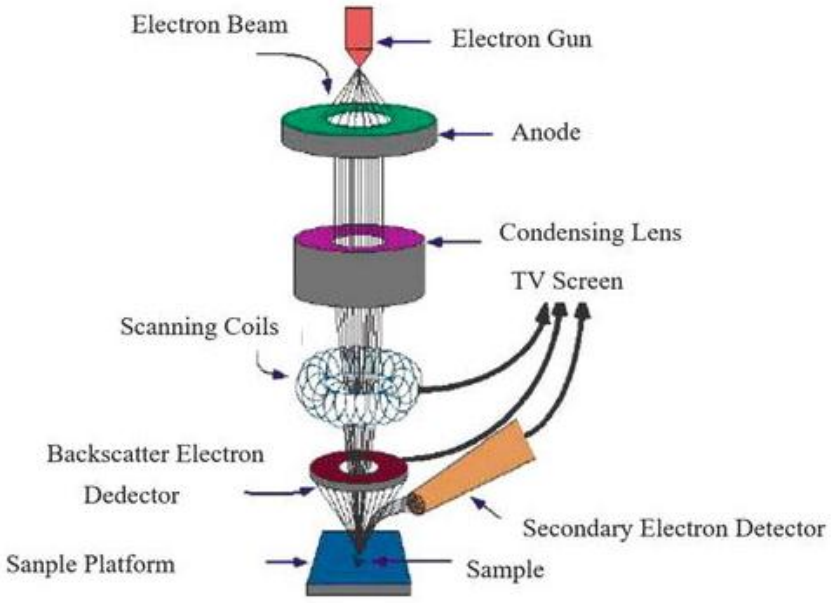

Figure 12: Schematic representation of Scanning Electron Microscopy (SEM). Image reproduced from reference 205.

Electrons are produced in the optical column of the microscope, held under vacuum, by means of an electronic gun situated at the top of the microscope, thus following a vertical path through the microscope (Figure 12). This beam of electrons is directed towards the specimen by passing through electromagnetic field, condensing and objective lenses, as well as apertures of varying diameters to adjust the density of the lens. When the electron beam strikes the specimen placed on a stage, secondary electrons, backscattered electrons, and characteristic X-rays are produced and then collected by one or more detectors to create an image. Figure 13 presents the process of specimen-electron beam interaction.[205-206]

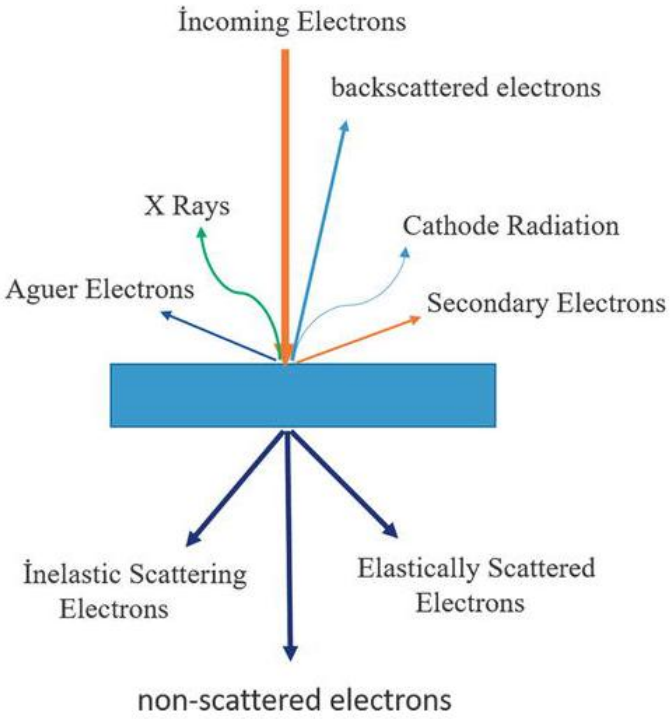

Figure 13: Schematic representation of the electron beam interacting with the specimen. Image reproduced from reference 205.

3.3.6 Adsorption-desorption studies- Brunauer-Emmett-Teller (BET) theory

Adsorption is a phenomenon where gas molecules or solute adhere onto the surface of the material or substance through chemical bonding (chemisorptions) or physical forces (physisorption). Chemisorption occurs when a chemical reaction occurs to form a strong chemical bond between the adsorbate and adsorbent usually resulting in a single-layer of adsorbed molecules. Physisorption occurs when the adsorbate adheres to the surface of the

adsorbent through weak Van der Waal forces thus allowing multi-layered adsorption and requires low activation energy. Various theories have been used to explain physisorption, however, the Brunauer-Emmett-Teller (BET) theory became the most popular for multilayer adsorption. The BET theory extends from the Langmuir theory used for monolayer adsorption and makes use of three (3) hypotheses;

i. All gas molecules are physically adsorbed onto the surface of the adsorbent such that only a monolayer is formed.
ii. Only one adsorbate is adsorbed onto each active site with no interaction occurs between adsorbates on different sites.
iii. All sites have the same heat of adsorption which is not dependent on the number of active sites available on the surface.

BET theory however, addresses the limitations presented by the Langmuir theory thus adding the following assumptions;

i. Gas molecules adsorb onto the surface of the adsorbent infinitely to form multiple layers of adsorbate.
ii. This results in molecule-molecule interactions of adjacent molecules however, different layers do not interact.
iii. The Langmuir theory is applied for each layer of adsorbates.

In BET analysis, an inert gas, typically Nitrogen or Argon, is passed though the material at cryogenic temperatures which then leads to physisoption of the gas on the surface and pores of the material. An adsorption isotherm is then produced, characteristic to the pore size of the pores (type I-V, see Figure 14).[207] The type I isotherm is used to describe materials with mocropores indicating the presence of only the monolayer. Type II isotherm is common for non-porous or macroporous materials with strong adsorbate–adsorbent interactions, the presence of a monolayer is observed at low pressures and then the sharp increase at medium pressures indicate the formation of multilayer. Type III and V isotherms form when weak interactions between the adsorbent and adsorbate exist thus the formed monolayer does not conform to the BET theory. Type V indicates mono and multilayer adsorption as well as when capillary condensation occurs as with type IV isotherm however, the latter generally observed with for mesoporous materials. [208]

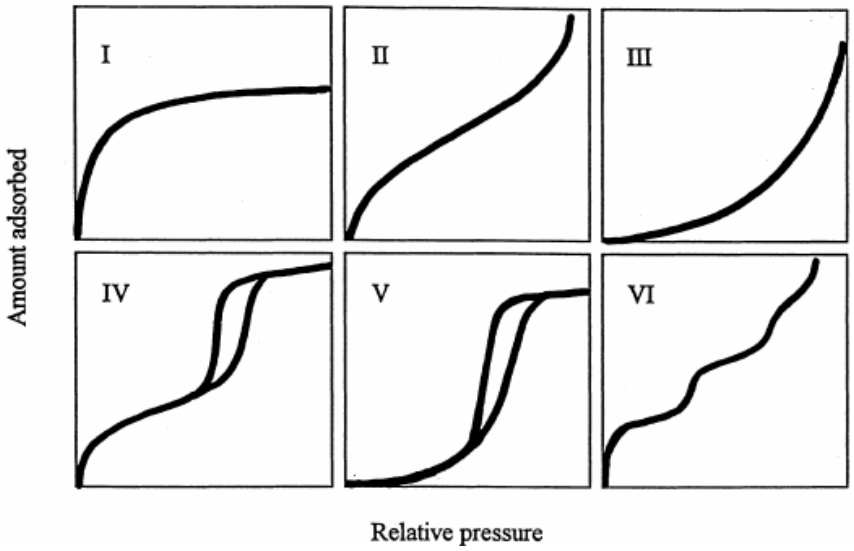

Figure 14: Adsorption Isotherms for gas as per the IUPAC classification. Reproduced from reference 207.

The amount of gas molecules adsorbed on the adsorbent material is generally used to calculate the surface area of the material. The BET equation defined in equation 3.2 is used to calculate the surface area of the material.

$$\frac{1}{v[(^{p_0}/_{p}) - 1]} = \frac{1}{v_m c} + \frac{c-1}{v_m c}\left(\frac{p}{p_0}\right)$$

BET equation (3.3.2)

Where, v is the amount of adsorbed gas molecules

p_0 - saturation pressure of the adsorbates

p - pressure of adsorbates at equilibrium

c - BET constant (energy of adsorption in the first adsorbed layer)

BET surface areas are obtained from the linear region of the N_2 isotherms. Prior to analysis, samples are degassed in the analysis tube under vacuum by heating at elevated temperatures to remove solvent molecules trapped in the pores of the materials whilst avoiding loss of framework crystallinity. Gas adsorption capacities (i.e CO_2 and H_2) can also determined at cryogenic temperatures (77K) and varying pressures to establish optimal conditions with maximum storage capabilities.

3.3.7 X-ray spectroscopy (XPS)

The surface chemistry of the Fe precipitates obtained from the AMD was analyzed using an XPS technique to quantitatively determine elemental composition, chemical and electronic state of the atoms that make up the Fe precipitates. This technique applies the concept of the photoelectric effect, a phenomenon whereby electrons at a state of rest absorb the energy of the electromagnetic radiation (eg. Light or x-rays) that hits the surface of the metal, these electrons then become electrically charged and move from the state of rest to the excited state thus being ejected from the surface of the metal (see the illustration in Figure 15).[209]

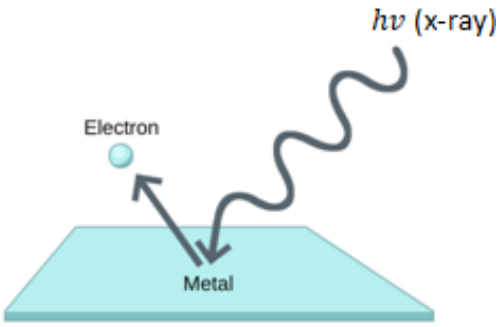

Figure 15: Representation of the photoelectric effect. Image reproduced from https://theory.labster.com/photoelectric-effect/, accessed on the 06/12/2022

$$E_{h\nu} = E_K + E_{\emptyset} + E_B(i) \qquad \textit{Energy conservation equation} \ (3.3.3)$$

$E_{h\nu}$ is the x-ray energy,

E_k is the kinetic energy of the ejected electron

$E_{\emptyset}$ is the spectrometer work function

$E_B(i)$ is the electron binding energy of the ith atomic orbital

The XPS technique uses a monoenergetic soft X-ray beam to excite the molecules on the surface of a sample, leading to photoelectrons being emitted from the surface of the material. Upon relaxation, the photoelectron gives off characteristic kinetic energy which is then measured by the detector thus providing information about the electronic states of the

atom and surface properties of the material.[210-211] Chemical shifts also can be used to determine how the atom is bonded thus providing the actual chemical state of the material.[212-213] XPS analysis of the obtained Fe precipitates was conducted using a Thermo ESCAlab 250Xi Spectrometer with X-rays of monochromatic Al kα (1486.7 eV). The survey spectra were examined at 100 eV, high resolution at 20 eV.

3.4 Chapter summary

The synthesis of MOFs from commercial precursors followed a conventional method-solvothermal synthesis owing to the simplicity and better understanding of the method. MOFs synthesized from PET-derived BDC have been widely reported in literature and proved to not affect the integrity of the MOFs. BDC was derived from PET by mixing with water and EG at elevated temperatures (210 °C), the resultant white powder was then used for the synthesis of MOFs by combining with commercial Fe source precursors or waste derived metal precursors. To synthesize MOFs from waste derived metal source, Fe was first extracted from the AMD using a chemical method (H_2O_2 and NaOH) and natural precipitation of Fe. The obtained Fe precipitates were then combined with commercial BDC or PET derived BDC to obtain either Fe-MIL-101 or Fe-MIL-88B. Characterization of the waste precursors and synthesized MOFs was the most important aspect as it proved whether the desired material had been obtained or not. Various analytical techniques were consulted in this regard to determine the morphology, crystal phases and sizes, textural and thermal properties chemical and electronic composition as well as the functional groups within the materials.

Chapter 4

4. Results and discussion: Fe-MIL-101

4.1 Chapter outline

Chapter 4 outlines and discusses the results of the synthesized Fe-MIL-101 MOFs from commercial and waste precursors. The chapter sets off by discussing the elemental composition of AMD prior to the extraction of Fe precipitates and then discusses structural properties of the latter. Textural, physical and chemical properties of MOFs derived from commercial precursors, partial and complete waste are also outlined. Weaknesses and strengths of the methods are identified and recommendations made for future investigations.

Holistic strategy for the synthesis of Fe-MIL-101 MOFs using Fe obtained from AMD and PET waste

Nqobile Mthembu[a,b], Xoliswa Dyosiba[a], Henrietta Langmi[b], Nicholas Musyoka[a*]

[a] Centre for Nanostructures and Advanced Materials (CeNAM), Chemicals Cluster, Council for Scientific and Industrial Research (CSIR), Pretoria, South Africa.

[b] Department of chemistry, university of Pretoria, Hatfield, 0002

**Corresponding author. Tel: +27 12 841 4806. Email: NMusyoka@csir.co.za*

Abstract

The successful synthesis of Fe-based MOFs using PET-derived BDC and AMD-derived Fe directly addresses the limitations of large-scale production of MOFs that is associated with high costs of starting materials. Fe-MIL-101 synthesized via the solvothermal route from waste precursor sources displayed similar properties to those synthesized from commercial grade precursors. XRD and FTIR spectra revealed characteristic diffraction peaks as well as vibrations and stretching bends that confirmed the coordination of BDC to the metal centre, respectively. The obtained MOFs had surface areas within the range of 500-1200 m^2/g and

pore size distribution in the micro- and mesoporous range. The MOFs proved to be thermally stable up to temperatures above 300 °C, typical of Fe-MIL-101 and further confirming the successful preparations of Fe-MIL-101 from both commercial and waste-derived precursors. Hydrogen adsorption studies on the Fe-MIL-101 from waste-precursors yielded material yielded 1.18 wt% at 1 bar and 77 K which is comparable to the values previously reported in literature relative to the surface area obtained.

Key words: Metal-organic frameworks, Acid mine drainage, Waste PET, Benzyl dicarboxylic acid, Fe-MIl-101, Fe-MIL-88B.

Introduction

Metal-Organic Frameworks (MOFs) are a group of porous materials that have attracted much attention over the years owing to their unique properties. As a result, MOFs have been found suitable for a wide range of applications including catalysis, sensors, supercapacitors, gas storage and separation/purification.[45, 47, 214] The high costs of starting materials, use of large amounts of solvents as well as long reaction times for the synthesis of MOFs pose limitations to the up-scaling of MOFs, resulting in limited industrial application of MOFs. A necessity to find cheaper and easy to source raw materials for the synthesis of MOFs, whilst maintaining the integrity of the MOF material, has risen over the years.[166] Deriving precursors from wastes such as polyethylene terephthalate (PET) bottles, waste batteries, coal fly ash or even wastewaters is an option worth exploring towards reducing costs associated with the synthesis of MOFs.[41, 161-163] Conventional recycling of PET waste has proven to be costly[215] with low efficiency and as a result, the degrading of PET to its monomers to be re-used in other reactions can be a better solution.[166, 216] The use of PET-derived 1,4-Benzenedicarboxylic acid (BDC) as an alternative to commercial grade BDC has been reported numerous times and the previously reported data proved that the use of waste PET-BDC does not compromise the integrity nor the textural properties of the derived MOFs.[165, 167, 217] However, a recent study by Dyosiba *et. al* (2019) informed that the use of colourful PET bottles to derive BDC linker in MOFs synthesis saw a decline in BET surface when compared to their counterparts synthesized from clear PET-derived BDC and commercial BDC.[159] Deleu *et al*. suggested a one-pot synthesis procedure using waste PET, which involved two stages: the hydrolysis of PET and simultaneous synthesis of MOFs.[169]

On the other hand, MOFs have also been synthesised from waste metal precursors such as spent Li-ion batteries as reported by Rambau *et al*.[170] Acid mine drainage (AMD) is known to be a great source for the harvest of metals as it is highly concentrated with heavy metals that can be recycled for reuse. AMD is a resultant waste from mining processes that is highly acidic, rich in heavy metals and sulfate.[172-173] AMD typically has low pH with high contents of Fe and a portion of other metals thus polluting underground and surface water which has devastating effects on biological activity.[174-175] While numerous technologies have been implemented to clean up the AMD that leaches into and pollute water systems. These technologies tend to be costly and are not efficient thus obtaining alternative use for the AMD waste is recommended.[176-177] The use of different alkaline reagent has served as one of the techniques used for the recovery of metals through precipitation thus yielding hydroxides or carbonates.[172, 176-177, 182-184] Flores *et al*. reported the use of Iron oxide particles recovered from AMD through a sequential precipitation as low-cost feedstock for the production of geothite, ferrihydrite and magnetite.[187] Seo *et al*. used three neutralizing reagents (NaOH, Na_2CO_3 and $Ca(OH)_2$) for the sequential selective precipitation of Fe, Al and Mn by control of the pH.[185]

By combining the use of waste PET as well as AMD-derived Fe metal, a completely green approach to Fe-MOFs synthesis is be achieved. In this study, Fe-MIL-101 synthesized from AMD-derived Fe metal and PET-derived BDC is reported, a comparison is provided for Fe-MIL-101 prepared from commercial grade precursors following the same synthesis approach.

Experimental

Materials and reagents

Iron (III) chloride hexahydrate ($FeCl_3 \cdot 6H_2O$), Sigma Aldrich, 97%), Iron (III) nonahydrate ($Fe(NO)_3 \cdot 9H_2O$, Sigma Aldrich, 98%), Terephthalic acid (1,4-BDC, Sigma Aldrich, 98%), ethylene glycol ($HOCH_2$-CH_2OH, Sigma Aldrich, 99.8%), *N,N*-dimethylformamide (DMF, Sigma Aldrich, 99.8%), hydrogen peroxide (H_2O_2, 50%), Sodium hydroxide (NaOH pellets, Sigma) and Ethanol (CH_3CH_2OH, Sigma Aldrich) were used without additional modification. Waste PET bottles were collected from household waste, caps, rings, and labels were removed and

then cleaned to avoid contamination. They were cut into small pieces. AMD water was collected from a gold mine in the Gauteng region of RSA.

PET depolymerization

The depolymerization of waste PET was carried out as per the procedure outlined by Dyosiba *et al.*[159] In a typical procedure, 125 g of PET flakes, 125 mL of ethylene glycol (EG) and 300 mL of H_2O were added into a 500 ml Teflon-lined high-pressure reactor and then heated to 210 °C and maintained for 8 h. The resultant product was centrifuged, washed twice with ethanol, and dried at 100 °C for 24 hours. The PET-derived BDC was then further used as a precursor in the synthesis of Fe-MOFs.

Fe extraction from AMD

Fe was precipitated by two methods, first by leaving AMD in open air at room temperature, which resulted in the oxidation of Fe^{2+} to Fe^{3+} which ultimately precipitated out. The precipitate was then filtered under vacuum, washed thoroughly with deionized water and dried at 100 °C overnight. The resultant product was ground to fine powder and labelled rAMD-Fe.

The second method was the selective precipitation of iron by pH control at room temperature using an alkaline reagent as reported by Seo *et al*.[185] In a typical procedure, Fe was first oxidized from Fe^{2+} to Fe^{3+} using 30 % H_2O_2, this solution was then neutralized with 4M NaOH solution to pH end points of 3.0-3.5. The precipitated product was recovered by filtration under vacuum and dried overnight at 100 °C.[190-191] The dried precipitate was grounded to fine powder and labelled $_{OHo}$AMD-Fe. To assess the effectiveness of the oxidation step, raw AMD was neutralized with 4M NaOH to a pH of 3.0-3.5 and the formed precipitate was washed with distilled water, dried at 100 °C and then labelled $_{OH}$AMD-Fe.

MIL-101 synthesis

Fe-MIL-101 was synthesized using $FeCl_3 \cdot 6H_2O$ (or $Fe(NO)_3 \cdot 9H_2O$) as a metal source and H_2BDC or PET-BDC as organic linkers. A procedure reported by Kholdeeva *et al.* (2019) was used with minor modifications.[192] In a typical procedure, 5.2 mmol of $FeCl_3 \cdot 6H_2O$ and 2.6 mmol of either H_2BDC or PET-BDC were fully dissolved in 30 mL DMF, transferred to a Teflon lined autoclave and heated at 110 ^{o} C for 20 h. The resultant red precipitate was then

centrifuged, followed by washing with DMF and hot ethanol (3 h) twice, respectively.[193] The product was then dried at 80 ^{o} C under vacuum overnight. MOFs prepared from commercial Fe source and commercial grade BDC were labelled as Fe-MIL-101(Cl) and Fe-MIL-101(NO_3) whereas those prepared from PET-derived PET were labelled Fe-MIL-101$(Cl)_{pet}$ and Fe-MIL-101$(NO_3)_{pet}$.

The synthesis of Fe-MIL-101 from rAMD-Fe and $_{OH}$AMD-Fe followed a similar procedure as with the commercial Fe sources. However, 5.2 mmol of rAMD-Fe or $_{OHo}$AMD-Fe were first dissolved in a stoichiometric amount of HCl or HNO_3 with heating at low temperatures (~60 °C) prior to mixing with a solution containing BDC dissolved in DMF. The MOFs synthesized by the dissolution of the precipitates in HCl were labelled as rAMD-Fe-MIL-101(Cl), rAMD-Fe-MIL-101- $(Cl)_{pet}$, $_{OHo}$AMD-Fe-MIL-101(Cl) and $_{OHo}$AMD-Fe-MIL-101$(Cl)_{pet}$. Samples prepared from HNO_3 were labelled as rAMD-Fe-MIL-101(NO_3), rAMD-Fe-MIL-101$(NO_3)_{pet}$, $_{OHo}$AMD-Fe-MIL-101(NO_3) and $_{OHo}$AMD-Fe-MIL-101$(NO_3)_{pet}$.

Characterization

Prior to Fe extraction, the AMD wastewater was analysed for pH and metal content as well as after the extraction of Fe. Elemental analysis was done using an ICP-OES Perkun Elmer, optima 2100 DV. X-ray diffraction (XRD) diffractograms were generated using a PANalytical X'Pert Pro powder diffractometer instrument consisting of a Pixcel detector. This instrument uses a Ni-filtered Cu-α radiation (0.154 nm) and was operated at 25 °C with a scanning rate set to 0.1°s^{-1} at 2θ angles between 3-90°. IR spectra of synthesized MOFs were obtained from the PerkinElmer Spectrum 100 Fourier transform infrared (FTIR) spectrometer. The scanning range was set at 4000 to 650 cm^{-1} and the resolution of 16 cm^{-1}, background was run prior to analysis. To determine the morphology of the MOFs, samples were first prepared for analysis by placing very tiny amounts on the carbon tape and then coating with carbon under vacuum. Analysis was then conducted on the Auriga Cobra Focused-Ion Beam Scanning Electron Microscope (FIB-SEM) instrument. Thermogravimetric analysis (TGA) of Fe-MIL-88B MOFs was determined using the Mettler, Toledo, TGA/SDTA 851e instrument. 10 mg of the MOF sample was weighed into a pan and steadily heated to 1000 °C at a rate of 10 °C min^{-1}. Any mass changes were monitored and a TGA profile generated. BET surface area and pore volume as well as Hydrogen (H_2) adsorption measurements were carried out on the ASAP 2020 HD analyzer (Micromeritics) instrument. Ultra-high purity grade

(99.999%) N_2 and H_2 gases were used to generate adsorption isotherms at 77 K and up to 1 bar. BET surface areas and pore volumes were obtained in the linear region of the N2 isotherms. Prior to analysis, 0.2-0.3 g of samples were weighed into the analysis tube and then degassed under vacuum (at a pressure of 10^{-7} bar) with heating at 150 °C overnight. XPS analysis was conducted using a Thermo ESCAlab 250Xi Spectrometer with X-rays of monochromatic Al kα (1486.7 eV) to generate survey spectra at 100 eV. The instrument had an X-ray power of 300 W, a spot size of 900 µm, and resolution at 20 eV at a pressure of 10^{-8} mbar.

Results and discussions

Elemental comparison of AMD

Fe, Al, Mn, Si, Ca and Mg were the typical elements found to be present in raw AMD with trace amounts of Zn, B, K, and Ce picked up by the instrument. Total Fe content was found to be 1251 mg/L with trace amounts for Na in the raw AMD sample. After the extraction of Fe with the use of an oxidant, Fe concentration decreased to 26 mg/L and Na content increased to 1784 mg/L. In the absence of H_2O_2, Fe concentration was measured to be 27 mg/L and that of Na at 1783 mg/L. This proves a recovery rate of ~98% was achieved whether the oxidant is used or not and is in accordance with the results obtained by Wei *et. al* (2005) and Menezes *et al*.[218-219] The increase in Na concentration is due to the NaOH added to the system for Fe precipitation. The Si content is also found to have decreased from 76 to 25 and 26 mg/L in the presence and absence of the oxidant, respectively. Fe^{3+} hydroxides precipitate at pH ~3.5 and the rest of the metals did not show any change in concentration.

Elemental composition of AMD-Fe precipitates

The XPS technique was used to confirm the elemental composition, chemical and electronic state of the atoms present in the AMD-Fe precipitates. XPS analysis was not done for $_{OH}$AMD-Fe since this precipitate exhibited similar behaviour as with $_{OHo}$AMD-Fe and the oxidant was found to have insignificant effect on the Fe precipitated from the AMD as confirmed by ICP-OES, XRD and FTIR techniques. The XPS survey and Fe2p spectra for rAMD-Fe and $_{OHo}$AMD-Fe are shown in Fig. 1. The XPS survey confirmed the predominant presence of Fe and O compounds with trace amounts of C and S compounds (see Equations 2.2.2 and

2.2.3 in page 29). rAMD-Fe also showed a presence of trace amounts for N compounds (Fig. 1b). The O1s spectrum for both precipitates (Fig. S3a and b) consisted of three (3) peaks at 533.7, 531.8 and 530.3 eV which were assigned to the carbonyl bond (C=O), hydroxide/sulphate and/or (C-O) and Fe(OH)O, respectively. The predominant peak at 530.3 eV in the Gaussian curve is attributed to the lattice oxygen confirming the presence of α-Fe_2O_3 as the XRD data had suggested. The peak at 531.8 is for SO_4^{2-} precipitated out as $FeSO_4$ and OH^- groups further confirming the deduction made about the materials being of hydroxides. The highest binding energy most likely originates from the hydroxyl groups adsorbed water molecules.[220]

The Fe2p spectra (see Fig. 1c and d) suggest that Fe species are present as two species, $FeSO_4$ and FeO(OH). Typical $Fe2p_{3/2}$ and $Fe2p_{1/2}$ peaks were observed at 712 and 25.8 eV, respectively, for both AMD-Fe precipitates. The Gaussian curve fitting revealed the appearance of a satellite peak centred at 720.2 eV which was exactly eight (8) units above the original $Fe2p_{3/2}$ peak with no overlapping with neither $Fe2p_{3/2}$ or $Fe2p_{1/2}$. The presence of this satellite peak and $Fe2p_{1/2}$ indicates the Fe^{3+} state of δ-FeOOH structure which is in correlation with the results from O1s spectrum and the XRD.[221-223] The presence of a satellite peak before the Fe $2p_{1/2}$ peak at 735 eV is an indication of Fe^{2+} being present within the precipitates as $FeSO_4$, however, the low intensity of the peak indicates very small quantities of this species.

The presence of sulphur (S) was also noted by the presence of a peak at 168.7 eV on both materials, as it can be observed in their respective S2p spectra (see supplemental data). The sulphur is present as both the sulfone (R_2SO_2 where R is the carbon atom) and sulphate species (SO_4^{2-}). Sulfate species are produced during the oxidation of metal sulfides (FeS_2) to form $FeSO_4$ as already revealed by the Fe 2p spectra. The sulfones are produced during the organic oxidation of sulfides and most likely precipitated out during the precipitation of Fe.[224] The presence of carbon species further confirms the presence of sulfone species which also correlates to the O1s spectrum peak for the carbonyl and C-O group. Four C1s peaks for C-C, C=C, C=O and O-C=O bonds were observed at 284.4, 282.9, 287.6 and 289.2 eV binding energy (see supplemental data). The presence of an O-C=O group suggests that the organic species that was present in the AMD was an ester molecule.

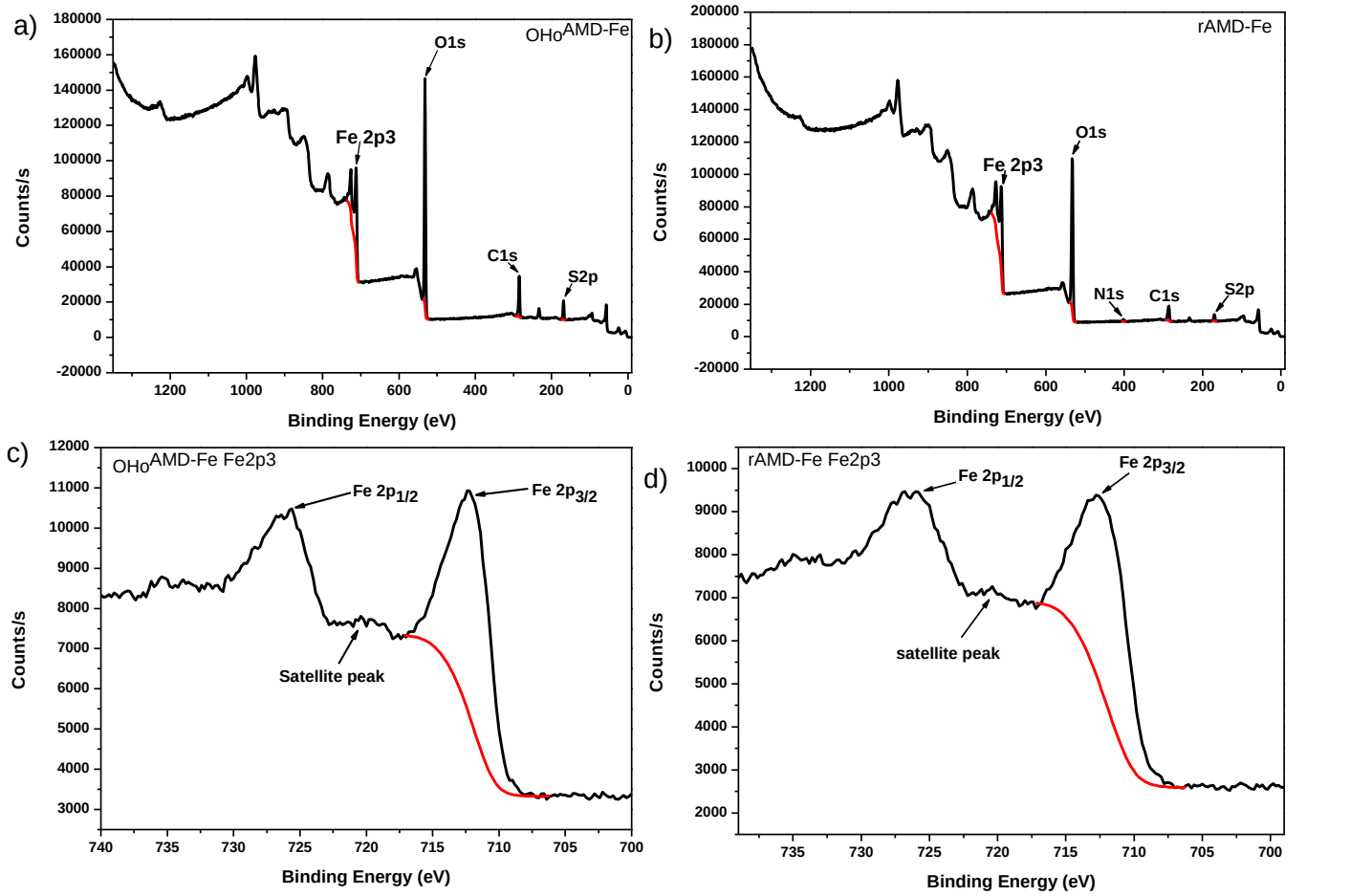

Figure 1: XPS spectra for AMD-Fe precipitates where a) and b) are survey spectra; c) and d) are Fe2p spectra for rAMD-Fe and $_{OHo}$AMD-Fe, respectively.

rAMD-Fe showed trace amounts of nitrogen molecules as impurities in the material (see supplemental data). The characteristic peak for cyanides and/or organic nitrogen compounds is observed at a binding energy of 400.1 eV. The lack of a peak at its specific binding energy shows that there is no Al species present as an impurity from the precipitation of AMD-Fe through both methods meaning that selective precipitation of Fe was achieved at pH 3.5.[161]

Structural analysis for Fe precipitates and BDC

XRD pattern for rAMD-Fe, $_{OHo}$AMD-Fe and $_{OH}$AMD-Fe are presented in Figure 2a. rAMD-Fe displays a typical ferric oxyhydroxide (FeOOH) diffractogram with a mixture of α- and β-phases observed in their characteristic positions (see Fig. 2a). From the XRD patterns, it can be concluded that β-FeOOH is predominant in rAMD-Fe, this is confirmed by the appearance of peaks at 2θ values of 8°, 34°(400), 35° (211) and 54° (600) which are characteristic for β-

FeOOH. The 2θ value at 23°(012) corresponds to the α-FeOOH phase which is assigned to the quartz (SiO_2) indicating that Si precipitated out during natural precipitation of Fe species, this corresponds to the decrease in Si content as indicated by the ICP-OES results.

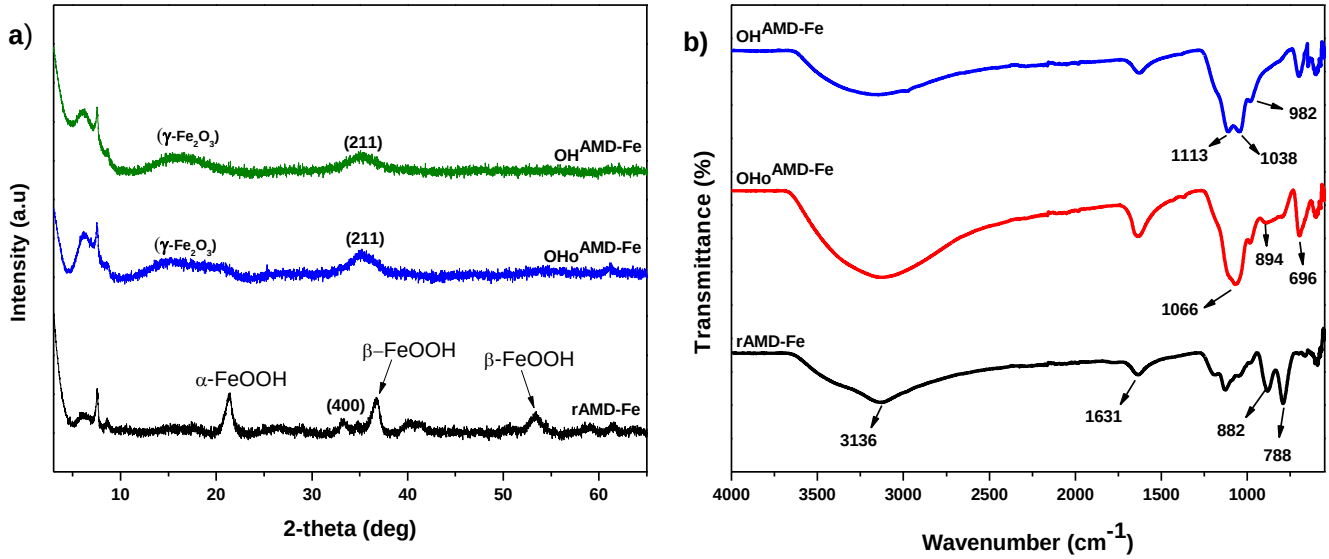

Figure 2: a) XRD pattern and b) FTIR spectra for AMD-Fe precipitates.

XRD patterns for $_{OHo}$AMD-Fe and $_{OH}$AMD-Fe were found to be almost similar, β-phases are observed at 2θ values of 8° and 35° whilst a broad peak at 15° is assigned to the γ phase. The broadness of the peaks is an indication of an amorphous material formed when NaOH is used to precipitate out Fe. NaOH treated AMD was rich in Fe species, hematite (Fe_2O_3) and magnetite (Fe_3O_4), the presence of the latter is represented by the peak at 35° and may be attributed to co-precipitation of Fe(II) and Fe(III) during neutralization.[176] This is in agreement with the results obtained from the ICP-OES which saw no difference in the Fe concentrations between the AMD samples in which an oxidant was used and the one where no oxidant was used. All iron precipitates from the AMD show a mixture of the hematite, magnetite and iron hydroxide peaks. Though rAMD-Fe shows a pattern typical for an iron oxyhydroxide, $_{OHo}$AMD-Fe and $_{OHo}$AMD-Fe XRD patterns are similar to those previously reported in literature for iron hydroxide nanoparticles.[186] Crystallite sizes were calculated to be 4.16 and 6.77 nm, respectively.

As shown in Figure 2b, the recovered precipitates consisted of an OH vibration peak represented by a broad peak at ~3140 cm^{-1} and H_2O molecules stretching mode at 1635 cm^{-1}. rAMD-Fe and $_{OHo}$AMD-Fe have peaks at 1113 cm^{-1} and 1064, respectively, that are representative of the S-O or S = O bond (refer to equation 2.2.1 and 2.2.2 in page 29). $_{OH}$AMD-Fe however, has a split peak where one is at 1108 cm^{-1} for the S-O or S=O bond and the one at 1037 cm^{-1} is for the Fe-O-OH stretching vibration mode thus confirming that the materials is indeed an Fe-hydroxide.

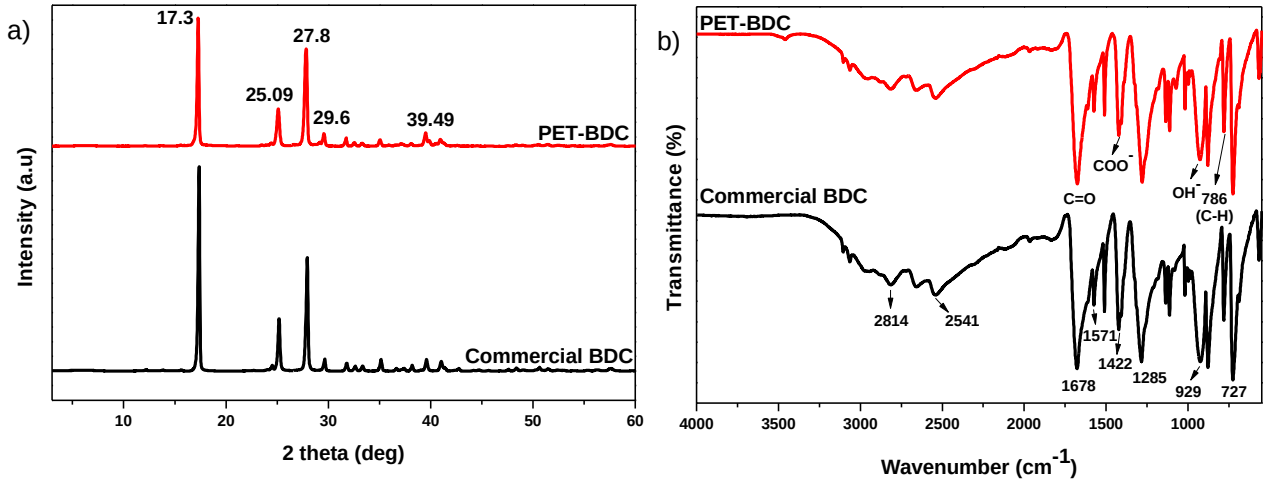

Figure 3: a) XRD pattern and b) FTIR spectra for commercial and PET derived BDC.

rAMD displays two peaks at 885 and 793 cm^{-1} which are both assigned to the Fe-O stretching mode whilst for $_{OHo}$AMD-Fe and $_{OH}$AMD-Fe this stretch mode appear at 697 and 701 cm^{-1}, respectively. The shoulder peaks at 980 and 986 cm^{-1} are assigned to the hematite Fe-O stretch mode and $_{OHo}$AMD-Fe has a peak at 895 cm^{-1} identified as the Fe-O stretching mode due to the presence of magnetite. The XRD pattern for the PET-BDC was identical to that of the commercial BDC (Fig. 3a), similar to those that have been previously reported in literature. The major characteristic peaks were observed at 17.3°, 25.09°, 27.8°, 29.6° and 39.49°.[159, 225]

Fig. 3b shows the FTIR spectras for commercial BDC and PET-BDC with major characteristic peaks observed for C=O stretch, COO^- stretch and O-H bending. The peak at 929 cm^{-1} assigned to -H bending is specifically due to the presence of the terephthalic acid dimmer via hydrogen bonds.[226] The carboxylic group (C=O) was identified by the absorption peaks at 3000-2541 cm^{-1} and the COO- stretch peaks at 1678, 1422 and 1285 cm^{-1}. The presence of

the benzene ring is confirmed by the presence of the C-H vibration mode represented by the peak at 727 cm^{-1}, which strongly supports the presence of the terephthalic acid monomer with the purity level similar to that of the commercial grade BDC.[227-228]

Fig. 4a and c are the XRD patterns for Fe-MIL-101 synthesized from chloride and nitrate precursors, respectively. XRD patterns for most synthesized Fe-MIL-101 MOFs exhibited characteristic Fe-MIL-101 peaks at 2θ values of 5.1, 5.85, 8.39, 9.04, 9.42 and 10.3. Further peaks were observed at 12.58, 16.47, 17.89, 18.86, 19.34 and 22° representative of trinuclear-transition metal based MOFs. The patterns of the prepared Fe-MIL-101 display fairly high intensities with very small areas under the peaks, indicating high crystallinity of the sample, which is in a good agreement with what was previously reported confirming that Fe-MIL-101 materials were indeed successfully synthesized.[193] $_{OHo}$AMD-Fe-MIL-101(Cl) and rAMD-Fe-MIL-101(NO_3) display very poor diffraction peaks possibly due to structural defects and small crystallite sizes. The slight shift in the XRD pattern for $_{OHo}$AMD-Fe-MIL-101$(Cl)_{pet}$ to higher diffraction angles is most likely due to change in the lattice structure of the material.

Figure 4b and d present FTIR spectra for Fe-MIL-101 samples prepared from chloride and nitrate precursors. All samples are similar in the structural vibrations, which is expected since they are all made up of trivalent metal centres and carboxylate linkers.[115] The carboxylate characteristic absorption peaks of C=O symmetric and asymmetric vibration bands are observed at 1396 and 1595 cm^{-1}, C-O stretching bands is at 1685 cm^{-1} indicating a successful coordination of the carboxylate ligand to the metal centre. The peak at 1020 and 750 cm^{-1} is attributed to the C-O-Fe stretching mode and C-H bending vibrations, respectively. This then further supports that BDC is indeed attached to the metal centre and the C-H vibrations mainly are due to the carboxylate group vibrations, similar to those reported in literature.[123-124, 229-230] Fe-MIL-101(NO_3) and Fe-MIL-101$(NO_3)_{pet}$ spectra (Fig. 3d) do not exhibit the shoulder peak at 604 cm^{-1} attributed to the stretching bend for Fe-O meaning that there is no connection through the μ_3-oxo atom as it would be expected for the octahedral.[231-232]

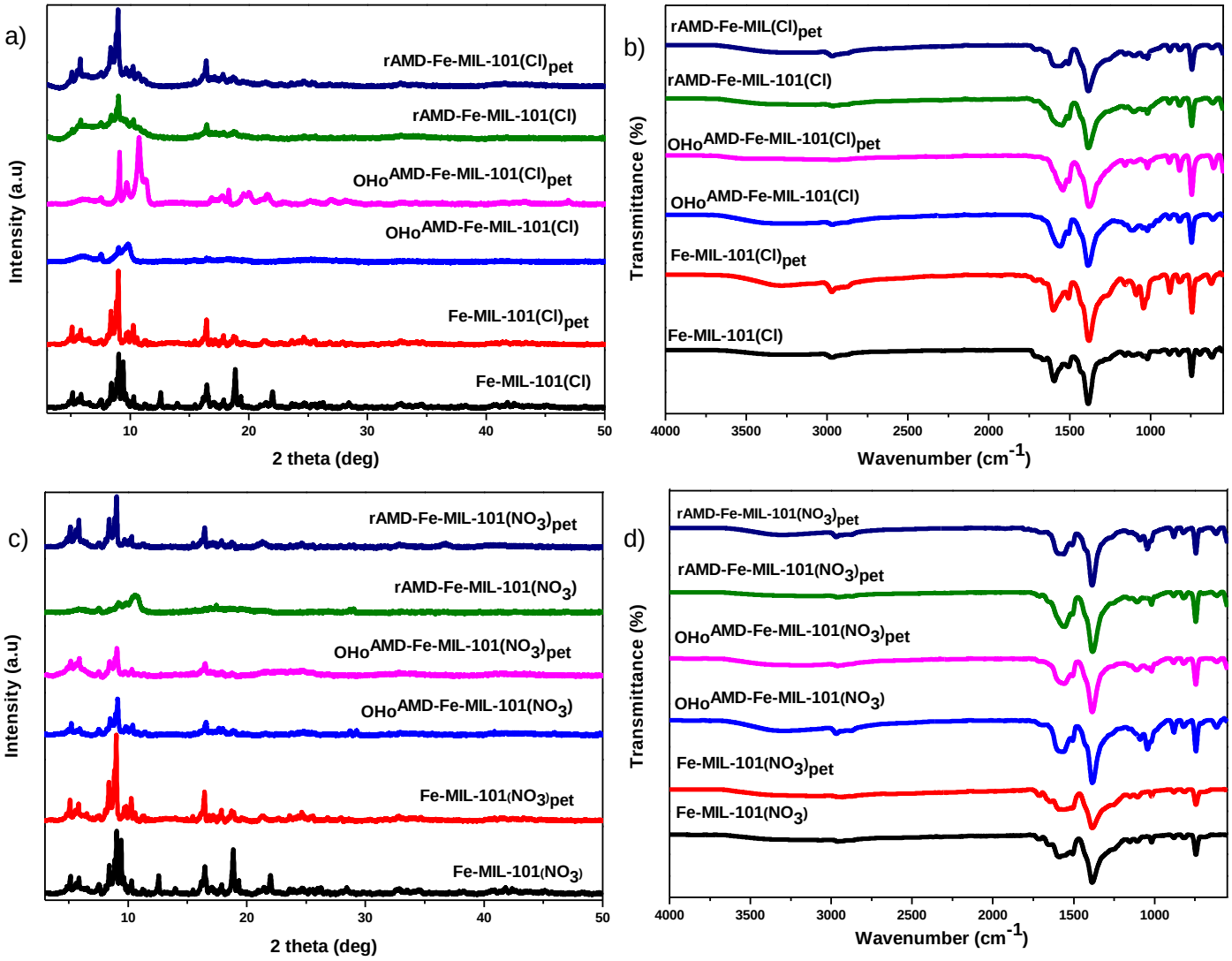

Figure 4: Showing XRD pattern and FTIR spectra for Fe-MIL-101 samples prepared using (a and b) Chloride (c and d) Nitrate precursors.

Morphological analysis of prepared MOFs

Fig. 5 presents SEM images for Fe-MIL-101 prepared from chloride (a and b) and nitrate (c and d) precursors. Samples prepared from the chloride precursors display an octahedral morphology except for $_{OHo}$AMD-Fe-MIL-101(Cl) (see supplemental data) which shows a bipyramidal hexagonal morphology and broken Fe-MIL-88B structures. This is due to a slow reaction within the reaction vessel caused by the HCl released in the system thus resulting in slow crystal growth and the formation of a thermodynamic phase, since MIL-101 and MIL-88B are topological framework isomers.[233] rAMD-Fe-MIL-101(Cl) and rAMD-Fe-MIL-101(Cl)$_{pet}$ were made up of mixed morphologies of Fe-MIL-101 and Fe-MIL-88B particles

(see Figure S5 and 6 in the supplemental data). The reaction synthesis for Fe-MIL-101 has been said to be a more sensitive reaction and any slight variations in any of the synthesis parameters can easily result in the formation of another MOF type.[234] Fe-MIL-53, Fe-MIL-101 and Fe-MIL-88B frameworks generally form as competing phases under certain reaction conditions.[235]

Fe-MIL-88B is the default structure that may be expected for connecting trigonal prisms and is the thermodynamic isomer, whereas Fe-MIL-101 is a kinetic isomer thus is likely to form where thermodynamic conditions are not favourable.

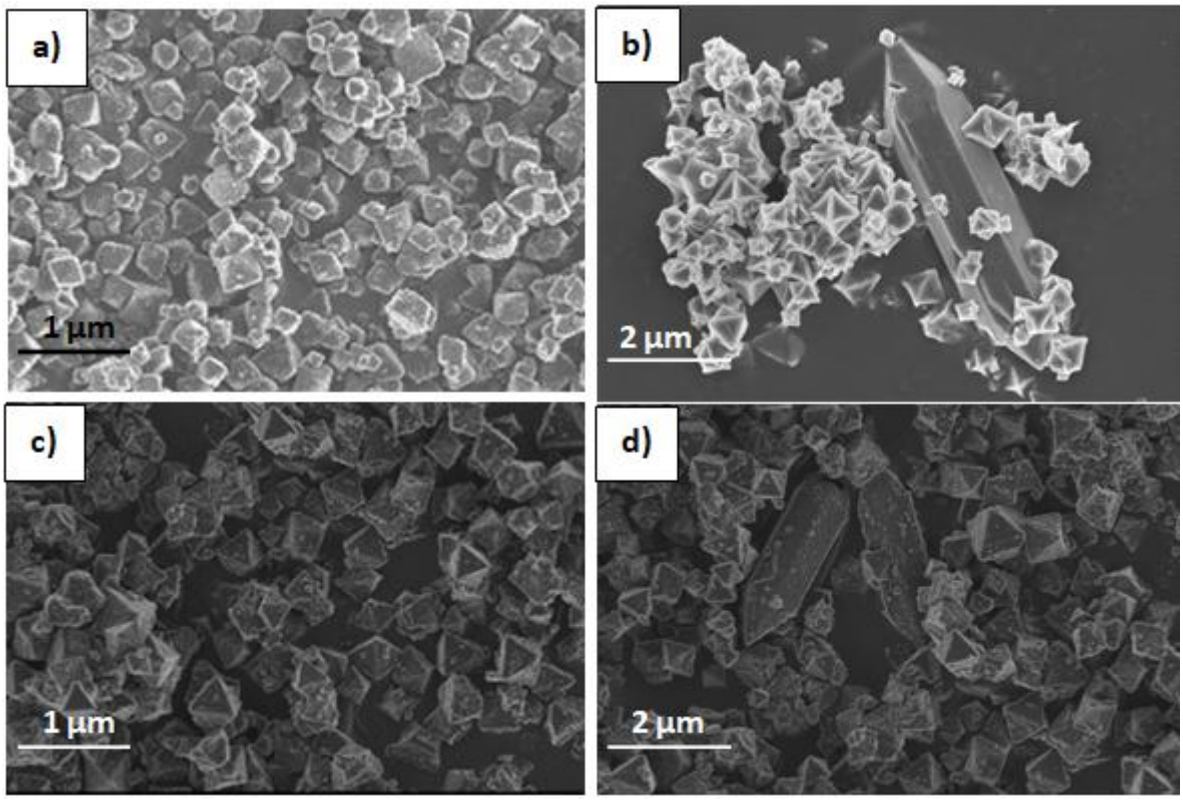

Figure 5: SEM images for Fe-MIL-101 MOFs where a) Fe-MIL-101(Cl)$_{pet}$ b) $_{OHo}$AMD-Fe-MIL-101(Cl) c) $_{OH}$oAMD-Fe-MIL-101(NO_3)$_{pet}$ d) rAMD-Fe-MIL-101(NO_3)$_{pet}$.

The commercial grade nitrate salt produced poorly crystalline solids of unknown phase (see supplemental data), this was expected as it had been reported in literature that for the synthesis of Fe-MIL-101 from the nitrate salt, the presence of a halogen is required otherwise a gel is formed. However, when rAMD-Fe and $_{OHo}$AMD-Fe were used in

replacement of the commercial grade Fe-nitrate salt (Fig. 5b-d), uniformly dispersed octahedral particles were obtained.

Thermal stability studies of obtained MOFs

In order to investigate the stability of synthesized Fe-MIL-101(Fe) MOFs, the thermal stability was assessed by thermogravimetric analysis (TGA). Figure 6a and b shows the TGA plots of the Fe-MIL-101 samples prepared from chloride and nitrate precursors, respectively. The analysis was carried out under N_2 atmosphere; a two-step weight loss was observed which is typical of the Fe-MIL-101 structures. The first weight loss within the region of ~30-200 °C shows about an 8% weight loss, which is due to the gradual loss of water molecule enclosed within the pores and bonded to the iron atoms as well as guest solvent molecules from the pores of Fe-MIL-101. The second weight loss in the region of 300 to 580 °C is ascribed to the breaking down of the Fe-MIL-101 and the decomposition of the carboxylate ligand.[133, 236]

All Fe-MOF samples exhibit good thermal stability and their structures are maintained up to 300 °C thereafter only metallic Fe is left as it cannot be further broken down. rAMD-Fe-MIL-101(Cl) and rAMD-Fe-MIL-101(Cl)$_{pet}$ display the highest thermal stabilities with lowest weight losses whilst Fe-MIL-101(Cl) and Fe-MIL-101(Cl)$_{pet}$ have the lowest thermal stabilities and the highest weight losses. This indicates that AMD derived Fe when dissolved in HCl yields high thermal stability MOFs compared to commercial Fe source, this may be due to the presence of both Fe^{2+} and Fe^{3+} whereas the latter consists of Fe^{3+}. $_{OHo}$AMD-Fe-MIL-101(Cl) and rAMD-Fe-MIL-101(Cl)$_{pet}$ display a three-step degradation and high thermal stabilities, commonly observed with Fe-MIL-88B (see Fig. 6a).

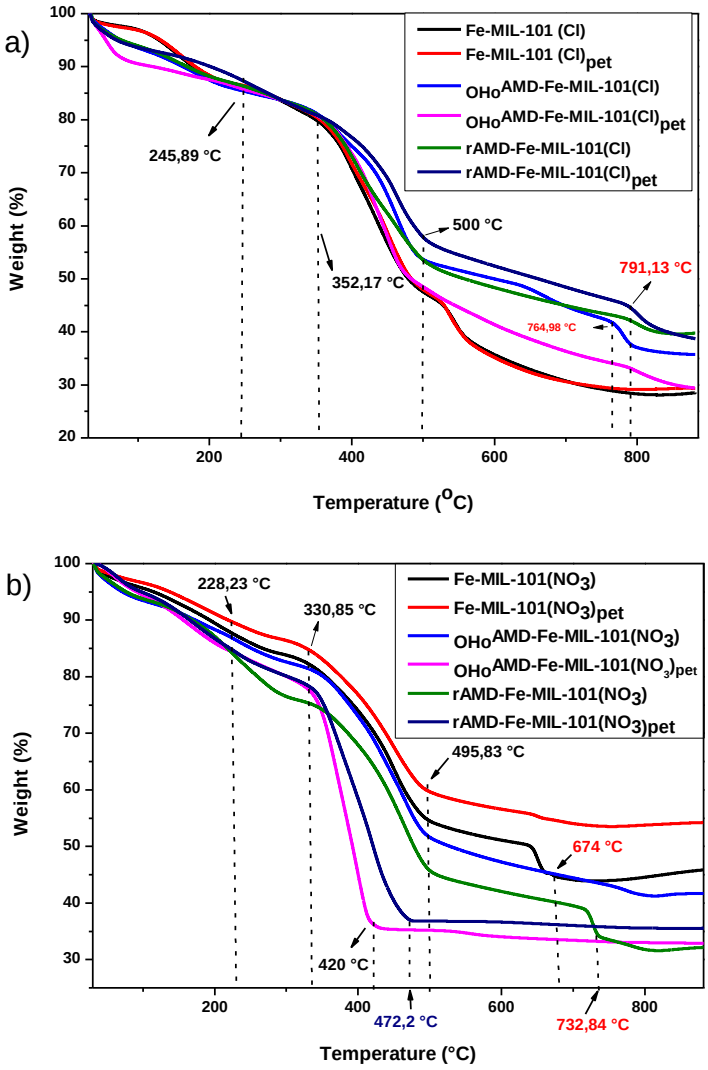

Figure 6: TGA profiles for the prepared Fe-MIL-101 samples using a) Chloride and b) Nitrate precursors.

This suggests that both these MOFs are not composed of pure Fe-MIL-101 phases and may consist of Fe-MIL-88B structures hence the observed deviation from the typical Fe-MIL-101 thermal properties. This is further confirmed by the SEM images in Figure 5b and d. The nitrate samples have weight losses not below 30%, $_{OHo}$AMD-Fe-MIL-101(NO_3)pet and rAMD-Fe-MIL-101(NO_3)pet have the highest losses and lower thermal stabilities compared to the rest of the nitrate profiles (397 and 419 °C, respectively).

Physical properties and hydrogen uptake measurements

Table 1 presents a summary of the BET surface areas and pore volumes obtained for the synthesized Fe-MIL-101, the synthesized materials displayed a type I N_2 isotherm (see supplemental data) that showed a hysteresis loop indicating presence of mesopores within the structure. This was further confirmed by the pore size distribution graphs (see supplemental data) which displayed the pores distribution within the micro- and mesoporous range (2-50 nm). Fe-MIL-101(Cl) and Fe-MIL-101 $(Cl)_{pet}$ had BET surface areas of 2052 and 501 m^2/g with pore volumes of 1.0 and 0.1904 cm^3/g. The huge difference in SA may be owed to the introduction of dye impurities into the MOF structure as well as BDC that could not be washed away, may have been deposited into the MOFs pores thus hindering the access of the N_2 gas during measurements.

Table 1: Summary table for BET surface areas and pore volumes obtained for MIL-101 samples.

MOF sample	BET surface area (m^2/g)	Pore volume (cm^3/g)
1. Fe-MIL-101(Cl)	2052	1.0013
2. Fe-MIL-101$(Cl)_{pet}$	501	0.1904
3. $_{OHo}$AMD-Fe-MIL-101$(Cl)_{pet}$	52.5	0.0623
4. $_{OHo}$-AMD-Fe-MIL-101(NO_3)	1104	0.6304
5. $_{OHo}$AMD-Fe-MIL-101$(NO_3)_{pet}$	565	0.3292
6. rAMD-Fe-MIL-101(NO_3)	701	0.4581
7. rAMD-Fe-MIL-101$(NO_3)_{pet}$	1179	0.7229

Surface areas for rAMD-Fe-MIL-101(NO_3), rAMD-Fe-MIL-101$(NO_3)_{pet}$, $_{OHo}$AMD-Fe-MIL-101(NO_3) and $_{OHo}$AMD-Fe-MIL-101$(NO_3)_{pet}$ were obtained as 701, 1179, 1104 and 565 m^2/g, respectively. BET surface areas obtained for the Fe-MIL-101 materials were much lower than what has been reported in literature (<3500 m^2/g)[237], this may be attributed to poor solvent exchange which ultimately led to poor activation of the MOFs. Solvent exchange in

the pores of the MOFs was carried out using ethanol at 60 °C for 3 hrs twice, though longer exchange times have been reported.[238] When commercial grade Fe source was replaced with rAMD-Fe and $_{OHo}$AMD-Fe dissolved in HCl, lower surface areas were expected due to the presence of Fe-MIL-88B particle (see supplementary data). SA measurements for rAMD-Fe-MIL-101(Cl), MIL-101-rAMD-Fe(Cl)$_{pet}$, and $_{OHo}$AMD-Fe-MIL-101(Cl) were not carried out due to poor XRD and SEM images indicating poor crystallinity and had mixed morphologies thus would not give conclusive results. Measurements for $_{OHo}$AMD-Fe-MIL-101(Cl)$_{pet}$, $_{OHo}$AMD-Fe-MIL-101(Cl)$_{pet}$ and $_{OHo}$AMD-Fe-MIL-101(NO_3)$_{pet}$ are reported in the supplemental data.

H_2 uptake analysis was conducted at a cryo-temperature (77K) to assess the adsorption properties of one of the Fe-MIL-101 synthesised materials. rAMD-Fe-MIL-101(NO_3)pet was selected since it had a superior surface area compared to all the other waste-derived Fe-based MIL-101 MOFs. Figure 7 presents the H_2 adsorption isotherm, the hydrogen uptake was fully reversible showing a typical IUPAC type I isotherm. The highest H_2 uptake value of 1.18 wt% at 1 bar and 77 K was obtained for this material. This is a relatively low value compared to those reported in literature for MOFs however, it is expected owing to the relatively low surface area obtained for this material. Latroche *et al*. reported MIL-101 surface areas of approximately 6000 m^2/g with the highest H_2 uptake of 6.1 wt%, which is comparable to the obtained value for this MOF considering that the surface area is ~3x less.[239]

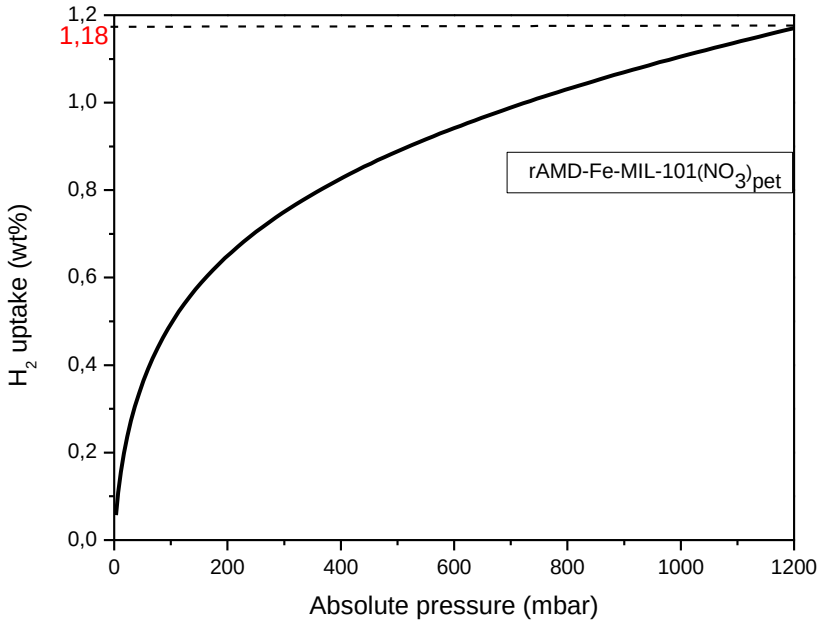

Figure 7: Hydrogen adsorption isotherms of rAMD-Fe-MIL-101$(NO_3)_{pet}$.

Porous materials with large pores usually have low hydrogen sorption capacity at low pressures since H_2 molecules in the centre of the void experience weak Van de Waal forces from pore walls.[240] It has been reported that MOFs with very high surface areas usually have low framework density therefore a compromise between the surface area and crystal density should be considered when pursuing porous MOFs with both high gravimetric and volumetric H_2 uptakes.[47, 241] Because the MOF H_2 uptake did not reach a point of saturation up to 1 bar, this means that conducting the analysis at higher pressures could result in higher H_2 uptakes capacities as more molecules are forced into the pores of the material.[242]

Conclusion

Fe-based MOFs were successfully synthesized from the waste precursors and displayed comparable textural and physical properties to the Fe-MOFs prepared from commercial grade precursors. This was supported by the XRD and FTIR that suggested the presence of a trinuclear metal centre and characteristic vibrations confirming the coordination of BDC to the Fe centre. Mixed MIL-101 and MIL-88B morphologies were observed with MOFs prepared by the dissolution of rAMD-Fe(Cl) and $_{OHo}$AMD-Fe(Cl), this resulted in decreased surface areas and pore volumes. Fe-MIL-101 prepared from rAMD-Fe(NO_3) and $_{OHo}$AMD-

$Fe(NO_3)$ displayed well dispersed octahedral morphologies with high degree of crystallinity and thermal stability superior to that of MOFs prepared from commercial grade precursors. The use of nitrate precursor for the synthesis of MIL-101(Fe) resulted in a material of unidentifiable morphology owing to the lack of a mineralizer usually added to aid the formation of the Fe-MIL-101 structure.

Fe-MIL-101 displayed relatively high H_2 storage capacities, comparable with the results previously reported by Ren *et al.* (0.99, 1.65 and 1.92 wt%) for Cr-MIL-101 MOFs.[148] Because of lower surface areas compared to the values reported (2000-6000 m^2),[243-244] the synthesized Fe-MIL-101 experienced lower H_2 adsorption. To enhance H_2 storage capacity in Fe-MIL-101, surface area and pore volume would first need to be optimized by supercritical activation as one of the methods. Another way of increasing H_2 uptake might be to composite Fe-MIL-101 with transition metals to create more active sites for the hydrogen molecule to adsorb.

The study has proved that it is possible to synthesize Fe-MIL-101 by following a holistic approach that utilizes two wastes. The study also revealed the limitations and weak points in using the waste materials for the synthesis of MOFs. Limitations such as mixed morphologies and lack of forming octahedral morphology when nitrate salt is used could be investigated in the future and the method could be adjusted to suit the synthesis of Fe-MIL-101 using these waste materials. Further studies would also elude into maximizing the surface area of the MOFs such that they match those of the commercial grade precursors for enhanced H_2 storage capacities.

Declaration

The authors would like to declare that there are no known competing financial interests or personal relationships that could have influenced this work in any way.

Acknowledgements

The authors would like to extend their sincere gratitude to the council for scientific and industrial research (CSIR), Future Leaders Africa Independent Research (FLAIR) grant and the University of Pretoria (UP) for the financial support and extending their resources such that this study was a success.

Appendix A. Supplementary data

Supplementary data to this article can be found online at https//www.

References

1. Ma, S.; Zhou, H.-C., Gas storage in porous metal–organic frameworks for clean energy applications. *Chemical Communications* **2010,** *46* (1), 44-53.

2. Cavenati, S.; Grande, C. A.; Rodrigues, A. E.; Kiener, C.; Müller, U., Metal Organic Framework Adsorbent for Biogas Upgrading. *Industrial & Engineering Chemistry Research* **2008,** *47* (16), 6333-6335.

3. Kriesten, M.; Vargas Schmitz, J.; Siegel, J.; Smith, C. E.; Kaspereit, M.; Hartmann, M., Shaping of Flexible Metal-Organic Frameworks: Combining Macroscopic Stability and Framework Flexibility. *European Journal of Inorganic Chemistry* **2019,** *2019* (43), 4700-4709.

4. Ren, J.; Dyosiba, X.; Musyoka, N. M.; Langmi, H. W.; North, B. C.; Mathe, M.; Onyango, M. S., Green synthesis of chromium-based metal-organic framework (Cr-MOF) from waste polyethylene terephthalate (PET) bottles for hydrogen storage applications. *International Journal of Hydrogen Energy* **2016,** *41* (40), 18141-18146.

5. Rambau, K. M.; Musyoka, N. M.; Panek, R.; Franus, W.; Wdowin, M.; Manyala, N., Preparation of coal fly ash derived metal organic frameworks and their carbon derivatives. *Materials Today Communications* **2021,** *27*, 102433.

6. Perez, E.; Andre, M.-L.; Navarro Amador, R.; Hyvrard, F.; Borrini, J.; Carboni, M.; Meyer, D., Recovery of metals from simulant spent lithium-ion battery as organophosphonate coordination polymers in aqueous media. *Journal of Hazardous Materials* **2016,** *317*, 617-621.

7. Perez, E.; Navarro Amador, R.; Carboni, M.; Meyer, D., In-situ precipitation of Metal–Organic Frameworks from a simulant battery waste solution. *Materials Letters* **2016,** *167*, 188-191.

8. Lagae Capelle, E.; Cognet, M.; Madhavi, S.; Carboni, M.; Meyer, D., Combining Organic and Inorganic Wastes to Form Metal–Organic Frameworks. *Materials* **2020,** *13*, 441.

9. Zhang, F.; Chen, S.; Nie, S.; Luo, J.; Lin, S.; Wang, Y.; Yang, H., Waste PET as a Reactant for Lanthanide MOF Synthesis and Application in Sensing of Picric Acid. *Polymers (Basel)* **2019,** *11* (12), 2015.

10. Huang, Y.-T.; Lai, Y.-L.; Lin, C.-H.; Wang, S.-L., Direct use of waste PET as unfailing source of organic reagents in the synthesis of intrinsic white/yellow luminescent nanoporous zincophosphates. *Green Chemistry* **2011,** *13* (8), 2000-2003.

11. El-Sayed, E.-S. M.; Yuan, D., Waste to MOFs: sustainable linker, metal, and solvent sources for value-added MOF synthesis and applications. *Green Chemistry* **2020,** *22* (13), 4082-4104.

12. Lo, S.-H.; Senthil Raja, D.; Chen, C.-W.; Kang, Y.-H.; Chen, J.-J.; Lin, C.-H., Waste polyethylene terephthalate (PET) materials as sustainable precursors for the synthesis of nanoporous MOFs, MIL-47, MIL-53(Cr, Al, Ga) and MIL-101(Cr). *Dalton Transactions* **2016,** *45* (23), 9565-9573.

13. Dyosiba, X.; Ren, J.; Musyoka, N. M.; Langmi, H. W.; Mathe, M.; Onyango, M. S., Preparation of value-added metal-organic frameworks (MOFs) using waste PET bottles as source of acid linker. *Sustainable Materials and Technologies* **2016,** *10*, 10-13.

14. Dyosiba, X.; Ren, J.; Musyoka, N. M.; Langmi, H. W.; Mathe, M.; Onyango, M. S., Feasibility of Varied Polyethylene Terephthalate Wastes as a Linker Source in Metal–Organic Framework UiO-66(Zr) Synthesis. *Industrial & Engineering Chemistry Research* **2019,** *58* (36), 17010-17016.

15. Deleu, W. P. R.; Stassen, I.; Jonckheere, D.; Ameloot, R.; De Vos, D. E., Waste PET (bottles) as a resource or substrate for MOF synthesis. *Journal of Materials Chemistry A* **2016,** *4* (24), 9519-9525.

16. Rambau, K.; Musyoka, N. M.; Palaniyandy, N.; Manyala, N., Manganese-Based Metal Organic Framework from Spent Li-Ion Batteries and its Electrochemical Performance as Anode Material in Li-ion Battery. *Journal of The Electrochemical Society* **2021,** *168* (1), 010527.

17. Johnson, D. B.; Hallberg, K. B., Acid mine drainage remediation options: a review. *Science of The Total Environment* **2005,** *338* (1), 3-14.

18. Das, P., Phytoremediation and Nanoremediation : Emerging Techniques for Treatment of Acid Mine Drainage Water. *Defence Life Science Journal* **2018,** *3*.

19. Mokgehle, T. M.; Tavengwa, N. T., Recent developments in materials used for the removal of metal ions from acid mine drainage. *Applied Water Science* **2021,** *11* (2), 42.

20. Norton, P. J., The control of acid mine drainage with Wetlands. *Mine Water and the Environment* **1992,** *11* (3), 27-34.

21. Masindi, V.; Tekere, M., Innovative Routes for Acid Mine Drainage (AMD) Valorization. 2020; pp 189-218.

22. Masindi, V.; Osman, M. S.; Shingwenyana, R., Valorization of acid mine drainage (AMD): A simplified approach to reclaim drinking water and synthesize valuable minerals – Pilot study. *Journal of Environmental Chemical Engineering* **2019,** *7* (3), 103082.

23. Nleya, Y.; Simate, G. S.; Ndlovu, S., Sustainability assessment of the recovery and utilisation of acid from acid mine drainage. *Journal of Cleaner Production* **2016,** *113*, 17-27.

24. Simate, G. S.; Ndlovu, S., Acid mine drainage: Challenges and opportunities. *Journal of Environmental Chemical Engineering* **2014,** *2* (3), 1785-1803.

25. Masindi, V.; Akinwekomi, V.; Maree, J. P.; Muedi, K. L., Comparison of mine water neutralisation efficiencies of different alkaline generating agents. *Journal of Environmental Chemical Engineering* **2017,** *5* (4), 3903-3913.

26. Flores, R. G.; Andersen, S. L. F.; Maia, L. K. K.; José, H. J.; Moreira, R. d. F. P. M., Recovery of iron oxides from acid mine drainage and their application as adsorbent or catalyst. *Journal of Environmental Management* **2012,** *111*, 53-60.

27. Seo, E. Y.; Cheong, Y. W.; Yim, G. J.; Min, K. W.; Geroni, J. N., Recovery of Fe, Al and Mn in acid coal mine drainage by sequential selective precipitation with control of pH. *CATENA* **2017,** *148*, 11-16.

28. Wei, X.; Viadero, R. C., Synthesis of magnetite nanoparticles with ferric iron recovered from acid mine drainage: Implications for environmental engineering. *Colloids and Surfaces A: Physicochemical and Engineering Aspects* **2007,** *294* (1), 280-286.

29. Wei, X.; Viadero, R. C.; Buzby, K. M., Recovery of Iron and Aluminum from Acid Mine Drainage by Selective Precipitation. *Environmental Engineering Science* **2005,** *22* (6), 745-755.

30. Du, P. D.; Thanh, H. T. M.; To, T. C.; Thang, H. S.; Tinh, M. X.; Tuyen, T. N.; Hoa, T. T.; Khieu, D. Q., Metal-Organic Framework MIL-101: Synthesis and Photocatalytic Degradation of Remazol Black B Dye. *Journal of Nanomaterials* **2019,** *2019*, 6061275.

31. Skobelev, I. Y.; Sorokin, A. B.; Kovalenko, K. A.; Fedin, V. P.; Kholdeeva, O. A., Solvent-free allylic oxidation of alkenes with O2 mediated by Fe- and Cr-MIL-101. *Journal of Catalysis* **2013,** *298*, 61-69.

32. Menezes, J. C. S. S.; Silva, R. A.; Arce, I. S.; Schneider, I. A. H., Production of a Poly-ferric Sulphate Chemical Coagulant by Selective Precipitation of Iron from Acidic Coal Mine Drainage. *Mine Water and the Environment* **2009,** *28* (4), 311.

33. Silva, R.; Menezes, J.; Lopes, F. c.; Kirchheim, A.; Schneider, I., Synthesis of a Goethite Pigment by Selective Precipitation of Iron from Acidic Coal Mine Drainage. *Mine Water and the Environment* **2017**.

34. Akinwekomi, V.; Maree, J. P.; Masindi, V.; Zvinowanda, C.; Osman, M. S.; Foteinis, S.; Mpenyana-Monyatsi, L.; Chatzisymeon, E., Beneficiation of acid mine drainage (AMD): A viable option for the synthesis of goethite, hematite, magnetite, and gypsum – Gearing towards a circular economy concept. *Minerals Engineering* **2020,** *148*, 106204.

35. Yoshioka, T.; Ota, M.; Okuwaki, A., Conversion of a Used Poly(ethylene terephthalate) Bottle into Oxalic Acid and Terephthalic Acid by Oxygen Oxidation in Alkaline Solutions at Elevated Temperatures. *Industrial & Engineering Chemistry Research* **2003,** *42* (4), 675-679.

36. Wang, H.; Kojtari, A.; Xu, X.; Ji, H.-F., Self-Assembled Microwires of Terephthalic Acid and Melamine. *Crystals* **2017,** *7* (8).

37. Singh, S.; Sharma, S.; Umar, A.; Mehta, S. K.; Bhatti, M. S.; Kansal, S. K., Recycling of Waste Poly(ethylene terephthalate) Bottles by Alkaline Hydrolysis and Recovery of Pure Nanospindle-Shaped Terephthalic Acid. *J Nanosci Nanotechnol* **2018,** *18* (8), 5804-5809.

38. Ravichandran, S. A.; Rajan, V. P.; Aravind, P. V.; Seenivasan, A.; Prakash, D. G.; Ramakrishnan, K., Characterization of Terephthalic Acid Monomer Recycled from Post-Consumer PET Polymer Bottles. *Macromolecular Symposia* **2016,** *361* (1), 30-33.

39. Li, X.; Guo, W.; Liu, Z.; Wang, R.; Liu, H., Fe-based MOFs for efficient adsorption and degradation of acid orange 7 in aqueous solution via persulfate activation. *Applied Surface Science* **2016,** *369*, 130-136.

40. Pham, H.; Ramos, K.; Sua, A.; Acuna, J.; Slowinska, K.; Nguyen, T.; Bui, A.; Weber, M. D. R.; Tian, F., Tuning Crystal Structures of Iron-Based Metal–Organic Frameworks for Drug Delivery Applications. *ACS Omega* **2020,** *5* (7), 3418-3427.

41. Tamames-Tabar, C.; Cunha, D.; Imbuluzqueta, E.; Ragon, F.; Serre, C.; Blanco-Prieto, M. J.; Horcajada, P., Cytotoxicity of nanoscaled metal–organic frameworks. *Journal of Materials Chemistry B* **2014,** *2* (3), 262-271.

42. Horcajada, P.; Salles, F.; Wuttke, S.; Devic, T.; Heurtaux, D.; Maurin, G.; Vimont, A.; Daturi, M.; David, O.; Magnier, E.; Stock, N.; Filinchuk, Y.; Popov, D.; Riekel, C.; Férey, G.; Serre, C., How Linker's Modification Controls Swelling Properties of Highly Flexible Iron(III) Dicarboxylates MIL-88. *Journal of the American Chemical Society* **2011,** *133* (44), 17839-17847.

43. Wang, Y.; Muramatsu, A.; Sugimoto, T., FTIR analysis of well-defined α-Fe2O3 particles. *Colloids and Surfaces A: Physicochemical and Engineering Aspects* **1998,** *134* (3), 281-297.

44. Liu, Z.; He, W.; Zhang, Q.; Shapour, H.; Bakhtari, M. F., Preparation of a GO/MIL-101(Fe) Composite for the Removal of Methyl Orange from Aqueous Solution. *ACS Omega* **2021,** *6* (7), 4597-4608.

45. Hamedi, A.; Trotta, F.; Borhani Zarandi, M.; Zanetti, M.; Caldera, F.; Anceschi, A.; Nateghi, M. R., In Situ Synthesis of MIL-100(Fe) at the Surface of Fe3O4@AC as Highly Efficient Dye Adsorbing Nanocomposite. *International Journal of Molecular Sciences* **2019,** *20* (22).

46. Carson, F.; Su, J.; Platero-Prats, A. E.; Wan, W.; Yun, Y.; Samain, L.; Zou, X., Framework Isomerism in Vanadium Metal–Organic Frameworks: MIL-88B(V) and MIL-101(V). *Crystal Growth & Design* **2013,** *13* (11), 5036-5044.

47. Zorainy, M. Y.; Gar Alalm, M.; Kaliaguine, S.; Boffito, D. C., Revisiting the MIL-101 metal–organic framework: design, synthesis, modifications, advances, and recent applications. *Journal of Materials Chemistry A* **2021,** *9* (39), 22159-22217.

48. Wu, W.; Decker, G. E.; Weaver, A. E.; Arnoff, A. I.; Bloch, E. D.; Rosenthal, J., Facile and Rapid Room-Temperature Electrosynthesis and Controlled Surface Growth of Fe-MIL-101 and Fe-MIL-101-NH2. *ACS Central Science* **2021,** *7* (8), 1427-1433.

49. Flak, D.; Chen, Q.; Mun, B. S.; Liu, Z.; Rękas, M.; Braun, A., In situ ambient pressure XPS observation of surface chemistry and electronic structure of α-Fe2O3 and γ-Fe2O3 nanoparticles. *Applied Surface Science* **2018,** *455*, 1019-1028.

50. Yamashita, T.; Hayes, P., Analysis of XPS spectra of Fe2+ and Fe3+ ions in oxide materials. *Applied Surface Science* **2008,** *254* (8), 2441-2449.

51. Zango, Z. U.; Jumbri, K.; Sambudi, N. S.; Hanif Abu Bakar, N. H.; Fathihah Abdullah, N. A.; Basheer, C.; Saad, B., Removal of anthracene in water by MIL-88(Fe), NH2-MIL-88(Fe), and mixed-MIL-88(Fe) metal–organic frameworks. *RSC Advances* **2019,** *9* (71), 41490-41501.

52. Sui, H.; Li, L.; Zhu, X.; Chen, D.; Wu, G., Modeling the adsorption of PAH mixture in silica nanopores by molecular dynamic simulation combined with machine learning. *Chemosphere* **2016,** *144*, 1950-1959.

53. Hornback, J. M., *Organic Chemistry*. Cengage Learning: 2005.

54. Tang, J.; Yang, M.; Yang, M.; Wang, J.; Dong, W.; Wang, G., Heterogeneous Fe-MIL-101 catalysts for efficient one-pot four-component coupling synthesis of highly substituted pyrroles. *New Journal of Chemistry* **2015,** *39* (6), 4919-4923.

55. Otun, K. O., Temperature-controlled activation and characterization of iron-based metal-organic frameworks. *Inorganica Chimica Acta* **2020,** *507*, 119563.

56. Férey, G.; Mellot-Draznieks, C.; Serre, C.; Millange, F.; Dutour, J.; Surblé, S.; Margiolaki, I., A Chromium Terephthalate-Based Solid with Unusually Large Pore Volumes and Surface Area. *Science* **2005,** *309* (5743), 2040-2042.

57. Karimi Alavijeh, R.; Akhbari, K., Biocompatible MIL-101(Fe) as a Smart Carrier with High Loading Potential and Sustained Release of Curcumin. *Inorganic Chemistry* **2020,** *59* (6), 3570-3578.

58. Latroche, M.; Surblé, S.; Serre, C.; Mellot-Draznieks, C.; Llewellyn, P. L.; Lee, J.-H.; Chang, J.-S.; Jhung, S. H.; Férey, G., Hydrogen Storage in the Giant-Pore Metal–Organic Frameworks MIL-100 and MIL-101. *Angewandte Chemie International Edition* **2006,** *45* (48), 8227-8231.

59. Li, H.; Wang, K.; Sun, Y.; Lollar, C. T.; Li, J.; Zhou, H.-C., Recent advances in gas storage and separation using metal–organic frameworks. *Materials Today* **2018,** *21* (2), 108-121.

60. MacGillivray, L. R., *Metal-organic frameworks: design and application*. John Wiley & Sons: 2010.

61. Musyoka, N. M.; Ren, J.; Annamalai, P.; Langmi, H. W.; North, B. C.; Mathe, M. K.; Cesar, D., Synthesis of a hybrid MIL-101(Cr)/ZTC composite for hydrogen storage applications. 2016.

62. Ren, J.; Musyoka, N. M.; Langmi, H. W.; Segakweng, T.; North, B. C.; Mathe, M.; Kang, X., Modulated synthesis of chromium-based metal-organic framework (MIL-101) with enhanced hydrogen uptake. *International Journal of Hydrogen Energy* **2014,** *39* (23), 12018-12023.

63. Lupu, D.; Ardelean, O.; Blanita, G.; Borodi, G.; Lazar, M. D.; Biris, A. R.; Ioan, C.; Mihet, M.; Misan, I.; Popeneciu, G., Synthesis and hydrogen adsorption properties of a new

iron based porous metal-organic framework. *International Journal of Hydrogen Energy* **2011,** *36* (5), 3586-3592.

64. Rallapalli, P. B. S.; Raj, M. C.; Senthilkumar, S.; Somani, R. S.; Bajaj, H. C., HF-free synthesis of MIL-101(Cr) and its hydrogen adsorption studies. *Environmental Progress & Sustainable Energy* **2016,** *35* (2), 461-468.

4.2 Chapter summary

Fe-MIL-101 were successfully synthesized using PET waste derived BDC and AMD derived Fe. Results obtained from these MOFs were compared with MOFs prepared from commercial precursors thus revealing that waste precursors do not compromise the integrity of the resultant MOF. However, the synthesis and activation methods proved ineffective as mixed morphologies and decreased surface areas were obtained with MOFs from complete waste. The replacement of one precursor with a waste precursor however, did not have severe effects on the morphology and textural properties of the MOFs. H2 adsorption proved viable as a comparable uptake was obtained when the experiment was carried out on rAMD-Fe-MIL-101$(NO_3)_{pet}$, a material prepared from complete waste (rAMD-Fe and PET-BDC) using HNO_3 to dissolve the Fe-precipitate.

Chapter 5

5. Results and discussion: Fe-MIL-88B

5.1 Chapter outline

In this chapter, results of the AMD, Fe precipitates and Fe-MIL-88B materials are discussed in detail. This chapter explicitly discusses elemental composition of AMD water, structural properties of PET-derived BDC and Fe precipitates as well as elemental composition of the latter. Results for Fe-MIL-88B MOFs from commercial, partial and absolute waste precursors are also discussed for textural, structural, morphology and H_2 uptake.

The use of complete waste-derived metal and organic ligand precursors for the holistic synthesis of MIL-88B(Fe) via the solvothermal route

Nqobile Mthembu[a,b], Xoliswa Dyosiba[a], Henrietta Langmi[b], Nicholas Musyoka[a*]

[a] Centre for Nanostructures and Advanced Materials (CeNAM), Chemicals Cluster, Council for Scientific and Industrial Research (CSIR), Pretoria, South Africa.

[b] Department of chemistry, university of Pretoria, Hatfield, 0002

**Corresponding author. Tel: +27 128414806. Email: NMusyoka@csir.co.za*

Abstract

The high cost associated with the synthesis processes of metal-organic frameworks has hindered their industrialization regardless of their potential use in a wide range of applications. The use of lower-grade materials as starting compounds for the production of MOF introduces a cost-effective and greener method that could allow for larger scale production of these porous materials. In this work, the synthesis of Fe-MIL-88B using AMD wastewater as the source for the Iron (Fe) metal as well as BDC derived from waste PET was achieved. Two extraction methods are explored thus yielding Fe of different phases/species. The synthesis procedure follows a widely reported solvothermal route and the waste-derived MOFs are compared to MOFs synthesized from commercial precursors. Waste

derived MOFs displayed similar morphologies, crystal phases as well as vibrations and stretching bands when compared to those prepared from commercial precursors. All MOFs showed a type I N_2 isotherm however, waste-derived MOFs had enhanced surface areas compared to MOFs prepared from commercial grade precursors that consisted of surface areas below 100 m^2/g. The pore size distribution were mostly seen in the micro porous range with some in the mesoporous range. The use of AMD as a source for Fe yielded MOFs with high thermal stabilities above 600 °C, elemental analysis revealed sulphur as an impurity in MOFs prepared from NaOH precipitated Fe ($_{OHo}$AMD-Fe). Hydrogen adsorption studies conducted at 77 K and 1 bar showed that waste derived Fe-MIL-88B MOFs were good candidates since a value of 0.81 wt% found to be consistent with the previously reported data for M-MIL-88B MOFs to date.

Key words: Metal-organic frameworks, Acid mine drainage, polyethylene terephthalate, Benzyl dicarboxylic acid (BDC), Fe-MIL-88B.

Introduction

The implementation of non-expensive approaches for the synthesis of MOFs has proved to be of great focus as it would see the industrial production of MOFs for a wide range of applications. The recycling of waste for valuable reuse is one way that researchers have opted for that serves as a double impact where the costs associated with MOF synthesis production are greatly reduced and harmful substance/materials are removed from the face of the earth. MOFs are a fairly new class of porous materials constructed from the coordination of metal clusters and organic linkers known for their high surface areas and pore volume.[245-246] The choice of linker allows for functionalization and tuneability to suit a specific application.[247-248] Materials Institute Lavoisier (MIL) MOFs are porous metal carboxylate salts composed of different trivalent metal cations (such as Cr, Al and Fe) and carboxylic acid ligands consisting of large pores and high-permanent porosity. MILs have been synthesized from nontoxic endogenous cations (such as Ca, Mg, Fe, and Zn) and ligands consisting of naturally occurring derivatives or biomolecules. These usually give rise to nontoxic and biologically and environmentally compatible MOFs, suitable for medical applications as well as for clean energy and environmental protection.

Fe-MOFs such as MIL-53, MIL-88, MIL-100 and MIL-101 are the most common and widely explored.[249] MIL-88B forms through a heterogeneous nucleation and exhibits a three-dimensional cage structure (hexagonal symmetry) with an **acs** topology.[107] Apart from being recognized as having a non-toxic nature, MIL-88B has a highly flexible framework, commonly referred to as the 'breathing' effect. The structural flexibility of MIL-88B makes them great candidates for use in various applications such as drug delivery as well as gas separation and storage. Serre *et. al* studied the 'breathing' effect of MIL-88 structures in different solvents which showed that MIL-88 structures are highly selective adsorbents, and the selectivity is strongly dependent on the nature of the organic linker.[122] Horcajada *et. al* further studied the effect of linker modification to the swelling of the MIL-88B and MIL-88D which revealed that the swelling behaviour of these MOFs was drastically affected by steric hinderance and the number of groups per aromatic ring thus leading either to permanent porosity or amplified swelling behaviour.[123]

Recent research has been focused on the use of PET-derived BDC as an organic linker for the synthesis of MOFs. The innovative use of recycled waste PET for MOF synthesis has proven to have no effect on the integrity and structural properties of the MOFs. Valuable reuse of waste PET would contribute to a suitable route for eliminating waste PET landfilling, decrease overall consumption of crude oil, and maintain the chemical value of polyester while creating a high-value end-use market for PET wastes.[166] Five nano porous trivalent MOFs were synthesized by Sheng-Han Lo and co-workers (2016) using PET-derived BDC as an organic linker instead of commercial terephthalic acid, all the characterization techniques strongly supported that the synthesized MOFs using PET are similar to their literature reports.[168] Similar studies were carried out by W. Deleu (2016) where MIL-53(Al) and MIL-47(V) were synthesized and J. Ren *et. al* (2016) studied the synthesis of Cr-based MOF, both studies looked at the synthesis of MOFs using PET-derived BDC as an organic linker as opposed to the commercial grade. The results were similar to those previously obtained in literature from commercial grade precursors and the Cr-MOF displayed superior textural and hydrogen storage properties.[166, 169] Dyosiba *et. al* (2019) focused on the use of various types of PET wastes as sources of BDC linker for the synthesis of the zirconium-based MOF, UiO-66(Zr). As expected, textural properties of the waste PET-derived UiO-66(Zr) MOFs were comparable to those of the MOFs derived from commercial BDC however, lower BET surface

areas were observed for MOFs synthesized from coloured PET waste bottles owing to the presence of organic dyes that then reside in the pores of the MOFs.[159] Eléonore Lagae-Capelle and co-workers (2020) reported the combination of PET-derived BDC with Al recovered from Li-ion batteries, a MIL-53 prepared had very similar properties to the material formed with high purity chemical compounds.[41]

Acid mine drainage serves as a potential alternative for the extraction of metals to be utilized in the synthesis of MOFs whilst abating pollution and lessening the expenses associated with MOF synthesis. AMD is a resultant of the natural oxidation of mine waste typically with low pH and high contents of iron metal and a portion of other metals which has adverse effects on the aquatic life and quality of water.[38] Many types of treatment to contain the damage to the environment are currently used worldwide, however operational costs are high and not effective[39-40] hence the need for an alternative approach to recover the dissolved metals for valuable reuse without further compromising the quality of the AMD wastewater. The synthesis of MOFs using the iron metal recycled from the AMD would greatly decrease the production costs of MOFs and eliminate mining waste therefore allowing for environmental and biological sustainability. According to our knowledge, the use of metals extracted from the AMD for MOF synthesis has not yet been reported. In this Article, we looked at the synthesis of MIL-88B from AMD-derived Fe using two different methods, and then combined with PET-derived BDC as an organic linker. These materials were then assessed for textural and physical properties in comparison to MIL-88B prepared from the commercial precursors.

Experimental

Materials and reagents

Iron (III) chloride hexahydrate ($FeCl_3 \cdot 6H_2O$), Sigma Aldrich, 97%), Iron (III) nonahydrate ($Fe(NO_3)_3 \cdot 9H_2O$, Sigma Aldrich, 98%), Terephthalic acid (1,4-BDC, Sigma Aldrich, 98%), ethylene glycol ($HOCH_2$-CH_2OH, Sigma Aldrich, 99.8%), *N,N*-dimethylformamide (DMF, Sigma Aldrich, 99.8%), hydrogen peroxide (H_2O_2, 50%), Sodium hydroxide (NaOH pellets, Sigma Aldrich), Glacial acetic acid (CH_3COOH, Sigma Aldrich, 60%), Ethanol (CH_3CH_2OH) and de-ionized water with no further purification. AMD water was collected in mines around the

Gauteng and PET coloured waste bottles were collected in household waste areas in the Gauteng region as well.

PET depolymerization

PET depolymerization was carried out using a procedure previously reported by Dyosiba *et al.* and J. Ren *et al*.[159, 166] The experiment was carried out in a 5000 ml Teflon-lined high-pressure reactor, in which 125 g of PET flakes were added along with 125 ml of ethylene glycol (EG) and 3000 ml of H_2O. The mixture was then gradually heated to 210 °C and maintained for 8 h. One completion, the final product was centrifuged, washed twice with ethanol, and dried at 100 °C for 24 hours. The PET-derived BDC was further used as a precursor in the synthesis of Fe-MOFs.

Fe extraction from AMD

Fe was precipitated by leaving AMD in open air at room temperature resulting in the oxidation of Fe^{2+} to Fe^{3+}. The resultant precipitate was then filtered under vacuum, washed thoroughly with deionized water, and then dried under vacuum and dried overnight at a temperature of 100 °C.[190-191] The resultant product was grounded to fine powder and labelled rAMD-Fe which was then used for the synthesis of MOFs. On the second method, Fe was precipitated out by first oxidizing with 30 % H_2O_2 and then 4M NaOH added, as outlined by Seo *et al.*[185] The resultant precipitate was treated as in the first method and labelled $_{OH}$AMD-Fe.[219]

Fe-MIL-88B synthesis

Fe-MIL-88B MOFs were synthesized using a procedure previously reported by Xu et al., (2016). In a typical procedure, 9.06 mmol of the metal source ($FeCl_3{\cdot}6H_2O$ or $Fe(NO_3)_3{\cdot}9H_2O$), 9.06 mmol of the organic linker (H_2BDC or PET-BDC), 0.30 g of NaOH and 4.47 mL of CH_3COOH were all dissolved in 50 ml DMF. The mixture was heated at 110 ^{o} C for 20 h using a teflon-lined stainless-steel bomb in a static oven. The resultant brown-red precipitate was separated from the solvent via centrifugation followed by washing with DMF and hot ethanol (3 h) twice.[193] The product was finally dried at 80 ^{o} C under vacuum

overnight. MOFs prepared from commercial Fe and commercial grade BDC were labelled as Fe-MIL-88B(Cl) and Fe-MIL88B(NO_3) whereas those prepared from PET-derived BDC were labelled Fe-MIL-88B$(Cl)_{pet}$ and MIL-88B$(NO_3)_{pet}$.

The synthesis of Fe-MIL-88B from rAMD-Fe and $_{OHo}$AMD-Fe followed a similar procedure as with the commercial Fe sources. However, 9.06 mmol of rAMD-Fe or $_{OH}$AMD-Fe was dissolved in in a stoichiometric amount of HCl or HNO_3 with heating at low temperatures (~60 °C) prior to mixing with a solution of terephthalic acid dissolved in DMF. The MOFs synthesized by the dissolution of the precipitates in HCl were labelled as rAMD-Fe-MIL-88B(Cl), rAMD-Fe-MIL-88B$(Cl)_{pet}$, $_{OHo}$AMD-Fe-MIL-88B(Cl) and $_{OHo}$AMD-Fe-MIL-88B- $(Cl)_{pet}$. Samples prepared from precipitates digested in HNO_3 were labelled as rAMD-Fe-MIL-88B(NO_3), rAMD-Fe-MIL-101$(NO_3)_{pet}$, $_{OHo}$AMD-Fe-MIL-88B(NO_3) and $_{OHo}$AMD-Fe-MIL-88B$(NO_3)_{pet}$.

Characterization

Raw AMD samples as well those samples derived from AMD after the extraction of Fe were measured for pH prior to the extraction of Fe at pH 3.5, the pH meter was first calibrated at pH 4 and 7 using standard solutions. To determine elemental content in the AMD samples, ICP-OES analysis was conducted using a PerkinElmer, optima 2100 DV instrument. Thermogravimetric analysis (TGA) was used to determine thermal stabilities of the Fe-MIL-88B using a Mettler, Toledo, TGA/SDTA 851e instrument. The analysis procedure involved weighing of the Fe-MIL-88B sample (10 mg) into a pan and then gradually heating to a temperature of 1000 °C (10 °C min^{-1}) under air flow at 10 mL/min. PerkinElmer Spectrum 100 Fourier transform infrared (FTIR) spectrometer, set to a range of 4000 to 550 cm^{-1} wavenumbers, 32 scans and a resolution of 16 cm^{-1}, was used to generate IR spectra of the materials. Prior to measurements, background was scanned to eliminate any noise or interferences. Measurements for BET surface areas and pore volumes of Fe-MIL-88B MOFs were carried out on the ASAP 2020 HD analyzer (Micromeritics) using N_2 as the adsorption gas at 77K. N_2 isotherms were obtained and then used to determine the BET surface areas. H_2 adsorption capacities were also measured on the same instrument at 77K and 1 bar. Samples (0.2-0.3 g) were first heated to 200 °C under vacuum for the removal of trapped

solvent molecules within the pores of the materials prior to analysis. isotherms were obtained using ultra-high purity grade (99.999%) gas. A PANalytical X'Pert Pro powder diffractometer operating on a Pixcel detector with a Ni-filtered Cu-Ka radiation (0.154 nm) was operated at ambient conditions to obtain X-ray diffraction (XRD) patterns at 2θ=3-90°, and a scanning rate of $0.1°s^{-1}$. SEM images were obtained with an Auriga Cobra Focused-Ion Beam Scanning Electron Microscope (FIB-SEM). Sample preparation entailed mounting samples on a carbon tape and then coated with carbon under vacuum to ensure no electrostatic charging scanning of the beam. A Thermo ESCAlab 250Xi Spectrometer with X-rays of monochromatic Al kα (1486.7 eV) was used to conduct high resolution X-ray photoelectron spectroscopy (XPS) analysis. The X-ray power was set at 300 W with a spot size of 900 µm to obtain survey spectra which were then examined at 100 eV, high resolution of 20 eV and pressure at 10^{-8} mbar.

Results and discussions

Elemental composition of AMD

ICP-OES revealed that the elements present in the raw AMD samples (as shown in table 1) samples were mainly iron (Fe), aluminum (Al), manganese (Mn), magnesium (Mg), calcium (Ca), silicon (Si) and sodium (Na). Raw AMD consisted of a high Fe content of 1251 mg/L with an initial pH of 1.92. Raising the pH to 3.5 ± 0.1 with and without the use of an oxidant, dissolved Fe was found to be 26 and 27 mg/L, respectively. A recovery of ~98% was achieved for both samples (with and without the oxidant), similar results to those reported by Wei *et. al* (2005) when a selective precipitation method was used for the recovery of Al and Fe.[218] At pH 3.5, the concentration of sodium increased significantly to concentrations of 1784 and 1783 mg/L with and without the use of an oxidant, respectively. This sharp increase of Na from a concentration of 29 mg/L is owing to the addition of NaOH solution for the precipitation of $Fe(OH)_3$. Contents of Al, Mn, Mg and Ca had negligible changes by either a slight decrease or increase which could have been an instrumental error. Si however, showed a consisted decrease in concentration on both AMD sample from which Fe had been precipitated out (with and without oxidant). The decrease in Si from a

concentration of 76 to 25 and 26 mg/L after the extraction of Fe with and without the oxidant, respectively, is an indication of Si co-precipitating out with Fe hydroxide. This implies that AMD-derived Fe hydroxide is not in the purest state.

Table 1: Concentration levels in AMD treated differently for the extraction of Fe.

Sample description	elements						
	Fe (mg/L)	**Al**	**Si**	**Mn**	**Mg**	**Ca**	**Na**
Raw AMD	1251	259	76	56	236	314	29
AMD With H_2O_2	26	266	25	52	224	318	1784
AMD Without H_2O_2	27	275	26	49	237	335	1783

Elemental and chemical composition of AMD-Fe precipitates

XPS survey spectra (Fig. 1a and b) revealed that the materials were mainly constituted by Fe and oxygen (O) whilst low amounts of S and C were detected, rAMD-Fe spectra however, also showed the presence of trace amounts of nitrogen (N) compounds. XPS spectra (Fig. 2a and b) for Fe 2p displayed characteristic peaks of Fe $2p_{3/2}$ and Fe $2p_{1/2}$ at 712 and 725.8 eV, respectively. Spectra for rAMD-Fe and $_{OHo}$-AMD-Fe revealed the presence of diamagnetic and paramagnetic peaks as well as satellite peaks at 720.2 and 71.8 eV, respectively. The presence of the satellite peak between the two Fe 2p3 peaks is an indication that the AMD-Fe precipitates are mainly composed of Fe^{3+}. The satellite peaks at 735 eV on both spectras however, are assigned to the electron-deficient Fe^{2+} sites created by the breaking of Fe-S bonds, thus suggesting the presence of $FeSO_4$. This explains why the ICP-OES never picked up any S concentrations since most of it had already precipitated out during the precipitation of Fe and may further confirm the findings from the XRD and FTIR regarding the presence of magnetite.[222-223]

The O1s spectra (Fig. 1c and d) showed characteristic peaks for oxygen (O) at 530.5, 532 and 533.4 eV for $_{OHo}$AMD-Fe. The O1s spectra for rAMD-Fe had characteristic peaks at 530.3, 531.8 and 533.7 eV. Peaks with the lowest binding energy in both O1s spectra (530.5 and

530.3 eV) were identified as lattice O attached to the Fe such that Fe-O bond exists. The hydroxide (OH), C-O and sulfate (SO_4^{2-}) peaks were identified as peaks appearing at 532 and 531.8 eV for rAMD-Fe and $_{OHo}$AMD-Fe, respectively, these peaks had the highest intensity and small area under the gaussian curve. Lastly, were the peaks that appears at the highest binding energy assigned to carbonyl groups (C=O).

C1s and S 2p3 spectra are shown in fig. S2a-d, further confirming the presence of organic and sulfur-containing compounds as suggested by the Fe2p3 and O1s spectra. C1s spectra shows the presence of four types of C-bonding at 282.9, 284.4, 287.6 and 289.2 eV binding energies. The peak at the lowest (282.9 eV) and highest (289.2 eV) binding energies observed on the $_{OHo}$AMD-Fe C1s spectra are assigned to the alkane bond (C-C) consisting of the highest number of electrons ejected and the ester bond (O-C=O) with the lowest number of electrons ejected off the surface of the sample. With rAMD-Fe however, the C-C and O-C=O bonds displayed equal peak height meaning the sample consisted of the same number of electrons. The C-O and C=O bonds were respectively assigned to the peaks appearing at 284.4 and 287.6 eV, for both Fe precipitates.

The presence of sulphur (S) was confirmed by the existence of a peak at 168 eV for both AMD-Fe samples and said to be present in the sulphate (SO_4^{2-}) or sulfone (R_2SO_2) form. The SO_4^{2-} is present as the FeSO4 as suggested by the Fe2p scan, also the presence of the sulfone compound also affirms the presence of organic groups as suggested by the C1s and O1s spectra.

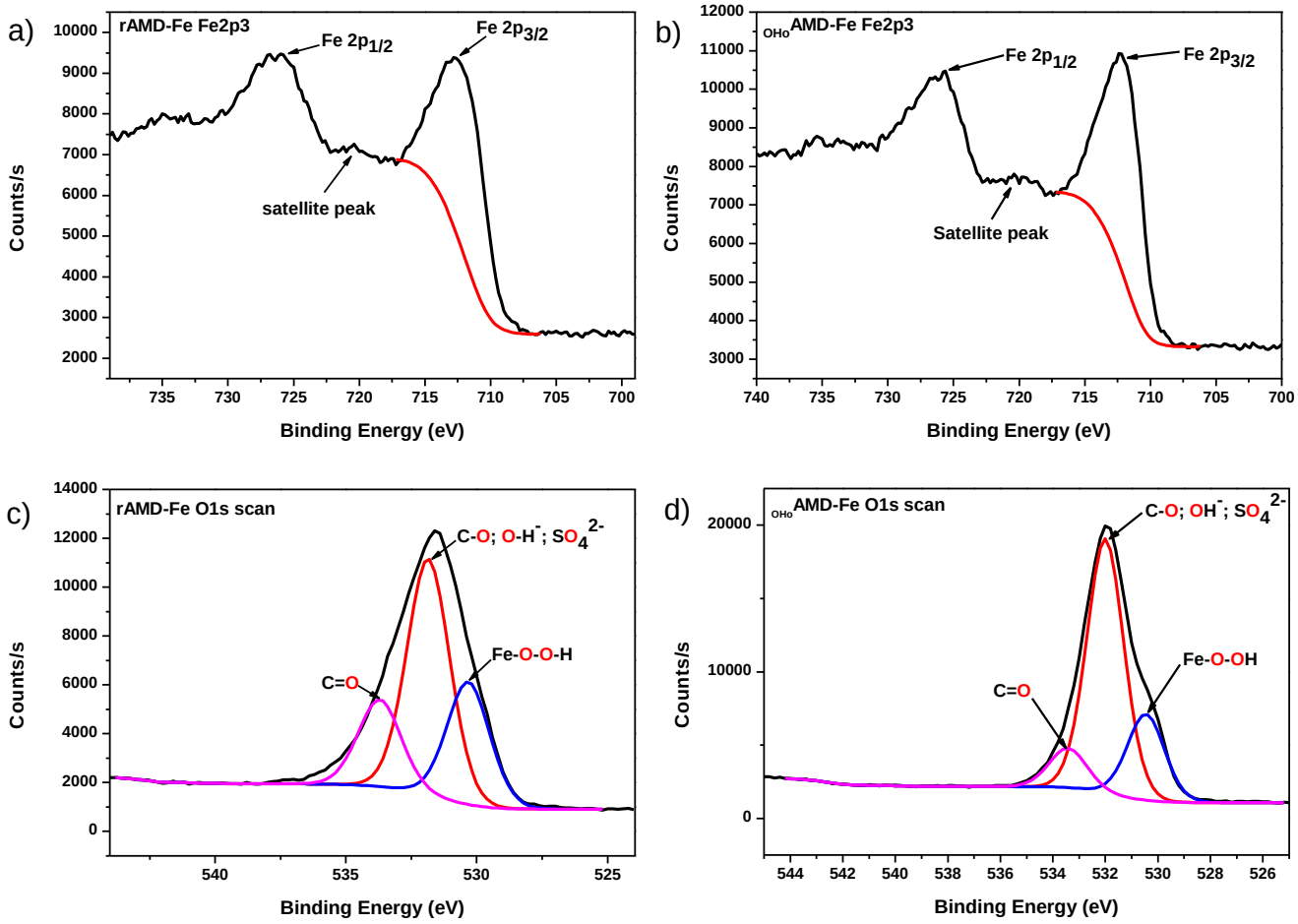

Figure 1: XPS spectra for AMD-Fe precipitates where a) and b) are broad spectra; c) and d) are Fe2p spectra for rAMD-Fe and $_{OHo}$AMD-Fe, respectively.

rAMD-Fe also displayed a very small peak at 400.1 eV (see Fig. S2e) that was assigned to nitrogen compounds (N) identified as cyanide or organic N. The deconvulsion of these peaks revealed that Si was bonded to O thus present as SiO_2, S present as FeS_2 and Al as Al_2O_3 species.[161]

Structural analysis for Fe precipitates and BDC

Fig. 2a depicts the XRD pattern of the iron recovered from AMD, it can be observed that the precipitates formed by the use of NaOH ($_{OH}$AMD-Fe and $_{OHo}$AMD-Fe) are of relatively low crystallinity with broad peaks compared to the one obtained by precipitation in open air (rAMD-Fe). This suggests that $_{OHo}$AMD-Fe and $_{OH}$AMD-Fe consists of very small crystallite particles (4.16 and 6.77 nm) and as a result are amorphous materials.[250] rAMD-Fe depicts a typical FeOOH diffractogram, consisting of typical α- and β-phases. The sharp peaks and small area under the peaks suggesting that these materials are of high crystallinity with

small crystallite size which was calculated to be 6.97 nm. Peaks that appear at 2θ values of 8°, 35°(400) and 54° which are characteristic for β-FeOOH, the peak observed at 23° corresponds to the α-FeOOH phase which is assigned to the quartz (SiO_2). The pattern for $_{OHo}$AMD-Fe and $_{OHo}$AMD-Fe shows that the material consists of haematite (15°), magnetite (35°) and Fe-OH (8°).

Fig. 2b is FTIR spectra for the AMD Fe precipitates, two common peaks across all three spectras are observed; the peak at ~3140 cm^{-1} is assigned to the OH vibration and the other at 1635 cm^{-1} is due to H_2O molecules stretching modes. Peaks at 1133 cm^{-1} and 1064 observed in rAMD-Fe and $_{OHo}$AMD-Fe spectras, respectively, are due to the stretching and vibration mode of the S-O or S = O bond. $_{OH}$AMD-Fe shows a split peak where one is at 1108 cm^{-1}, assigned to the S-O or S=O bond and the one at 1037 cm^{-1} is assigned to the Fe-O-OH stretching vibration mode thus confirming that the material indeed consists of Fe-hydroxide. The two peaks observed with rAMD at 885 (magnetite) and 793 cm^{-1} are both assigned to the Fe-O stretching mode whilst for $_{OHo}$AMD-Fe and $_{OH}$AMD-Fe this stretch mode appears at 697 and 701 cm^{-1}, respectively. The shoulder peaks at 980 and 986 cm^{-1} observed with $_{OHo}$AMD-Fe and $_{OH}$AMD-Fe are assigned to the hematite Fe-O stretch mode; $_{OHo}$AMD-Fe also has a short peak at 895 cm-^{1} identified as the Fe-O stretching mode due to the presence of magnetite.

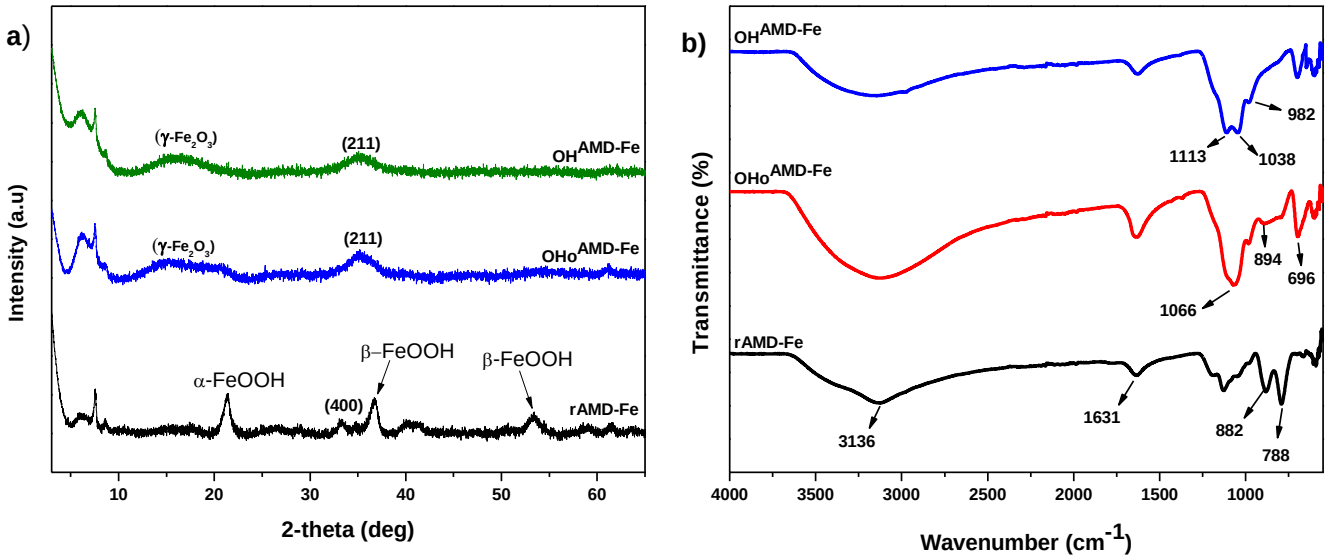

Figure 2: a) XRD and b) FTIR spectra for AMD-Fe precipitates.

The XRD pattern for the two BDC is shown in Figure 3a., the two materials are displaying similar diffraction pattern at similar diffraction angles which implies that the PET-derived BDC is identical to the commercial BDC. The major diffraction peaks are observed at 17.3, 25.09, 27.8, 29.6 and 39.49° as previously reported in literature. Fig. 3b shows the FTIR spectra for commercial BDC and PET-BDC with major characteristic peaks observed at 1678, 1420 and 922 cm^{-1} for both materials respectively assigned to C=O, COO^- and O-H bending. The peak at 922 cm-1 is specifically due to the presence of the TPA dimmer via hydrogen bonds and the broad band around 2800 cm^{-1} is attributed to the presence of water molecules in the microwires.[226] No difference is observed between the two BDC spectra and are similar to the results previously reported.[165, 167, 251]

The powder X-ray diffraction (PXRD) patterns of Fe-MIL-88B synthesized from chloride and nitrate precursors are shown in Fig. 4a. and 4b., respectively. Fe-MIL- 88B exhibited three characteristic diffraction peaks at 9.12°, 10.73°, 11.48°, 17.2°, 18.3° and 20.7° representing the 002, 100, 101, 103, 202 and 211 crystal facets, respectively. The PXRD patterns displayed a group of prominent diffraction peaks confirming the crystalline nature of the prepared Fe-MIL-88B samples and that the crystallinity is not affected by replacing commercial grade precursors with waste derived precursors.

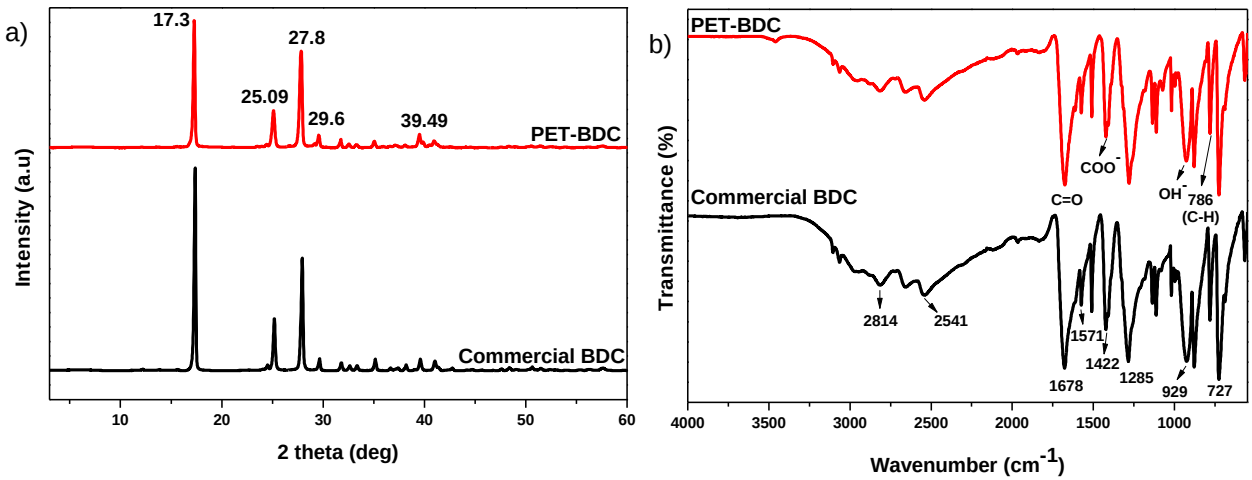

Figure 3: XRD and b) FTIR spectra for commercial BDC vs PET-derived BDC.

To identify functional groups present in Fe-MIL-88B samples, FTIR technique was applied. Figure 4c. and 4d. depict FTIR spectra for the all the Fe-MIL-88B materials that were prepared from the chloride and nitrate precursors, respectively. For the synthesized Fe-

MIL-88B samples, the results obtained seemed to be in agreement with what had been obtained in literature. The slightly broad peaks at 2969 cm^{-1} are attributed to the presence of the OH groups, the peaks are quite narrow owing to the low Fe/BDC ratio of 1. A broadened OH band is a consequence of the increased number of unsaturated metal sites and widened pores of which clearly these materials do not possess. The carboxylate C=O symmetric and asymmetric vibrations as well as that of C-O stretching are observed at ~1381 cm^{-1}, 1594 cm^{-1} and 1649 cm^{-1}. These peaks are consistent with those previously reported in literature, they indicate that BDC is coordinated to the metal center and in a crystallite state, thus MOF structures were successfully formed.[123-124, 252]

Further confirming the coordination of Fe to BDC are the two peaks assigned to C-H bending vibration and Fe-O stretching are observed at 741 cm^{-1} and 604 cm^{-1}, respectively. Lastly, is the peak at 1090 cm^{-1} attributed to the C-O-Fe stretching mode and further confirms the attachment of Fe to BDC via the oxygen. The absence of peaks at 1063 nor at 2861 cm^{-1} proves that DMF molecules were successfully removed from the pores during the solvent exchange with ethanol. A peak characteristic of free BDC trapped in the pores is normally observed at 1704 cm^{-1} in the FTIR spectra and the absence of this peak indicates that all the H_2BDC was deprotonated during MOF formation or the DMF washing was effective at removing the unreacted BDC.[253]

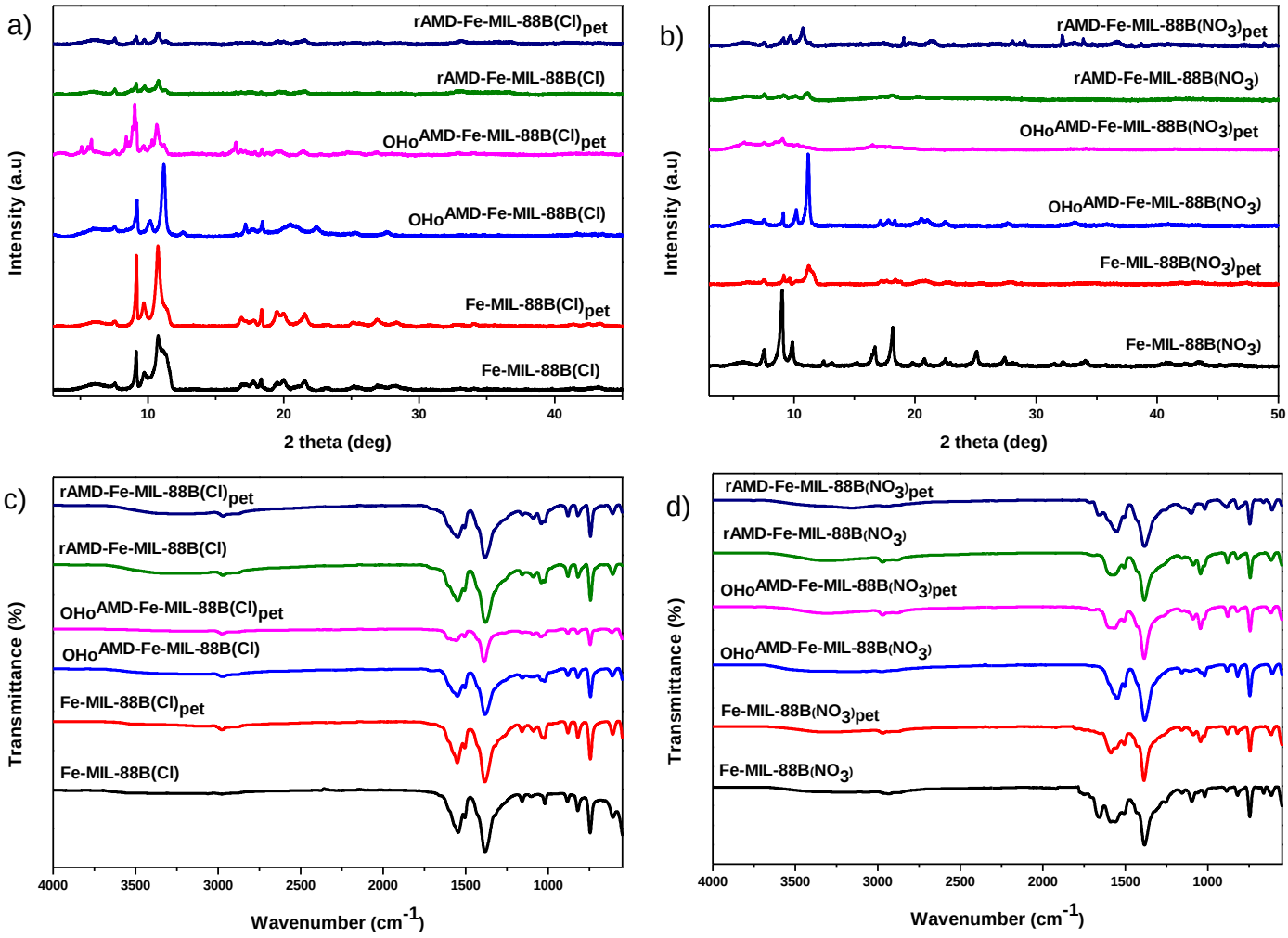

Figure 4: XRD patterns (a and b) and FTIR) spectra (c and d) for Fe-MIL-88B samples.

Morphological analysis of prepared MOFs

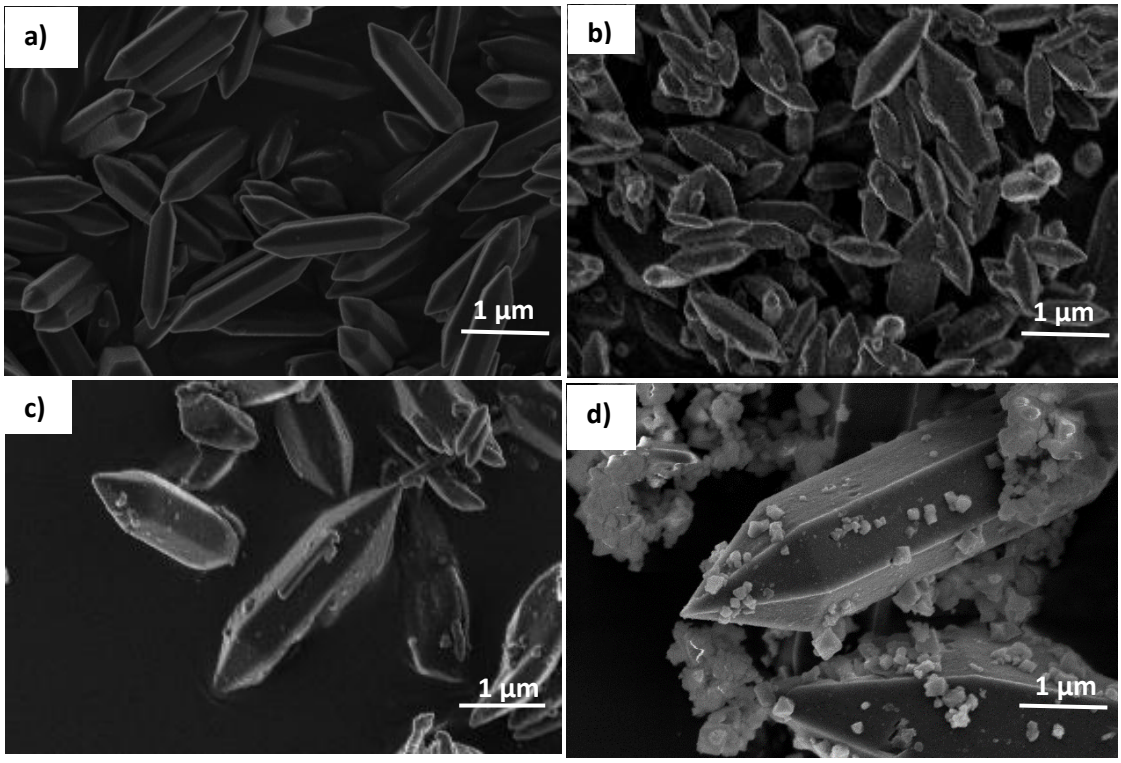

Figure 5: SEM images of a) Fe-MIL-88B(Cl) b) $_{OHo}$AMD-Fe-MIL-88B(Cl) c) $_{OHo}$AMD-Fe-MIL-88B $(Cl)_{pet}$ d) rAMD-Fe-MIL-88B $(Cl)_{pet}$ materials prepared from the chloride precursors.

Fig. 5a-d is the SEM images for MIL-88B prepared from chloride precursors. From the images it can be observed that spindle-like morphologies were obtained for all samples with uniform dispersibility as previously reported in literature. However, mixed morphologies were also observed more specifically with MIL-88B prepared from AMD-Fe precipitates whereas commercial Fe sources resulted in the formation of pure Fe-MIL-88B morphology even when commercial BDC was replaced with PET-BDC. When HCl is used for the dissolution of $_{OHo}$AMD-Fe (Fig. 5b. and c.), pure Fe-MIL-88B morphology is obtained though for $_{OHo}$AMD-Fe-MIL-88B(Cl) broken Fe-MIL-88B structures were observed. When rAMD-Fe (Fig. 5d) is dissolved in HCl, mixed morphologies of Fe-MIL-101 and Fe-MIL-88B were obtained. This is because Fe-MIL-53, Fe-MIL-101 and Fe-MIL-88B frameworks are often formed as competing phases under certain solvothermal conditions.[235]

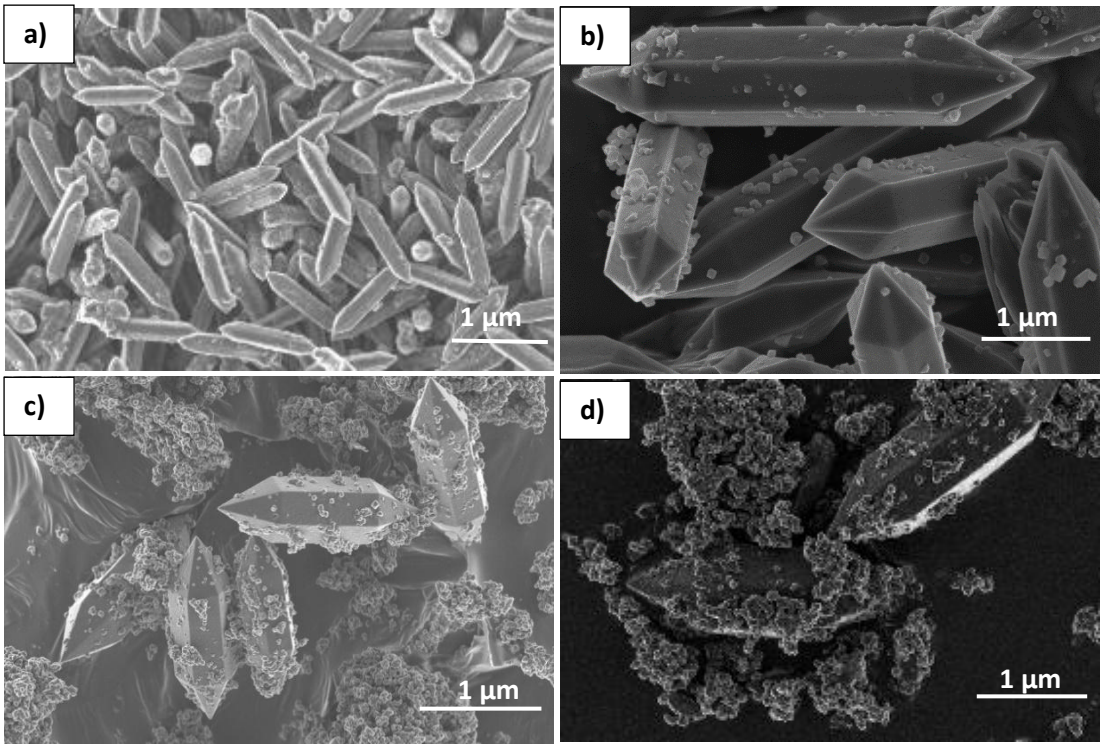

Figure 6: SEM images of a) MIL-88B(NO_3)pet b) MIL-88B-$_{OHo}$AMD-Fe(NO_3) c) MIL-88B-rAMD-Fe(NO_3) d) MIL-88B-rAMD-Fe(NO_3)$_{pet}$ materials prepared from the nitrate precursors.

A spindle-like morphology is still observed for all materials from nitrate precursors as shown in Fig. 6a-d. MOFs prepared from AMD-Fe precipitates however, no longer had a Fe-MIL-88B pure phase whether commercial or PET-derived BDC is used as it is observed in Fig. 6b-d. The deposits do not have a specific morphology and were unfamiliar, it could be concluded that they are undigested contaminants from the AMD-derived Fe, since HNO_3 is a weak acid and the dissolution of the Fe materials was not complete as observed with HCl. The Fe concentration during the synthesis of Fe-MIL-88B also plays a major role as there is a concentration threshold that favours the formation of either the Fe-MIL-101 or Fe-MIL-88B phase. High concentrations of Fe yield more of Fe-MIL-101 crystallites whereas at lower Fe concentrations, Fe-MIL-88B crystallites are observed.[235] NaOH was added as a base which was used to scavenge protons liberated from the terephthalic acid upon MOF formation.[233, 254-255] Large crystals were observed for Fe-MIL-88B samples prepared from AMD-Fe precipitates which may have been a result of slow crystal growth within the system due to high volumes of acid, the modulator and acid used for the dissolution of Fe precipitates. The

observed large crystals agree with the calculated average crystal sizes from the XRD results (Fig. 2a).

Thermal stability studies of obtained MOFs

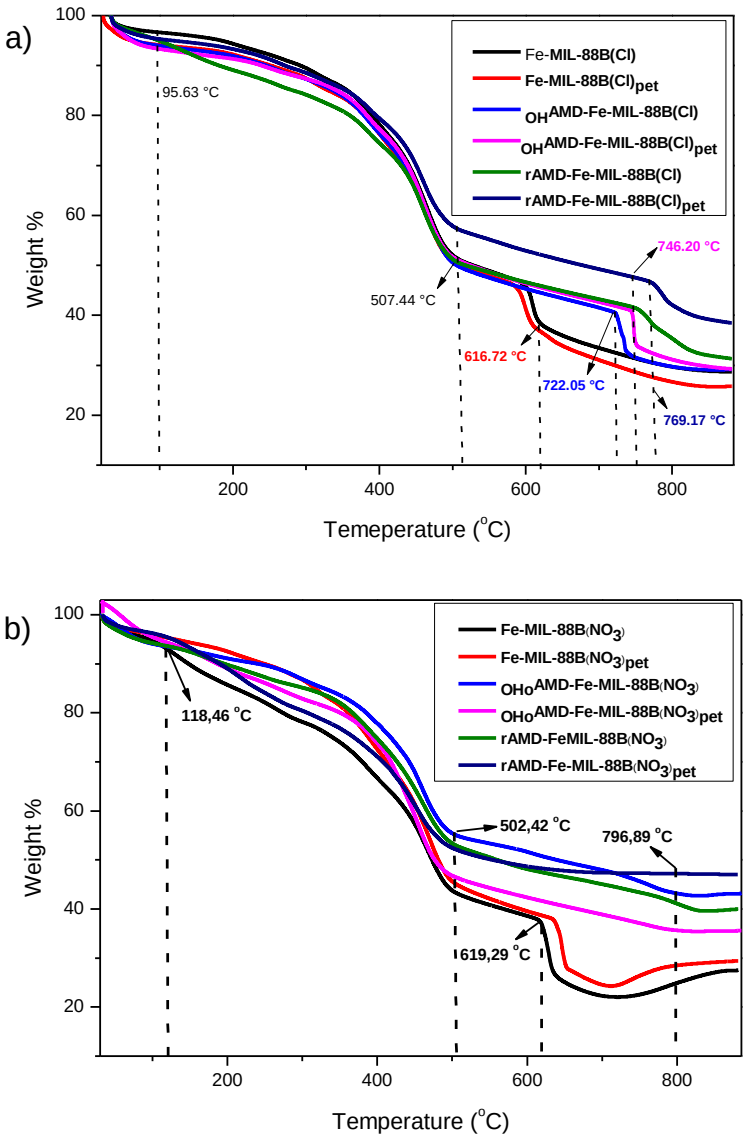

Figure 7: TGA profiles for MIL-88B samples prepared from a) Chloride and b) Nitrate precursors.

Figure 7a and b display TGA profiles obtained for all the MIL-88B samples prepared, they are in correlation with what has been obtained and reported in literature for a typical Fe-MIL-88B MOF. The TGA profiles display a three-step loss typical of the Fe-MIL-88B MOF, where the first loss around 25-136 °C is the loss of water and solvent molecules trapped within the

pores of the material. The second loss at ~460 °C is due to the decomposition of BDC, complete decomposition is observed at temperatures around 600-700 °C where CO_2 is released as a consequence of carboxylate decomposition. Total decomposition of the organic structure is observed at temperature around 460-700 °C for Fe-MIL-88B prepared using AMD derived Fe compared to those from commercial precursors decomposing between 460-600 °C, thus Fe-MIL-88B from AMD derived Fe have much higher stabilities.

An overlap is observed for all the Fe-MIL-88 suggesting identical thermal stabilities were maintained through the MOFs.[117, 222] in Fig. 3a, Fe-MIL-88B$(Cl)_{pet}$ depicts the highest weight loss of 74.2% whilst rAMD-Fe-MIL-88B$(Cl)_{pet}$ has the lowest weight loss of 61.6%. However, the difference in weight losses is negligible amongst the commercial grade and MOFs derived from waste as none of the materials exhibited weight losses of above 75%. Fe-MIL-88B from the nitrate commercial salt exhibited high thermal stabilities with the lowest weight losses when compared to those prepared from chloride commercial precursors. Fe-MIL-88B(NO_3) and Fe-MIL-88B$(NO_3)_{pe}$t were of lowest thermal stabilities compared to materials prepared for rAMD-Fe and $_{OHo}$AMD-Fe in HNO_3. The mass left after total decomposition of all the materials is assumed to be that of Fe_2O_3 which had been identified to be present from the XRD measurements.[233]

Physical properties and hydrogen uptake measurements

Table 2: Showing surface areas and pore volumes of prepared Fe-MIL-88B materials.

Sample	**Surface area (m^2/g)**	**Pore volume (cm^3/g)**
Fe-MIL-88B(Cl)	21.42	0.0791
Fe-MIL-88B$(Cl)_{pet}$	42.49	0.1428
$_{OHo}$AMD-Fe-MIL-88B(Cl)	414.07	0.2244
rAMD-Fe-MIL-88B(Cl)	474.22	0.3366
Fe-MIL-88B(NO_3)	272.39	0.2534
Fe-MIL-88B$(NO_3)_{pet}$	159.43	0.1154
$_{OHo}$AMD-Fe-MIL-88B(NO_3)	60.21	0.0654
rAMD-Fe-MIL-88B(NO_3)	1294.99	0.7614

Figure S7 (see supplementary data) depicts the N_2 adsorption–desorption Isotherms obtained for the prepared Fe-MIL-88B. rAMD-Fe-MIL-88B(NO_3) MOF had the highest surface area (1294 m^2/g) and displayed type I isotherms indicating that the material is micro-porous in nature. To further support this, high N_2 sorption capacities which occurred at low relative pressures are typically observed in the presence of micro-pores thus indicating the presence of micro-pores in the pore structure of the synthesized Fe-MIL-88B sample. MOFs synthesized with BDC derived from PET waste bottles (Fe-MIL-88B$(Cl)_{pet}$ and Fe-MIL-88B$(NO_3)_{pet}$) measured low BET surface areas (42.49 and 159.43, respectively) compared to those obtained with $_{OHo}$AMD-Fe-MIL-88B(Cl) and rAMD-Fe-MIL-88B(Cl) (414.04 and 474 m^2/g, respectively) where commercial BDC is used with AMD-derived Fe. Fe-MIL-88B(Cl) had even lower surface areas of 21.42 m^2/g with a type III isotherm (see supplementary data), indicating that this material is non-porous in nature. Normally, Fe-MIL-88B has a low surface area because of its conformational flexibility and channels that yield a denser structure. The weak uptake of N_2 gas by the material, even at high relative pressures is assumed to be due to the weak interaction of the framework with N_2 that prevents the structure from expanding.[233, 256]

The use of Fe precipitates that were dissolved in HNO_3 somehow yielded high surface areas as compared to those of HCl, this is expected owing to the introduction of structural defects observed with Fe-MIL-88B structures from HNO_3 as observed in Fig. 6b-d. This surface area is then therefore not conclusive or representative of the materials. The NDLFT plots shown in the supplementary section (Fig. S8) are indicating that the synthesized Fe-MIL-88B samples consist mostly of meso-pores (pore size <2 nm) with the presence of macro-pores (<50 nm) as opposed to micro-pores as previously reported in literature.[253] The presence of large pores in the Fe-MIL-88B is an indication of the collapsed pores within the materials to form larger pores, this may be due to the poor solvent exchange method that resulted in DMF molecules not being replaced by ethanol. DMF has a higher surface tension thus vacuum drying forcibly removed the DMF molecule therefore leaving a collapsed pore.

Hydrogen adsorption studies were conducted on the Fe-MIL-88B materials to determine their hydrogen uptake capacities as well as the effects of using waste-derived precursors. Figure 8 is depicting a hydrogen uptake isotherm for rAMD-Fe-MIL-88B(NO_3) with the highest uptake of 0.81 wt% at 77k and absolute pressure of 1 bar. The total gravimetric

uptake at cryogenic conditions is linearly proportional to surface area, this is consistent with the previously reported data for Fe-MIL-88B to date and the Chahine rule.[152, 257] Hydrogen uptakes is dependent on the surface area and the pore volume of the MOF material with physisorption prevailing as indicated by the sharp increase of the isotherm at low pressures due to the presence of open metal sites.[114, 258]

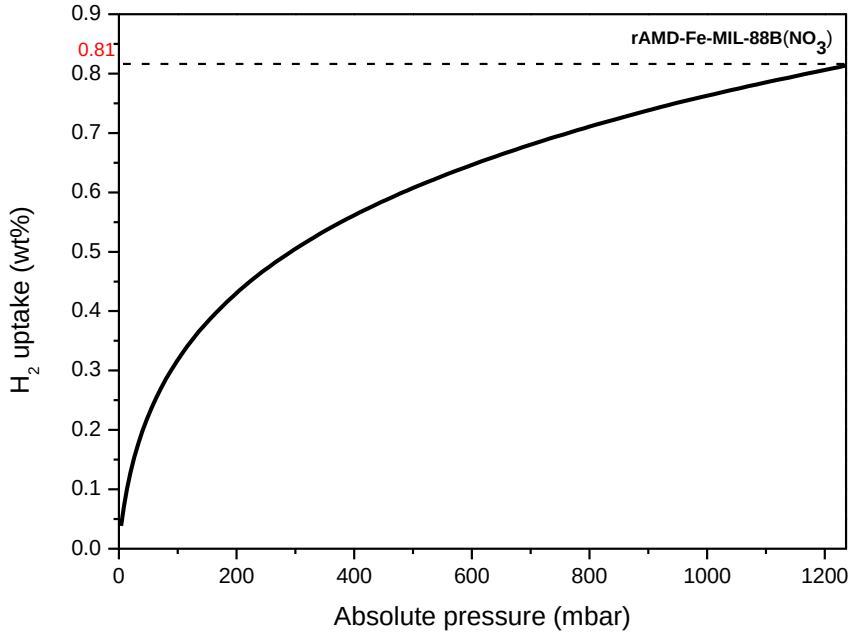

Figure 8: Hydrogen adsorption isotherm of rAMD-Fe-MIL-88B(NO_3).

Conclusion

Fe-based MIL-88B samples were successfully synthesized using unconventional feedstock and they exhibited properties similar to those synthesized from commercial grade precursors. XRD, FTIR and SEM results confirmed this with characteristic diffraction peaks at 2θ angle, vibration and stretching bands at previously reported range as well as hexagonal bipyramidal morphologies dominating though some MOFs exhibited mixed morphologies, respectively. TGA revealed that MOFs from AMD-derived Fe were much more stable compared to when commercial Fe is used and the replacement of commercial grade BDC with PET-derived BDC did not compromise the stability of the MOFs. The materials had very

low BET surface areas owing to their breathing nature though they displayed type I N_2 isotherms with little or no hysteresis loop, agreeing with results obtained from literature.

Hydrogen adsorption results also proved that the synthesized Fe-MIL-88B from waste were suitable for H_2 storage as the results obtained were comparable to those reported in literature (0.47 wt%, at 298 K and 7.6 bar) and adheres to the Chahine rule.[152, 257] Fe-MIL-88B does not have high surface area, as a result very poor H_2 adsorption results are obtained thus post-synthetic methods might be explored to enhance H_2 storage properties of the materials. To avoid mixed morphologies in future, the precursors should be mixed and sealed in a vial, and then heated on a hot plate with continuous stirring, this will allow the mixture to react homogeneously, avoids particle aggregation, and permits formation of highly uniform particles. Other studies have looked at using bulky anionic surfactants for uniform synthesis of MIL-88B, the method could be employed in future to determine if pure morphologies can be obtained with AMD-derived Fe as they did with commercial grade precursors.

Declaration

The authors would like to declare that there are no known competing financial interests or personal relationships that could have influenced this work in any way.

Acknowledgements

The authors would like to extend their sincere gratitude to the council for scientific and industrial research (CSIR), Department of science and innovation (DSI), Future Leaders Africa Independent Research (FLAIR) grant and the University of Pretoria (UP) for financial support and extending their resources such that this study became a success.

Appendix A. Supplementary data

Supplementary data to this article can be found online at http//www.

References

1. Kazemi, S.; Safarifard, V., Carbon dioxide capture in MOFs: The effect of ligand functionalization. *Polyhedron* **2018,** *154*, 236-251.

2. Kong, X.-J.; Li, J.-R., An Overview of Metal–Organic Frameworks for Green Chemical Engineering. *Engineering* **2021,** *7* (8), 1115-1139.

3. Li, H.; Li, L.; Lin, R.-B.; Zhou, W.; Zhang, Z.; Xiang, S.; Chen, B., Porous metal-organic frameworks for gas storage and separation: Status and challenges. *EnergyChem* **2019,** *1* (1), 100006.

4. Bilal, M.; Adeel, M.; Rasheed, T.; Iqbal, H. M. N., Multifunctional metal–organic frameworks-based biocatalytic platforms: recent developments and future prospects. *Journal of Materials Research and Technology* **2019,** *8* (2), 2359-2371.

5. Liao, X.; Wang, F.; Wang, F.; Cai, Y.; Yao, Y.; Teng, B.-T.; Hao, Q.; Shuxiang, L., Synthesis of (100) surface oriented MIL-88A-Fe with rod-like structure and its enhanced fenton-like performance for phenol removal. *Applied Catalysis B: Environmental* **2019,** *259*, 118064.

6. Pham, H.; Ramos, K.; Sua, A.; Acuna, J.; Slowinska, K.; Nguyen, T.; Bui, A.; Weber, M. D. R.; Tian, F., Tuning Crystal Structures of Iron-Based Metal-Organic Frameworks for Drug Delivery Applications. *ACS Omega* **2020,** *5* (7), 3418-3427.

7. Serre, C.; Mellot-Draznieks, C.; Surblé, S.; Audebrand, N.; Filinchuk, Y.; Férey, G., Role of solvent-host interactions that lead to very large swelling of hybrid frameworks. *Science* **2007,** *315* (5820), 1828-31.

8. Horcajada, P.; Salles, F.; Wuttke, S.; Devic, T.; Heurtaux, D.; Maurin, G.; Vimont, A.; Daturi, M.; David, O.; Magnier, E.; Stock, N.; Filinchuk, Y.; Popov, D.; Riekel, C.; Férey, G.; Serre, C., How Linker's Modification Controls Swelling Properties of Highly Flexible Iron(III) Dicarboxylates MIL-88. *Journal of the American Chemical Society* **2011,** *133* (44), 17839-17847.

9. Ren, J.; Dyosiba, X.; Musyoka, N. M.; Langmi, H. W.; North, B. C.; Mathe, M.; Onyango, M. S., Green synthesis of chromium-based metal-organic framework (Cr-MOF) from waste polyethylene terephthalate (PET) bottles for hydrogen storage applications. *International Journal of Hydrogen Energy* **2016,** *41* (40), 18141-18146.

10. Lo, S.-H.; Senthil Raja, D.; Chen, C.-W.; Kang, Y.-H.; Chen, J. J.; Lin, C.-H., Waste polyethylene terephthalate (PET) materials as sustainable precursors for the synthesis of nanoporous MOFs, MIL-47, MIL-53(Cr, Al, Ga) and MIL-101(Cr). *Dalton Trans.* **2016,** *45*.

11. Deleu, W. P. R.; Stassen, I.; Jonckheere, D.; Ameloot, R.; De Vos, D. E., Waste PET (bottles) as a resource or substrate for MOF synthesis. *Journal of Materials Chemistry A* **2016,** *4* (24), 9519-9525.

12. Dyosiba, X.; Ren, J.; Musyoka, N. M.; Langmi, H. W.; Mathe, M.; Onyango, M. S., Feasibility of Varied Polyethylene Terephthalate Wastes as a Linker Source in Metal–Organic Framework UiO-66(Zr) Synthesis. *Industrial & Engineering Chemistry Research* **2019,** *58* (36), 17010-17016.

13. Lagae Capelle, E.; Cognet, M.; Madhavi, S.; Carboni, M.; Meyer, D., Combining Organic and Inorganic Wastes to Form Metal–Organic Frameworks. *Materials* **2020,** *13*, 441.

14. Macingova, E.; Luptakova, A., Recovery of Metals from Acid Mine Drainage. *Chemical Engineering Transactions* **2012,** *28*, 109-114.

15. Silva, R. d. A.; Secco, M. P.; Lermen, R. T.; Schneider, I. A. H.; Hidalgo, G. E. N.; Sampaio, C. H., Optimizing the selective precipitation of iron to produce yellow pigment from acid mine drainage. *Minerals Engineering* **2019,** *135*, 111-117.

16. RoyChowdhury, A.; Sarkar, D.; Datta, R., Removal of Acidity and Metals from Acid Mine Drainage-Impacted Water using Industrial Byproducts. *Environmental Management* **2019,** *63* (1), 148-158.

17. Wei, X.; Viadero, R. C., Synthesis of magnetite nanoparticles with ferric iron recovered from acid mine drainage: Implications for environmental engineering. *Colloids and Surfaces A: Physicochemical and Engineering Aspects* **2007,** *294* (1), 280-286.

18. Wei, X.; Viadero, R. C.; Buzby, K. M., Recovery of Iron and Aluminum from Acid Mine Drainage by Selective Precipitation. *Environmental Engineering Science* **2005,** *22* (6), 745-755.

19. Seo, E. Y.; Cheong, Y. W.; Yim, G. J.; Min, K. W.; Geroni, J. N., Recovery of Fe, Al and Mn in acid coal mine drainage by sequential selective precipitation with control of pH. *CATENA* **2017,** *148*, 11-16.

20. Silva, R.; Menezes, J.; Lopes, F. c.; Kirchheim, A.; Schneider, I., Synthesis of a Goethite Pigment by Selective Precipitation of Iron from Acidic Coal Mine Drainage. *Mine Water and the Environment* **2017**.

21. Skobelev, I. Y.; Sorokin, A. B.; Kovalenko, K. A.; Fedin, V. P.; Kholdeeva, O. A., Solvent-free allylic oxidation of alkenes with O2 mediated by Fe- and Cr-MIL-101. *Journal of Catalysis* **2013,** *298*, 61-69.

22. Menezes, J. C. S. S.; Silva, R. A.; Arce, I. S.; Schneider, I. A. H., Production of a Poly-ferric Sulphate Chemical Coagulant by Selective Precipitation of Iron from Acidic Coal Mine Drainage. *Mine Water and the Environment* **2009,** *28* (4), 311.

23. Zango, Z. U.; Jumbri, K.; Sambudi, N. S.; Hanif Abu Bakar, N. H.; Fathihah Abdullah, N. A.; Basheer, C.; Saad, B., Removal of anthracene in water by MIL-88(Fe), NH2-MIL-88(Fe), and mixed-MIL-88(Fe) metal–organic frameworks. *RSC Advances* **2019,** *9* (71), 41490-41501.

24. Sui, H.; Li, L.; Zhu, X.; Chen, D.; Wu, G., Modeling the adsorption of PAH mixture in silica nanopores by molecular dynamic simulation combined with machine learning. *Chemosphere* **2016,** *144*, 1950-1959.

25. Rambau, K. M.; Musyoka, N. M.; Panek, R.; Franus, W.; Wdowin, M.; Manyala, N., Preparation of coal fly ash derived metal organic frameworks and their carbon derivatives. *Materials Today Communications* **2021,** *27*, 102433.

26. Jönsson, J.; Jönsson, J.; Lövgren, L., Precipitation of secondary Fe(III) minerals from acid mine drainage. *Applied Geochemistry - APPL GEOCHEM* **2006,** *21*, 437-445.

27. Wang, H.; Kojtari, A.; Xu, X.; Ji, H.-F., Self-Assembled Microwires of Terephthalic Acid and Melamine. *Crystals* **2017,** *7* (8).

28. Pham, H.; Ramos, K.; Sua, A.; Acuna, J.; Slowinska, K.; Nguyen, T.; Bui, A.; Weber, M. D. R.; Tian, F., Tuning Crystal Structures of Iron-Based Metal–Organic Frameworks for Drug Delivery Applications. *ACS Omega* **2020,** *5* (7), 3418-3427.

29. Nehra, M.; Dilbaghi, N.; Singhal, N. K.; Hassan, A. A.; Kim, K.-H.; Kumar, S., Metal organic frameworks MIL-100(Fe) as an efficient adsorptive material for phosphate management. *Environmental Research* **2019,** *169*, 229-236.

30. Yurduşen, A.; Yürüm, Y., A Controlled Synthesis Strategy To Enhance the CO2 Adsorption Capacity of MIL-88B Type MOF Crystallites by the Crucial Role of Narrow Micropores. *Industrial & Engineering Chemistry Research* **2019,** *58* (31), 14058-14072.

31. Wu, W.; Decker, G. E.; Weaver, A. E.; Arnoff, A. I.; Bloch, E. D.; Rosenthal, J., Facile and Rapid Room-Temperature Electrosynthesis and Controlled Surface Growth of Fe-MIL-101 and Fe-MIL-101-NH2. *ACS Central Science* **2021,** *7* (8), 1427-1433.

32. Carson, F.; Su, J.; Platero-Prats, A. E.; Wan, W.; Yun, Y.; Samain, L.; Zou, X., Framework Isomerism in Vanadium Metal–Organic Frameworks: MIL-88B(V) and MIL-101(V). *Crystal Growth & Design* **2013,** *13* (11), 5036-5044.

33. Horcajada, P.; Salles, F.; Wuttke, S.; Devic, T.; Heurtaux, D.; Maurin, G.; Vimont, A.; Daturi, M.; David, O.; Magnier, E.; Stock, N.; Filinchuk, Y.; Popov, D.; Riekel, C.; Férey, G.; Serre, C., *J. Am. Chem. Soc.* **2011,** *133*, 17839.

34. Taylor-Pashow, K. M. L.; Rocca, J. D.; Xie, Z.; Tran, S.; Lin, W., *J. Am. Chem. Soc.* **2009,** *131*, 14261.

35. Hou, S.; Wu, Y.-n.; Feng, L.; Chen, W.; Wang, Y.; Morlay, C.; Li, F., Green synthesis and evaluation of an iron-based metal–organic framework MIL-88B for efficient decontamination of arsenate from water. *Dalton Transactions* **2018,** *47* (7), 2222-2231.

36. Xiao, Y.; Guo, X.; Huang, H.; Yang, Q.; Huang, A.; Zhong, C., Synthesis of MIL-88B(Fe)/Matrimid mixed-matrix membranes with high hydrogen permselectivity. *RSC Advances* **2015,** *5* (10), 7253-7259.

37. García-Holley, P.; Schweitzer, B.; Islamoglu, T.; Liu, Y.; Lin, L.; Rodriguez, S.; Weston, M. H.; Hupp, J. T.; Gómez-Gualdrón, D. A.; Yildirim, T.; Farha, O. K., Benchmark Study of Hydrogen Storage in Metal–Organic Frameworks under Temperature and Pressure Swing Conditions. *ACS Energy Letters* **2018,** *3* (3), 748-754.

38. Yurduşen, A.; Yürüm, A.; Yürüm, Y., Engineering MIL-88B crystallites for enhanced H2 uptake capacity: The role of ultramicropores. *International Journal of Energy Research* **2020,** *44* (4), 2875-2888.

39. Xuan Huynh, N. T.; Chihaia, V.; Son, D. N., Hydrogen storage in MIL-88 series. *Journal of Materials Science* **2019,** *54* (5), 3994-4010.

40. Zeleňák, V.; Saldan, I., Factors Affecting Hydrogen Adsorption in Metal-Organic Frameworks: A Short Review. *Nanomaterials (Basel)* **2021,** *11* (7).

5.2 Chapter summary

This chapter outlines the successful synthesis of Fe-MIL-88B was demonstrated through the various characterization techniques. Fe was found to be the predominant metal in the AMD waste as outlined by the results from the ICP-OES shown in Table 1. XPS was then used to study elemental and chemical composition of Fe precipitates which revealed that most Fe present in the materials was in the +2 state, deeming both oxidation methods used effective. FTIR and XRD confirmed structural properties of Fe precipitates, PET-BDC and Fe-MIL-88B MOFs prepared from commercial and waste starting materials. The lowered BET

surface areas and large pore volumes are a result of collapsed pores in the Fe-MIL-88B MOFs due to poor activation of the pores. Fe-MIL-88B from waste showed improved BET surface areas compared to those prepared from commercial precursors.

Chapter 6

6. Conclusions

Fe-MIL-88B samples were successfully synthesized using unconventional feed stock and they exhibited properties similar to those synthesized from commercial grade precursors. XRD, FTIR and SEM results confirmed this with characteristic diffraction peaks at 2θ angle, vibration and stretching bands at previously reported range as well as hexagonal bipyramidal morphologies (spindle-like). MOFs prepared from waste precursors such as rAMD-Fe-MIL-88B$(NO_3)_{pet}$ and rAMD-Fe-MIL-88B, no longer had a MIL-88B pure phase instead exhibited mixed morphologies. TGA revealed that MOFs from AMD-derived Fe were much more stable compared to when commercial Fe is used and the replacement of commercial grade BDC with PET-derived BDC did not compromise the stability of the MOFs. The materials had very low BET surface areas which could be attributed to their breathing nature though they displayed type I N_2 isotherms with little or no hysteresis loop, agreeing with results obtained from literature.

To avoid mixed morphologies in future, the precursors should be mixed and sealed in a vial, and then heated on a hot plate with continuous stirring, this will allow the mixture to react homogeneously, avoids particle aggregation, and permits formation of highly uniform particles. Other studies have looked at using bulky anionic surfactants for uniform synthesis of MIL-88B, the method could be employed in future to determine if pure morphologies can be obtained with AMD-derived Fe as they did with commercial grade precursors. The use of HCl and HNO_3 played a huge role in identifying an acid suitable for the dissolution of the Fe precursor from the AMD. HCl yielded purer morphologies (no deposits) whilst HNO_3 resulted in larger quantities (>1 mg) of Fe-based MOFs. Hydrogen adsorption results also proved that the synthesized Fe-MIL-88B from waste were suitable for H_2 storage as the results obtained were comparable to those reported in literature (0.47 wt%, at 298 K and 7.6 bar) and adheres to the Chahine rule.[152, 257] Fe-MIL-88B does not have high surface area, as a result very poor H_2 adsorption results are obtained thus post-synthetic methods might be explored to enhance H_2 storage properties of the materials.

Fe-MIL-101 was successfully synthesized from the waste precursors and displayed comparable textural and physical properties to the Fe-MOFs prepared from commercial

grade precursors. This was supported by the XRD and FTIR that suggested the presence of a trinuclear metal center and characteristic vibrations confirming the coordination of BDC to the Fe center. Mixed Fe-MIL-101 and Fe-MIL-88B morphologies were observed with MOFs prepared by the dissolution of rAMD-Fe(HCl) and $_{OHo}$AMD-Fe(HCl), this resulted in decreased surface areas and pore volumes. Fe-MIL-101 prepared from rAMD-Fe(HNO_3) and $_{OHo}$AMD-Fe(HNO_3) displayed well dispersed octahedral morphologies with high degree of crystallinity and thermal stability superior to that of MOFs prepared from commercial grade precursors. The use of the nitrate commercial precursor for the synthesis of MIL-101 resulted in a material of unfamiliar morphology owing to the lack of a mineralizer usually added to aid the formation of the Fe-MIL-101 structure.

Fe-MIL-101 displayed relatively high H_2 storage capacities, comparable with the results previously reported by Ren *et al.* (0.99, 1.65 and 1.92 wt%) for Cr-MIL-101 MOFs.[148] Because of lower surface areas compared to the values reported (2000-6000 m^2),[243-244] the synthesized Fe-MIL-101 experienced lower H_2 adsorption. To enhance H_2 storage capacity in Fe-MIL-101, surface area and pore volume would first need to be optimized by supercritical activation as one of the methods. Another way of increasing H_2 uptake might be to composite Fe-MIL-101 with transition metals to create more active sites for the hydrogen molecule to adsorb.

6.1 Future work

The study has, without a doubt, proved that it is possible to synthesize Fe-MIL-101 and Fe-MIL-88B using complete waste, PET and AMD. From the study, the limitations and weak points in using the waste materials for the synthesis of MOFs were discovered. Limitations such as mixed morphologies and lack of forming octahedral morphology when nitrate salt (Fe-MIL-101) is used could be investigated in the future. This could allow for an opportunity to develop/adjust a method such that it is suitable for the synthesis of pure Fe-MIL-101 and Fe-MIL-88B using these waste materials. Further studies would also elude into the optimization of the surface areas of the MOFs such that they match if not surpass those of MOFs prepared from commercial grade precursors. The latter would enable the use of waste-based MOFs to be used in numerous applications, more especially for hydrogen storage.

References

1. Day, G. S.; Drake, H. F.; Zhou, H.-C.; Ryder, M. R., Evolution of porous materials from ancient remedies to modern frameworks. *Communications Chemistry* **2021,** *4* (1), 114.

2. Novel porous materials for emerging applications. *Journal of Materials Chemistry* **2006,** *16* (7), 623-625.

3. Zhang, J.; Chen, J.; Peng, S.; Peng, S.; Zhang, Z.; Tong, Y.; Miller, P. W.; Yan, X.-P., Emerging porous materials in confined spaces: from chromatographic applications to flow chemistry. *Chemical Society Reviews* **2019,** *48* (9), 2566-2595.

4. Huo, Q., Chapter 16 - Synthetic Chemistry of the Inorganic Ordered Porous Materials. In *Modern Inorganic Synthetic Chemistry*, Xu, R.; Pang, W.; Huo, Q., Eds. Elsevier: Amsterdam, 2011; pp 339-373.

5. Bennett, T. D.; Coudert, F.-X.; James, S. L.; Cooper, A. I., The changing state of porous materials. *Nature Materials* **2021,** *20* (9), 1179-1187.

6. Rashidi, S.; Esfahani, J.; Hormozi, F., Classifications of Porous Materials for Energy Applications. 2020.

7. Wu, Y.; Weckhuysen, B. M., Separation and Purification of Hydrocarbons with Porous Materials. *Angewandte Chemie International Edition* **2021,** *60* (35), 18930-18949.

8. Sircar, S.; Myers, A. L., Gas separation by zeolites. *Handbook of zeolite science and technology* **2003,** *1063*.

9. Kosinov, N.; Gascon, J.; Kapteijn, F.; Hensen, E. J. M., Recent developments in zeolite membranes for gas separation. *Journal of Membrane Science* **2016,** *499*, 65-79.

10. Lin, R.-B.; Xiang, S.; Zhou, W.; Chen, B., Microporous Metal-Organic Framework Materials for Gas Separation. *Chem* **2020,** *6* (2), 337-363.

11. Mohamedali, M.; Nath, D.; Ibrahim, H.; Henni, A., Review of Recent Developments in CO2 Capture Using Solid Materials: Metal Organic Frameworks (MOFs). 2016; pp 115-154.

12. Saxena, R.; Singh, V. K.; Kumar, E. A., Carbon Dioxide Capture and Sequestration by Adsorption on Activated Carbon. *Energy Procedia* **2014,** *54*, 320-329.

13. de Zeeuw, J., CHROMATOGRAPHY: GAS | Gas–Solid Gas Chromatography. In *Encyclopedia of Separation Science*, Wilson, I. D., Ed. Academic Press: Oxford, 2000; pp 481-489.

14. Kim, H.-J.; Yang, H.-C.; Chung, D.-Y.; Yang, I.-H.; Choi, Y.; Moon, J.-K., Functionalized Mesoporous Silica Membranes for CO 2 Separation Applications. *Journal of Chemistry* **2015,** *2015*, 1-9.

15. Pal, N.; Lee, J.-H.; Cho, E.-B., Recent Trends in Morphology-Controlled Synthesis and Application of Mesoporous Silica Nanoparticles. *Nanomaterials* **2020,** *10*, 2122.

16. Chang, F.; Zhou, J.; Chen, P.; Chen, Y.; Jia, H.; Saad, S.; Gao, Y.; Cao, X.; Zheng, T., Microporous and mesoporous materials for gas storage and separation: A review. *Asia-Pacific Journal of Chemical Engineering* **2013,** *8*.

17. Thomas, K., Hydrogen adsorption and storage on porous materials. *Catalysis Today* **2007,** *120*, 389-398.

18. Dong, J.; Wang, X.; Xu, H.; Zhao, Q.; Li, J., Hydrogen storage in several microporous zeolites. *International Journal of Hydrogen Energy* **2007,** *32* (18), 4998-5004.

19. Regli, L.; Zecchina, A.; Vitillo, J. G.; Cocina, D.; Spoto, G.; Lamberti, C.; Lillerud, K. P.; Olsbye, U.; Bordiga, S., Hydrogen storage in Chabazite zeolite frameworks. *Physical Chemistry Chemical Physics* **2005,** *7* (17), 3197-3203.

20. Stephanie-Victoire, F.; Goulay, A. M.; de Lara, E. C., Adsorption and coadsorption of molecular hydrogen isotopes in zeolites. 1. Isotherms of H-2, HD, and D-2 in NaA by thermomicrogravimetry. *Langmuir* **1998,** *14* (25), 7255-7259.

21. Li, Y.; Yang, R. T., Hydrogen Storage in Low Silica Type X Zeolites. *The Journal of Physical Chemistry B* **2006,** *110* (34), 17175-17181.

22. Yue, M.; Lambert, H.; Pahon, E.; Roche, R.; Jemei, S.; Hissel, D., Hydrogen energy systems: A critical review of technologies, applications, trends and challenges. *Renewable and Sustainable Energy Reviews* **2021,** *146*, 111180.

23. Andersson, J.; Grönkvist, S., Large-scale storage of hydrogen. *International Journal of Hydrogen Energy* **2019,** *44* (23), 11901-11919.

24. Dincă, M.; Long, J. R., Hydrogen storage in microporous metal-organic frameworks with exposed metal sites. *Angew Chem Int Ed Engl* **2008,** *47* (36), 6766-79.

25. Kuppler, R. J.; Timmons, D. J.; Fang, Q.-R.; Li, J.-R.; Makal, T. A.; Young, M. D.; Yuan, D.; Zhao, D.; Zhuang, W.; Zhou, H.-C., Potential applications of metal-organic frameworks. *Coordination Chemistry Reviews* **2009,** *253* (23), 3042-3066.

26. Introduction to Metal–Organic Frameworks. *Chemical Reviews* **2012,** *112* (2), 673-674.

27. Furukawa, H.; Cordova Kyle, E.; O'Keeffe, M.; Yaghi Omar, M., The Chemistry and Applications of Metal-Organic Frameworks. *Science* **2013,** *341* (6149), 1230444.

28. Lee, Y.-R.; Kim, J.; Ahn, W.-S., Synthesis of metal-organic frameworks: A mini review. *Korean Journal of Chemical Engineering* **2013,** *30* (9), 1667-1680.

29. Kumar, S.; Jain, S.; Nehra, M.; Dilbaghi, N.; Marrazza, G.; Kim, K.-H., Green synthesis of metal–organic frameworks: A state-of-the-art review of potential environmental and medical applications. *Coordination Chemistry Reviews* **2020,** *420*, 213407.

30. Reinsch, H., "Green" Synthesis of Metal-Organic Frameworks. *European Journal of Inorganic Chemistry* **2016,** *2016* (27), 4290-4299.

31. Hirscher, M.; Panella, B., Hydrogen storage in metal–organic frameworks. *Scripta Materialia* **2007,** *56* (10), 809-812.

32. Lubitz, W.; Tumas, W., Hydrogen: An Overview. *Chemical Reviews* **2007,** *107* (10), 3900-3903.

33. Hwang, H. T.; Varma, A., Hydrogen storage for fuel cell vehicles. *Current Opinion in Chemical Engineering* **2014,** *5*, 42-48.

34. Thomas, K. M., Hydrogen adsorption and storage on porous materials. *Catalysis Today* **2007,** *120* (3), 389-398.

35. Ren, J.; Musyoka, N. M.; Langmi, H. W.; Mathe, M.; Liao, S., Current research trends and perspectives on materials-based hydrogen storage solutions: A critical review. *International Journal of Hydrogen Energy* **2017,** *42* (1), 289-311.

36. Uranga Piña, L.; Martínez Mesa, A.; Seifert, G., Adsorption of molecular hydrogen on nanostructered surfaces. **2015**.

37. Suh, M. P.; Park, H. J.; Prasad, T. K.; Lim, D.-W., Hydrogen Storage in Metal–Organic Frameworks. *Chemical Reviews* **2012,** *112* (2), 782-835.

38. Macingova, E.; Luptakova, A., Recovery of Metals from Acid Mine Drainage. *Chemical Engineering Transactions* **2012,** *28*, 109-114.

39. Silva, R. d. A.; Secco, M. P.; Lermen, R. T.; Schneider, I. A. H.; Hidalgo, G. E. N.; Sampaio, C. H., Optimizing the selective precipitation of iron to produce yellow pigment from acid mine drainage. *Minerals Engineering* **2019,** *135*, 111-117.

40. RoyChowdhury, A.; Sarkar, D.; Datta, R., Removal of Acidity and Metals from Acid Mine Drainage-Impacted Water using Industrial Byproducts. *Environmental Management* **2019,** *63* (1), 148-158.

41. Lagae Capelle, E.; Cognet, M.; Madhavi, S.; Carboni, M.; Meyer, D., Combining Organic and Inorganic Wastes to Form Metal–Organic Frameworks. *Materials* **2020,** *13*, 441.

42. Li, Z.; Liu, P.; Ou, C.; Dong, X., Porous Metal–Organic Frameworks for Carbon Dioxide Adsorption and Separation at Low Pressure. *ACS Sustainable Chemistry & Engineering* **2020,** *8* (41), 15378-15404.

43. Hu, Z.; Wang, Y.; Shah, B. B.; Zhao, D., CO2 Capture in Metal–Organic Framework Adsorbents: An Engineering Perspective. *Advanced Sustainable Systems* **2019,** *3* (1), 1800080.

44. Zhou, Introduction to MetalOrganic Frameworks. *Chemical Reviews* **2012,** *112* (2), 673-674.

45. Cavenati, S.; Grande, C. A.; Rodrigues, A. E.; Kiener, C.; Müller, U., Metal Organic Framework Adsorbent for Biogas Upgrading. *Industrial & Engineering Chemistry Research* **2008,** *47* (16), 6333-6335.

46. Kidanemariam, A.; Lee, J.; Park, J., Recent Innovation of Metal-Organic Frameworks for Carbon Dioxide Photocatalytic Reduction. *Polymers* **2019,** *11*.

47. Ma, S.; Zhou, H.-C., Gas storage in porous metal–organic frameworks for clean energy applications. *Chemical Communications* **2010,** *46* (1), 44-53.

48. Liu, J.; Chen, L.; Cui, H.; Zhang, J.; Zhang, L.; Su, C.-Y., Applications of metal–organic frameworks in heterogeneous supramolecular catalysis. *Chemical Society Reviews* **2014,** *43* (16), 6011-6061.

49. Rasheed, T.; Rizwan, K.; Bilal, M.; Iqbal, H. M. N., Metal-Organic Framework-Based Engineered Materials—Fundamentals and Applications. *Molecules* **2020,** *25* (7).

50. Kitagawa, S.; Matsuda, R., Chemistry of coordination space of porous coordination polymers. *Coordination Chemistry Reviews* **2007,** *251* (21), 2490-2509.

51. Li, G.; Xia, L.; Dong, J.; Chen, Y.; Li, Y., 10 - Metal-organic frameworks. In *Solid-Phase Extraction*, Poole, C. F., Ed. Elsevier: 2020; pp 285-309.

52. Van Vleet, M. J.; Weng, T.; Li, X.; Schmidt, J. R., In Situ, Time-Resolved, and Mechanistic Studies of Metal–Organic Framework Nucleation and Growth. *Chemical Reviews* **2018,** *118* (7), 3681-3721.

53. Sharmin, E.; Zafar, F., Introductory Chapter: Metal Organic Frameworks (MOFs). 2016.

54. Kitagawa, S.; Kondo, M., Functional Micropore Chemistry of Crystalline Metal Complex-Assembled Compounds. *Bulletin of the Chemical Society of Japan* **1998,** *71* (8), 1739-1753.

55. Liu, J.; Chen, L.; Cui, H.; Zhang, J.; Zhang, L.; Su, C.-Y., ChemInform Abstract: Applications of Metal-Organic Frameworks in Heterogeneous Supramolecular Catalysis. *Chemical Society reviews* **2014,** *43*.

56. Zhao, P.; Tsang, S. C. E.; Fairen-Jimenez, D., Structural heterogeneity and dynamics in flexible metal-organic frameworks. *Cell Reports Physical Science* **2021,** *2* (9), 100544.

57. Kitagawa, S.; Kitaura, R.; Noro, S.-i., Functional Porous Coordination Polymers. *Angewandte Chemie International Edition* **2004,** *43* (18), 2334-2375.

58. Zhang, S.-Y.; Jensen, S.; Tan, K.; Wojtas, L.; Roveto, M.; Cure, J.; Thonhauser, T.; Chabal, Y. J.; Zaworotko, M. J., Modulation of Water Vapor Sorption by a Fourth-Generation Metal–Organic Material with a Rigid Framework and Self-Switching Pores. *Journal of the American Chemical Society* **2018,** *140* (39), 12545-12552.

59. Kurzydym, I.; Czekaj, I., Modelling of porous metal-organic framework (MOF) materials used in catalysis. *Technical Transactions* **2020**, 1-24.

60. Kitagawa, S., Porous Materials and the Age of Gas. *Angewandte Chemie International Edition* **2015,** *54* (37), 10686-10687.

61. Kitagawa, S., Future Porous Materials. *Accounts of Chemical Research* **2017,** *50* (3), 514-516.

62. Li, H.; Cosio, M.; Wang, K.; Burtner, W.; Zhou, H.-C., Design and Construction of Chemically Stable Metal-Organic Frameworks. In *Elaboration and Applications of Metal-Organic Frameworks*, WORLD SCIENTIFIC: 2017; Vol. Volume 2, pp 1-35.

63. Serre, C.; Devic, T., Iron and Groups V- and VI-based MOFs. 2016; pp 171-202.

64. De Toni, M.; Pullumbi, P.; Coudert, F.-X.; Fuchs, A. H., Understanding the Effect of Confinement on the Liquid−Gas Transition: A Study of Adsorption Isotherms in a Family of Metal−Organic Frameworks. *The Journal of Physical Chemistry C* **2010,** *114* (49), 21631-21637.

65. Li, H.; Eddaoudi, M.; O'Keeffe, M.; Yaghi, O. M., Design and synthesis of an exceptionally stable and highly porous metal-organic framework. *Nature* **1999,** *402* (6759), 276-279.

66. Kapil, V.; Wieme, J.; Vandenbrande, S.; Lamaire, A.; Speybroeck, V.; Ceriotti, M., *Modeling the structural and thermal properties of loaded metal-organic frameworks. An interplay of quantum and anharmonic fluctuations*. 2019.

67. Liu, Y.; Pang, H.; Wang, X.; Yu, S.; Chen, Z.; Zhang, P.; Chen, L.; Song, G.; Saleh Alharbi, N.; Omar Rabah, S.; Wang, X., Zeolitic imidazolate framework-based nanomaterials for the capture of heavy metal ions and radionuclides: A review. *Chemical Engineering Journal* **2021,** *406*, 127139.

68. Chen, B.; Yang, Z.; Zhu, Y.; Xia, Y., Zeolitic imidazolate framework materials: recent progress in synthesis and applications. *Journal of Materials Chemistry A* **2014,** *2* (40), 16811-16831.

69. Park, K. S.; Ni, Z.; Côté, A. P.; Choi, J. Y.; Huang, R.; Uribe-Romo, F. J.; Chae, H. K.; O'Keeffe, M.; Yaghi, O. M., Exceptional chemical and thermal stability of zeolitic imidazolate frameworks. *Proceedings of the National Academy of Sciences* **2006,** *103* (27), 10186.

70. Zeolitic Imidazolate Frameworks. In *Introduction to Reticular Chemistry*, 2019; pp 463-479.

71. Liu, Y.; Cheng, H.; Cheng, M.; Liu, Z.; Huang, D.; Zhang, G.; Shao, B.; Liang, Q.; Luo, S.; Wu, T.; Xiao, S., The application of Zeolitic imidazolate frameworks (ZIFs) and their derivatives based materials for photocatalytic hydrogen evolution and pollutants treatment. *Chemical Engineering Journal* **2021,** *417*, 127914.

72. Bhunia, M. K.; Hughes, J. T.; Fettinger, J. C.; Navrotsky, A., Thermochemistry of Paddle Wheel MOFs: Cu-HKUST-1 and Zn-HKUST-1. *Langmuir* **2013,** *29* (25), 8140-8145.

73. Goyal, P.; Paruthi, A.; Menon, D.; Behara, R.; Jaiswal, A.; V, K.; Kumar, A.; Krishnan, V.; Misra, S. K., Fe doped bimetallic HKUST-1 MOF with enhanced water stability for trapping Pb(II) with high adsorption capacity. *Chemical Engineering Journal* **2021**, 133088.

74. Ru, J.; Wang, X.; Wang, F.; Cui, X.; Du, X.; Lu, X., UiO series of metal-organic frameworks composites as advanced sorbents for the removal of heavy metal ions: Synthesis, applications and adsorption mechanism. *Ecotoxicology and Environmental Safety* **2021,** *208*, 111577.

75. Han, Y.; Yang, H.; Guo, X., Synthesis Methods and Crystallization of MOFs. 2020.

76. Stock, N.; Biswas, S., Synthesis of Metal-Organic Frameworks (MOFs): Routes to Various MOF Topologies, Morphologies, and Composites. *Chemical Reviews* **2012,** *112* (2), 933-969.

77. Raptopoulou, C. P., Metal-Organic Frameworks: Synthetic Methods and Potential Applications. *Materials* **2021,** *14* (2).

78. Bian, Y.; Xiong, N.; Zhu, G., Technology for the Remediation of Water Pollution: A Review on the Fabrication of Metal Organic Frameworks. *Processes* **2018,** *6* (8).

79. Klinowski, J.; Almeida Paz, F. A.; Silva, P.; Rocha, J., Microwave-Assisted Synthesis of Metal–Organic Frameworks. *Dalton Transactions* **2011,** *40* (2), 321-330.

80. Zhao, Z.; Li, H.; Zhao, K.; Wang, L.; Gao, X., Microwave-assisted synthesis of MOFs: Rational design via numerical simulation. *Chemical Engineering Journal* **2022,** *428*, 131006.

81. Morsali, A.; Hashemi, L., Chapter Two - Nanoscale coordination polymers: Preparation, function and application. In *Advances in Inorganic Chemistry*, Ruiz-Molina, D.; van Eldik, R., Eds. Academic Press: 2020; Vol. 76, pp 33-72.

82. Grewal, A.; Kumar, K.; Redhu, S.; Bhardwaj, S., Microwave assisted synthesis: a green chemistry approach. *International Research Journal of Pharmaceutical and Applied Sciences* **2013,** *3*, 278-285.

83. Kharissova, O. V.; Kharisov, B. I.; Oliva González, C. M.; Méndez, Y. P.; López, I., Greener synthesis of chemical compounds and materials. *Royal Society Open Science 6* (11), 191378.

84. Xu, H.; Zeiger, B. W.; Suslick, K. S., Sonochemical synthesis of nanomaterials. *Chemical Society Reviews* **2013,** *42* (7), 2555-2567.

85. Bang, J. H.; Suslick, K. S., Applications of Ultrasound to the Synthesis of Nanostructured Materials. *Advanced Materials* **2010,** *22* (10), 1039-1059.

86. Al-Kutubi, H.; Gascon, J.; Sudhölter, E. J. R.; Rassaei, L., Electrosynthesis of Metal–Organic Frameworks: Challenges and Opportunities. *ChemElectroChem* **2015,** *2* (4), 462-474.

87. M. V, V.; Nageswaran, G., Review—Direct Electrochemical Synthesis of Metal Organic Frameworks. *Journal of The Electrochemical Society* **2020,** *167* (15), 155527.

88. Ghoorchian, A.; Afkhami, A.; Madrakian, T.; Ahmadi, M., Chapter 9 - Electrochemical synthesis of MOFs. In *Metal-Organic Frameworks for Biomedical Applications*, Mozafari, M., Ed. Woodhead Publishing: 2020; pp 177-195.

89. Tanaka, S., Chapter 10 - Mechanochemical synthesis of MOFs. In *Metal-Organic Frameworks for Biomedical Applications*, Mozafari, M., Ed. Woodhead Publishing: 2020; pp 197-222.

90. Szczęśniak, B.; Borysiuk, S.; Choma, J.; Jaroniec, M., Mechanochemical synthesis of highly porous materials. *Materials Horizons* **2020,** *7* (6), 1457-1473.

91. Chen, D.; Zhao, J.; Zhang, P.; Dai, S., Mechanochemical synthesis of metal–organic frameworks. *Polyhedron* **2019,** *162*, 59-64.

92. Yan, Y., 7 - Tribology and tribo-corrosion testing and analysis of metallic biomaterials. In *Metals for Biomedical Devices*, Niinomi, M., Ed. Woodhead Publishing: 2010; pp 178-201.

93. Vernon-Parry, K. D., Scanning electron microscopy: an introduction. *III-Vs Review* **2000,** *13* (4), 40-44.

94. Rani, M.; Keshu; Shanker, U., Chapter 3 - Green nanomaterials: An overview. In *Green Functionalized Nanomaterials for Environmental Applications*, Shanker, U.; Hussain, C. M.; Rani, M., Eds. Elsevier: 2022; pp 43-80.

95. Mohamed Shameer, P.; Mohamed Nishath, P., Chapter 8 - Exploration and enhancement on fuel stability of biodiesel: A step forward in the track of global commercialization. In *Advanced Biofuels*, Azad, A. K.; Rasul, M., Eds. Woodhead Publishing: 2019; pp 181-213.

96. Sindhu, R.; Binod, P.; Pandey, A., Chapter 17 - Microbial Poly-3-Hydroxybutyrate and Related Copolymers. In *Industrial Biorefineries & White Biotechnology*, Pandey, A.; Höfer, R.; Taherzadeh, M.; Nampoothiri, K. M.; Larroche, C., Eds. Elsevier: Amsterdam, 2015; pp 575-605.

97. Carta, M., Gas Separation. 2015; pp 852-855.

98. Rosi, N. L.; Eckert, J.; Eddaoudi, M.; Vodak, D. T.; Kim, J.; O'Keeffe, M.; Yaghi, O. M., Hydrogen storage in microporous metal-organic frameworks. *Science* **2003,** *300* (5622), 1127-9.

99. Sculley, J.; Yuan, D.; Zhou, H.-C., The current status of hydrogen storage in metal–organic frameworks—updated. *Energy & Environmental Science* **2011,** *4* (8), 2721-2735.

100. Wong-Foy, A. G.; Matzger, A. J.; Yaghi, O. M., Exceptional H2 Saturation Uptake in Microporous Metal−Organic Frameworks. *Journal of the American Chemical Society* **2006,** *128* (11), 3494-3495.

101. Rowsell, J. L. C.; Millward, A. R.; Park, K. S.; Yaghi, O. M., Hydrogen Sorption in Functionalized Metal−Organic Frameworks. *Journal of the American Chemical Society* **2004,** *126* (18), 5666-5667.

102. Dincă, M.; Dailly, A.; Liu, Y.; Brown, C. M.; Neumann, D. A.; Long, J. R., Hydrogen Storage in a Microporous Metal−Organic Framework with Exposed Mn2+ Coordination Sites. *Journal of the American Chemical Society* **2006,** *128* (51), 16876-16883.

103. Ma, T.; Li, H.; Ma, J.-G.; Cheng, P., Application of MOF-based materials in electrochemical sensing. *Dalton Transactions* **2020,** *49* (47), 17121-17129.

104. Ma, B.; Guo, H.; Wang, M.; Li, L.; Jia, X.; Chen, H.; Xue, R.; Yang, W., Electrocatalysis of Cu−MOF/Graphene Composite and its Sensing Application for Electrochemical Simultaneous Determination of Dopamine and Paracetamol. *Electroanalysis* **2019,** *31* (6), 1002-1008.

105. He, S.; Wu, L.; Li, X.; Sun, H.; Xiong, T.; Liu, J.; Huang, C.; Xu, H.; Sun, H.; Chen, W.; Gref, R.; Zhang, J., Metal-organic frameworks for advanced drug delivery. *Acta Pharmaceutica Sinica B* **2021,** *11* (8), 2362-2395.

106. Abánades Lázaro, I.; Forgan, R. S., Application of zirconium MOFs in drug delivery and biomedicine. *Coordination Chemistry Reviews* **2019,** *380*, 230-259.

107. Pham, H.; Ramos, K.; Sua, A.; Acuna, J.; Slowinska, K.; Nguyen, T.; Bui, A.; Weber, M. D. R.; Tian, F., Tuning Crystal Structures of Iron-Based Metal-Organic Frameworks for Drug Delivery Applications. *ACS Omega* **2020,** *5* (7), 3418-3427.

108. Li, H.-Y.; Zhao, S.-N.; Zang, S.-Q.; Li, J., Functional metal–organic frameworks as effective sensors of gases and volatile compounds. *Chemical Society Reviews* **2020,** *49* (17), 6364-6401.

109. Kumar, P.; Deep, A.; Kim, K.-H., Metal organic frameworks for sensing applications. *TrAC Trends in Analytical Chemistry* **2015,** *73*, 39-53.

110. Dong, J.; Zhao, D.; Lu, Y.; Sun, W.-Y., Photoluminescent metal–organic frameworks and their application for sensing biomolecules. *Journal of Materials Chemistry A* **2019,** *7* (40), 22744-22767.

111. Zhang, H.; Chen, S.; Zhang, H.; Fan, X.; Gao, C.; Yu, H.; Quan, X., Carbon nanotubes-incorporated MIL-88B-Fe as highly efficient Fenton-like catalyst for degradation of organic pollutants. *Frontiers of Environmental Science & Engineering* **2019,** *13* (2), 18.

112. Zhong, G.; Liu, D.; Zhang, J., Applications of Porous Metal–Organic Framework MIL-100(M) (M = Cr, Fe, Sc, Al, V). *Crystal Growth & Design* **2018,** *18* (12), 7730-7744.

113. Millange, F.; Walton, R. I., MIL-53 and its Isoreticular Analogues: a Review of the Chemistry and Structure of a Prototypical Flexible Metal-Organic Framework. *Israel Journal of Chemistry* **2018,** *58* (9-10), 1019-1035.

114. Xuan Huynh, N. T.; Chihaia, V.; Son, D. N., Hydrogen storage in MIL-88 series. *Journal of Materials Science* **2019,** *54* (5), 3994-4010.

115. Li, X.; Guo, W.; Liu, Z.; Wang, R.; Liu, H., Fe-based MOFs for efficient adsorption and degradation of acid orange 7 in aqueous solution via persulfate activation. *Applied Surface Science* **2016,** *369*, 130-136.

116. Geng, N.; Chen, W.; Xu, H.; Ding, M.; Lin, T.; Wu, Q.; Zhang, L., Insights into the novel application of Fe-MOFs in ultrasound-assisted heterogeneous Fenton system: Efficiency, kinetics and mechanism. *Ultrasonics Sonochemistry* **2021,** *72*, 105411.

117. Hou, S.; Wu, Y.-n.; Feng, L.; Chen, W.; Wang, Y.; Morlay, C.; Li, F., Green synthesis and evaluation of an iron-based metal–organic framework MIL-88B for efficient decontamination of arsenate from water. *Dalton Transactions* **2018,** *47* (7), 2222-2231.

118. Vu, T.; Le, G.; Vũ Thị, H.; Nguyen, K.; Quan, T.; quang, n.; Tran, H.; Phuong, D.; Loi, V.; Lee, G., Highly photocatalytic activity of novel Fe-MIL-88B/GO nanocomposite in the degradation of reactive dye from aqueous solution. *Materials Research Express* **2017,** *4*.

119. Zhang, H.; Gong, X.; Song, Z.; Zhang, S.; Du, W.; Nguyen, T. T.; Guo, M.; Gao, X., Wood-based carbon quantum dots for enhanced photocatalysis of MIL-88B(Fe). *Optical Materials* **2021,** *113*, 110865.

120. J. Kepert, C.; J. Rosseinsky, M., Zeolite-like crystal structure of an empty microporous molecular framework. *Chemical Communications* **1999,** (4), 375-376.

121. Alhamami, M.; Doan, H.; Cheng, C.-H., A Review on Breathing Behaviors of Metal-Organic-Frameworks (MOFs) for Gas Adsorption. *Materials* **2014,** *7*.

122. Serre, C.; Mellot-Draznieks, C.; Surblé, S.; Audebrand, N.; Filinchuk, Y.; Férey, G., Role of solvent-host interactions that lead to very large swelling of hybrid frameworks. *Science* **2007,** *315* (5820), 1828-31.

123. Horcajada, P.; Salles, F.; Wuttke, S.; Devic, T.; Heurtaux, D.; Maurin, G.; Vimont, A.; Daturi, M.; David, O.; Magnier, E.; Stock, N.; Filinchuk, Y.; Popov, D.; Riekel, C.; Férey, G.; Serre, C., How Linker's Modification Controls Swelling Properties of Highly Flexible Iron(III) Dicarboxylates MIL-88. *Journal of the American Chemical Society* **2011,** *133* (44), 17839-17847.

124. Pham, H.; Ramos, K.; Sua, A.; Acuna, J.; Slowinska, K.; Nguyen, T.; Bui, A.; Weber, M. D. R.; Tian, F., Tuning Crystal Structures of Iron-Based Metal–Organic Frameworks for Drug Delivery Applications. *ACS Omega* **2020,** *5* (7), 3418-3427.

125. Zhao, J.; Yin, F.; Ji, L.; Wang, C.; Shi, C.; Liu, X.; Yang, H.; Wang, X.; Kong, L., Development of a Tau-Targeted Drug Delivery System Using a Multifunctional Nanoscale Metal–Organic Framework for Alzheimer's Disease Therapy. *ACS Applied Materials & Interfaces* **2020,** *12* (40), 44447-44458.

126. Sivakumar, P.; Priyatharshni, S.; Nagashanmugam, K. B.; Thanigaivelan, A.; Kumar, K., Chitosan capped nanoscale Fe-MIL-88B-NH2 metal-organic framework as drug carrier material for the pH responsive delivery of doxorubicin. *Materials Research Express* **2017,** *4* (8), 085023.

127. Zango, Z. U.; Sambudi, N. S.; Jumbri, K.; Abu Bakar, N. H. H.; Saad, B., Removal of Pyrene from Aqueous Solution Using Fe-based Metal-organic Frameworks. *IOP Conference Series: Earth and Environmental Science* **2020,** *549* (1), 012061.

128. Maksimchuk, N.; Zalomaeva, O.; Skobelev, I.; Kovalenko, K.; Fedin, V.; Kholdeeva, O., ChemInform Abstract: Metal-Organic Frameworks of the MIL-101 Family as Heterogeneous Single-Site Catalysts. *Proceedings of The Royal Society A Mathematical Physical and Engineering Sciences* **2012,** *468*, 2017-2034.

129. Zhang, X.; Li, F.; Ren, J.; Feng, H.; Hou, X.; Ma, C., Synthesis of Metal Organic Framework Material MIL-101. *IOP Conference Series: Earth and Environmental Science* **2019,** *295* (3), 032022.

130. Sun, J.; Yu, G.; Huo, Q.; Kan, Q.; Guan, J., Epoxidation of styrene over Fe(Cr)-MIL-101 metal–organic frameworks. *RSC Adv.* **2014,** *4*.

131. Hong, D.-Y.; Hwang, Y. K.; Serre, C.; Férey, G.; Chang, J.-S., Porous Chromium Terephthalate MIL-101 with Coordinatively Unsaturated Sites: Surface Functionalization, Encapsulation, Sorption and Catalysis. *Advanced Functional Materials* **2009,** *19* (10), 1537-1552.

132. Bhattacharjee, S.; Chen, C.; Ahn, W.-S., Chromium terephthalate metal–organic framework MIL-101: synthesis, functionalization, and applications for adsorption and catalysis. *RSC Advances* **2014,** *4* (94), 52500-52525.

133. Tang, J.; Yang, M.; Yang, M.; Wang, J.; Dong, W.; Wang, G., Heterogeneous Fe-MIL-101 catalysts for efficient one-pot four-component coupling synthesis of highly substituted pyrroles. *New Journal of Chemistry* **2015,** *39* (6), 4919-4923.

134. Niknam, E.; Panahi, F.; Daneshgar, F.; Bahrami, F.; Khalafi-Nezhad, A., Metal–Organic Framework MIL-101(Cr) as an Efficient Heterogeneous Catalyst for Clean Synthesis of Benzoazoles. *ACS Omega* **2018,** *3* (12), 17135-17144.

135. Kim, D.-W.; Kim, H.-G.; Cho, D.-H., Catalytic performance of MIL-100 (Fe, Cr) and MIL-101 (Fe, Cr) in the isomerization of endo- to exo-dicyclopentadiene. *Catalysis Communications* **2016,** *73*, 69-73.

136. Vu, T. A.; Le, G. H.; Dao, C. D.; Dang, L. Q.; Nguyen, K. T.; Dang, P. T.; Tran, H. T. K.; Duong, Q. T.; Nguyen, T. V.; Lee, G. D., Isomorphous substitution of Cr by Fe in MIL-101 framework and its application as a novel heterogeneous photo-Fenton catalyst for reactive dye degradation. *RSC Advances* **2014,** *4* (78), 41185-41194.

137. Hartmann, M.; Fischer, M., Amino-functionalized basic catalysts with MIL-101 structure. *Microporous and Mesoporous Materials* **2012,** *164*, 38-43.

138. Barbosa, A. D. S.; Julião, D.; Fernandes, D. M.; Peixoto, A. F.; Freire, C.; de Castro, B.; Granadeiro, C. M.; Balula, S. S.; Cunha-Silva, L., Catalytic performance and electrochemical behaviour of Metal–organic frameworks: MIL-101(Fe) versus NH2-MIL-101(Fe). *Polyhedron* **2017,** *127*, 464-470.

139. Chen, M.-L.; Lu, T.-H.; Long, L.-L.; Xu, Z.; Ding, L.; Cheng, Y.-H., NH2-Fe-MILs for effective adsorption and Fenton-like degradation of imidacloprid: Removal performance and mechanism investigation. *Environmental Engineering Research* **2022,** *27* (2), 200702-0.

140. Zhao, F.; Liu, Y.; Hammouda, S. B.; Doshi, B.; Guijarro, N.; Min, X.; Tang, C.-J.; Sillanpää, M.; Sivula, K.; Wang, S., MIL-101(Fe)/g-C3N4 for enhanced visible-light-driven photocatalysis toward simultaneous reduction of Cr(VI) and oxidation of bisphenol A in aqueous media. *Applied Catalysis B: Environmental* **2020,** *272*, 119033.

141. Yan, D.; Hu, H.; Gao, N.; Ye, J.; Ou, H., Fabrication of carbon nanotube functionalized MIL-101(Fe) for enhanced visible-light photocatalysis of ciprofloxacin in aqueous solution. *Applied Surface Science* **2019,** *498*, 143836.

142. Günduğar, K.; Semerci, F., Compositing of MIL-101(Fe) with reduced graphene oxide and polyaniline for capacitive energy storage. *Materials Chemistry and Physics* **2022,** *278*, 125641.

143. Lee, S.-J.; Yoon, J. W.; Seo, Y.-K.; Kim, M.-B.; Lee, S.-K.; Lee, U. H.; Hwang, Y. K.; Bae, Y.-S.; Chang, J.-S., Effect of purification conditions on gas storage and separations in a chromium-based metal–organic framework MIL-101. *Microporous and Mesoporous Materials* **2014,** *193*, 160-165.

144. Chong, K. C.; Ho, P. S.; Lai, S. O.; Lee, S. S.; Lau, W. J.; Lu, S.-Y.; Ooi, B. S., Solvent-Free Synthesis of MIL-101(Cr) for CO2 Gas Adsorption: The Effect of Metal Precursor and Molar Ratio. *Sustainability* **2022,** *14* (3).

145. Liu, Q.; Ning, L.; Zheng, S.; Tao, M.; Shi, Y.; He, Y., Adsorption of Carbon Dioxide by MIL-101(Cr): Regeneration Conditions and Influence of Flue Gas Contaminants. *Scientific Reports* **2013,** *3* (1), 2916.

146. Hong, W. Y.; Perera, S. P.; Burrows, A. D., Comparison of MIL-101(Cr) metal-organic framework and 13X zeolite monoliths for CO2 capture. *Microporous and Mesoporous Materials* **2020,** *308*, 110525.

147. Joshi, J. N.; Zhu, G.; Lee, J. J.; Carter, E. A.; Jones, C. W.; Lively, R. P.; Walton, K. S., Probing Metal–Organic Framework Design for Adsorptive Natural Gas Purification. *Langmuir* **2018,** *34* (29), 8443-8450.

148. Ren, J.; Musyoka, N. M.; Langmi, H. W.; Segakweng, T.; North, B. C.; Mathe, M.; Kang, X., Modulated synthesis of chromium-based metal-organic framework (MIL-101) with enhanced hydrogen uptake. *International Journal of Hydrogen Energy* **2014,** *39* (23), 12018-12023.

149. Klyamkin, S. N.; Chuvikov, S. V.; Maletskaya, N. V.; Kogan, E. V.; Fedin, V. P.; Kovalenko, K. A.; Dybtsev, D. N., High-pressure hydrogen storage on modified MIL-101 metal–organic framework. *International Journal of Energy Research* **2014,** *38* (12), 1562-1570.

150. Ghoufi, A.; Deschamps, J.; Maurin, G., Theoretical Hydrogen Cryostorage in Doped MIL-101(Cr) Metal–Organic Frameworks. *The Journal of Physical Chemistry C* **2012,** *116* (19), 10504-10509.

151. Karikkethu Prabhakaran, P.; Deschamps, J., Hydrogen adsorption in lithium doped MIL-101 and MIL-53(Al) at 77 and 298 K up to 100 bar: effect of lithium concentration. *Journal of Porous Materials* **2015,** *22* (4), 1073-1081.

152. Yurduşen, A.; Yürüm, A.; Yürüm, Y., Engineering MIL-88B crystallites for enhanced H2 uptake capacity: The role of ultramicropores. *International Journal of Energy Research* **2020,** *44* (4), 2875-2888.

153. Huynh, N. T. X.; Chihaia, V.; Son, D. N., Enhancing hydrogen storage by metal substitution in MIL-88A metal-organic framework. *Adsorption* **2020,** *26* (4), 509-519.

154. Al-Othman, A.; Tawalbeh, M.; Temsah, O.; Al Murisi, M., Industrial Challenges of MOFs in Energy Applications. 2021; pp 1-8.

155. He, Q.; Zhan, F.; Wang, H.; Xu, W.; Wang, H.; Chen, L., Recent progress of industrial preparation of metal–organic frameworks: synthesis strategies and outlook. *Materials Today Sustainability* **2022,** *17*, 100104.

156. Ma, Q.; Zhang, T.; Wang, B., Shaping of metal-organic frameworks, a critical step toward industrial applications. *Matter* **2022,** *5* (4), 1070-1091.

157. Chai, W.; Shen, Y.; Wang, J.; Zhang, G., Applications of Metal-Organic Framework Materials. *Journal of Physics: Conference Series* **2022,** *2194* (1), 012014.

158. Zhang, L.; Liand, F.; Luo, L., Preparation Methods of Metal Organic Frameworks and Their Capture of CO2. *IOP Conference Series: Earth and Environmental Science* **2018,** *108*, 042104.

159. Dyosiba, X.; Ren, J.; Musyoka, N. M.; Langmi, H. W.; Mathe, M.; Onyango, M. S., Feasibility of Varied Polyethylene Terephthalate Wastes as a Linker Source in Metal–Organic Framework UiO-66(Zr) Synthesis. *Industrial & Engineering Chemistry Research* **2019,** *58* (36), 17010-17016.

160. DOAN VAN HUAN, V. T., Use of waste TPA in the synthesis of a metal organic framework (MOF) for use in hydrogen storage. In *Scientific conference on Oil Refining and Pertrochemical Engineering (ORPE 2014)*, Hanoi, Vietnam, 2014; pp pp. 47-53.

161. Rambau, K. M.; Musyoka, N. M.; Panek, R.; Franus, W.; Wdowin, M.; Manyala, N., Preparation of coal fly ash derived metal organic frameworks and their carbon derivatives. *Materials Today Communications* **2021,** *27*, 102433.

162. Perez, E.; Andre, M.-L.; Navarro Amador, R.; Hyvrard, F.; Borrini, J.; Carboni, M.; Meyer, D., Recovery of metals from simulant spent lithium-ion battery as organophosphonate coordination polymers in aqueous media. *Journal of Hazardous Materials* **2016,** *317*, 617-621.

163. Perez, E.; Navarro Amador, R.; Carboni, M.; Meyer, D., In-situ precipitation of Metal–Organic Frameworks from a simulant battery waste solution. *Materials Letters* **2016,** *167*, 188-191.

164. Kaur, R.; Marwaha, A.; Chhabra, V. A.; Kaushal, K.; Kim, K.-H.; Tripathi, S. K., Facile synthesis of a Cu-based metal-organic framework from plastic waste and its application as a sensor for acetone. *Journal of Cleaner Production* **2020,** *263*, 121492.

165. Dyosiba, X.; Ren, J.; Musyoka, N. M.; Langmi, H. W.; Mathe, M.; Onyango, M. S., Preparation of value-added metal-organic frameworks (MOFs) using waste PET bottles as source of acid linker. *Sustainable Materials and Technologies* **2016,** *10*, 10-13.

166. Ren, J.; Dyosiba, X.; Musyoka, N. M.; Langmi, H. W.; North, B. C.; Mathe, M.; Onyango, M. S., Green synthesis of chromium-based metal-organic framework (Cr-MOF) from waste polyethylene terephthalate (PET) bottles for hydrogen storage applications. *International Journal of Hydrogen Energy* **2016,** *41* (40), 18141-18146.

167. El-Sayed, E.-S. M.; Yuan, D., Waste to MOFs: sustainable linker, metal, and solvent sources for value-added MOF synthesis and applications. *Green Chemistry* **2020,** *22* (13), 4082-4104.

168. Lo, S.-H.; Senthil Raja, D.; Chen, C.-W.; Kang, Y.-H.; Chen, J. J.; Lin, C.-H., Waste polyethylene terephthalate (PET) materials as sustainable precursors for the synthesis of nanoporous MOFs, MIL-47, MIL-53(Cr, Al, Ga) and MIL-101(Cr). *Dalton Trans.* **2016,** *45*.

169. Deleu, W. P. R.; Stassen, I.; Jonckheere, D.; Ameloot, R.; De Vos, D. E., Waste PET (bottles) as a resource or substrate for MOF synthesis. *Journal of Materials Chemistry A* **2016,** *4* (24), 9519-9525.

170. Rambau, K.; Musyoka, N. M.; Palaniyandy, N.; Manyala, N., Manganese-Based Metal Organic Framework from Spent Li-Ion Batteries and its Electrochemical Performance as Anode Material in Li-ion Battery. *Journal of The Electrochemical Society* **2021,** *168* (1), 010527.

171. Cognet, M.; Condomines, J.; Cambedouzou, J.; Madhavi, S.; Carboni, M.; Meyer, D., An original recycling method for Li-ion batteries through large scale production of Metal Organic Frameworks. *Journal of Hazardous Materials* **2020,** *385*, 121603.

172. Johnson, D. B.; Hallberg, K. B., Acid mine drainage remediation options: a review. *Science of The Total Environment* **2005,** *338* (1), 3-14.

173. Das, P., Phytoremediation and Nanoremediation : Emerging Techniques for Treatment of Acid Mine Drainage Water. *Defence Life Science Journal* **2018,** *3*.

174. Mokgehle, T. M.; Tavengwa, N. T., Recent developments in materials used for the removal of metal ions from acid mine drainage. *Applied Water Science* **2021,** *11* (2), 42.

175. Norton, P. J., The control of acid mine drainage with Wetlands. *Mine Water and the Environment* **1992,** *11* (3), 27-34.

176. Masindi, V.; Osman, M. S.; Shingwenyana, R., Valorization of acid mine drainage (AMD): A simplified approach to reclaim drinking water and synthesize valuable minerals – Pilot study. *Journal of Environmental Chemical Engineering* **2019,** *7* (3), 103082.

177. Masindi, V.; Tekere, M., Innovative Routes for Acid Mine Drainage (AMD) Valorization. 2020; pp 189-218.

178. Netinger Grubeša, I.; Barišić, I.; Fucic, A.; Bansode, S. S., 3 - Environmental impact of ferrous slag usage in civil engineering. In *Characteristics and Uses of Steel Slag in Building Construction*, Netinger Grubeša, I.; Barišić, I.; Fucic, A.; Bansode, S. S., Eds. Woodhead Publishing: 2016; pp 31-50.

179. Egiebor, N.; Oni, B., Acid Rock Drainage Formation and Treatment: A Review. *Asia-Pacific Journal of Chemical Engineering* **2007,** *2*, 47-62.

180. Dold, B., Evolution of Acid Mine Drainage Formation in Sulphidic Mine Tailings. *Minerals* **2014,** *4* (3), 621-641.

181. Florence, K.; Sapsford, D. J.; Johnson, D. B.; Kay, C. M.; Wolkersdorfer, C., Iron-mineral accretion from acid mine drainage and its application in passive treatment. *Environmental Technology* **2016,** *37* (11), 1428-1440.

182. Nleya, Y.; Simate, G. S.; Ndlovu, S., Sustainability assessment of the recovery and utilisation of acid from acid mine drainage. *Journal of Cleaner Production* **2016,** *113*, 17-27.

183. Simate, G. S.; Ndlovu, S., Acid mine drainage: Challenges and opportunities. *Journal of Environmental Chemical Engineering* **2014,** *2* (3), 1785-1803.

184. Masindi, V.; Akinwekomi, V.; Maree, J. P.; Muedi, K. L., Comparison of mine water neutralisation efficiencies of different alkaline generating agents. *Journal of Environmental Chemical Engineering* **2017,** *5* (4), 3903-3913.

185. Seo, E. Y.; Cheong, Y. W.; Yim, G. J.; Min, K. W.; Geroni, J. N., Recovery of Fe, Al and Mn in acid coal mine drainage by sequential selective precipitation with control of pH. *CATENA* **2017,** *148*, 11-16.

186. Akinwekomi, V.; Maree, J. P.; Masindi, V.; Zvinowanda, C.; Osman, M. S.; Foteinis, S.; Mpenyana-Monyatsi, L.; Chatzisymeon, E., Beneficiation of acid mine drainage (AMD): A viable option for the synthesis of goethite, hematite, magnetite, and gypsum – Gearing towards a circular economy concept. *Minerals Engineering* **2020,** *148*, 106204.

187. Flores, R. G.; Andersen, S. L. F.; Maia, L. K. K.; José, H. J.; Moreira, R. d. F. P. M., Recovery of iron oxides from acid mine drainage and their application as adsorbent or catalyst. *Journal of Environmental Management* **2012,** *111*, 53-60.

188. Li, B.; Wang, H.; Chen, B., Microporous Metal–Organic Frameworks for Gas Separation. *Chemistry – An Asian Journal* **2014,** *9* (6), 1474-1498.

189. Akcil, A.; Agcasulu, I.; Swain, B., Valorization of waste LCD and recovery of critical raw material for circular economy: A review. *Resources, Conservation and Recycling* **2019,** *149*, 622-637.

190. Wei, X.; Viadero, R. C., Synthesis of magnetite nanoparticles with ferric iron recovered from acid mine drainage: Implications for environmental engineering. *Colloids and Surfaces A: Physicochemical and Engineering Aspects* **2007,** *294* (1), 280-286.

191. Wei, X.; Viadero, R. C.; Buzby, K. M., Recovery of Iron and Aluminum from Acid Mine Drainage by Selective Precipitation. *Environmental Engineering Science* **2005,** *22* (6), 745-755.

192. Du, P. D.; Thanh, H. T. M.; To, T. C.; Thang, H. S.; Tinh, M. X.; Tuyen, T. N.; Hoa, T. T.; Khieu, D. Q., Metal-Organic Framework MIL-101: Synthesis and Photocatalytic Degradation of Remazol Black B Dye. *Journal of Nanomaterials* **2019,** *2019*, 6061275.

193. Skobelev, I. Y.; Sorokin, A. B.; Kovalenko, K. A.; Fedin, V. P.; Kholdeeva, O. A., Solvent-free allylic oxidation of alkenes with O2 mediated by Fe- and Cr-MIL-101. *Journal of Catalysis* **2013,** *298*, 61-69.

194. Gabbott, P., *Principles and Applications of Thermal Analysis*. Wiley: 2008.

195. Loganathan, S.; Valapa, R. B.; Mishra, R. K.; Pugazhenthi, G.; Thomas, S., Chapter 4 - Thermogravimetric Analysis for Characterization of Nanomaterials. In *Thermal and Rheological Measurement Techniques for Nanomaterials Characterization*, Thomas, S.; Thomas, R.; Zachariah, A. K.; Mishra, R. K., Eds. Elsevier: 2017; pp 67-108.

196. Gomes, J.; Batra, J.; Chopda, V. R.; Kathiresan, P.; Rathore, A. S., Chapter 25 - Monitoring and Control of Bioethanol Production From Lignocellulosic Biomass. In *Waste*

Biorefinery, Bhaskar, T.; Pandey, A.; Mohan, S. V.; Lee, D.-J.; Khanal, S. K., Eds. Elsevier: 2018; pp 727-749.

197. Borghetti, G. S.; Carini, J. P.; Honorato, S. B.; Ayala, A. P.; Moreira, J. C. F.; Bassani, V. L., Physicochemical properties and thermal stability of quercetin hydrates in the solid state. *Thermochimica Acta* **2012,** *539*, 109-114.

198. Chauhan, A.; Chauhan, P., Powder XRD Technique and its Applications in Science and Technology. *Journal of analytical and bioanalytical techniques* **2014,** *5*, 1-5.

199. Vogt, F. G.; Williams, G. R., Advanced Approaches to Effective Solid-State Analysis: X-Ray Diffraction, Vibrational Spectroscopy and Solid-State NMR. *ChemInform* **2011,** *42*.

200. Elzwawi, S. Cathodic Arc Zinc Oxide for Active Electronic Devices. 2015.

201. Berna, F., Fourier Transform Infrared Spectroscopy (FTIR). In *Encyclopedia of Geoarchaeology*, Gilbert, A. S., Ed. Springer Netherlands: Dordrecht, 2017; pp 285-286.

202. Jaggi, N.; Vij, D. R., FOURIER TRANSFORM INFRARED SPECTROSCOPY. In *Handbook of Applied Solid State Spectroscopy*, Vij, D. R., Ed. Springer US: Boston, MA, 2006; pp 411-450.

203. Patrizi, B.; Cumis, S.; Viciani; D'Amato, Dioxin and Related Compound Detection: Perspectives for Optical Monitoring. *International Journal of Molecular Sciences* **2019,** *20*, 2671.

204. Khare, T.; Oak, U.; Shriram, V.; Verma, S. K.; Kumar, V., Chapter Ten - Biologically synthesized nanomaterials and their antimicrobial potentials. In *Comprehensive Analytical Chemistry*, Verma, S. K.; Das, A. K., Eds. Elsevier: 2019; Vol. 87, pp 263-289.

205. Cengiz, T., Scanning Electron Microscopy. In *Electron Microscopy*, Mohsen, M., Ed. IntechOpen: Rijeka, 2022; p Ch. 1.

206. Abdullah, A.; Mohammed, A., *Scanning Electron Microscopy (SEM): A Review*. 2019.

207. Donohue, M.; Aranovich, G. L., Classification of Gibbs adsorption isotherms. *Advances in Colloid and Interface Science* **1998,** *76*, 137-152.

208. Ambroz, F.; Macdonald, T. J.; Martis, V.; Parkin, I. P., Evaluation of the BET Theory for the Characterization of Meso and Microporous MOFs. *Small Methods* **2018,** *2* (11), 1800173.

209. Fadley, C. S., X-ray photoelectron spectroscopy: Progress and perspectives. *Journal of Electron Spectroscopy and Related Phenomena* **2010,** *178-179*, 2-32.

210. Engelhard, M. H.; Droubay, T. C.; Du, Y., X-Ray Photoelectron Spectroscopy Applications. In *Encyclopedia of Spectroscopy and Spectrometry (Third Edition)*, Lindon, J. C.; Tranter, G. E.; Koppenaal, D. W., Eds. Academic Press: Oxford, 2017; pp 716-724.

211. Guy, O. J.; Walker, K.-A. D., Chapter 4 - Graphene Functionalization for Biosensor Applications. In *Silicon Carbide Biotechnology (Second Edition)*, Saddow, S. E., Ed. Elsevier: 2016; pp 85-141.

212. Baer, D. R.; Thevuthasan, S., Chapter 16 - Characterization of Thin Films and Coatings. In *Handbook of Deposition Technologies for Films and Coatings (Third Edition)*, Martin, P. M., Ed. William Andrew Publishing: Boston, 2010; pp 749-864.

213. Briggs, D., Handbook of X-ray Photoelectron Spectroscopy C. D. Wanger, W. M. Riggs, L. E. Davis, J. F. Moulder and G. E.Muilenberg Perkin-Elmer Corp., Physical Electronics Division, Eden Prairie, Minnesota, USA, 1979. 190 pp. $195. *Surface and Interface Analysis* **1981,** *3* (4), v-v.

214. Kriesten, M.; Vargas Schmitz, J.; Siegel, J.; Smith, C. E.; Kaspereit, M.; Hartmann, M., Shaping of Flexible Metal-Organic Frameworks: Combining Macroscopic Stability and Framework Flexibility. *European Journal of Inorganic Chemistry* **2019,** *2019* (43), 4700-4709.

215. Zhang, F.; Chen, S.; Nie, S.; Luo, J.; Lin, S.; Wang, Y.; Yang, H., Waste PET as a Reactant for Lanthanide MOF Synthesis and Application in Sensing of Picric Acid. *Polymers (Basel)* **2019,** *11* (12), 2015.

216. Huang, Y.-T.; Lai, Y.-L.; Lin, C.-H.; Wang, S.-L., Direct use of waste PET as unfailing source of organic reagents in the synthesis of intrinsic white/yellow luminescent nanoporous zincophosphates. *Green Chemistry* **2011,** *13* (8), 2000-2003.

217. Lo, S.-H.; Senthil Raja, D.; Chen, C.-W.; Kang, Y.-H.; Chen, J.-J.; Lin, C.-H., Waste polyethylene terephthalate (PET) materials as sustainable precursors for the synthesis of nanoporous MOFs, MIL-47, MIL-53(Cr, Al, Ga) and MIL-101(Cr). *Dalton Transactions* **2016,** *45* (23), 9565-9573.

218. Menezes, J. C. S. S.; Silva, R. A.; Arce, I. S.; Schneider, I. A. H., Production of a Poly-ferric Sulphate Chemical Coagulant by Selective Precipitation of Iron from Acidic Coal Mine Drainage. *Mine Water and the Environment* **2009,** *28* (4), 311.

219. Silva, R.; Menezes, J.; Lopes, F. c.; Kirchheim, A.; Schneider, I., Synthesis of a Goethite Pigment by Selective Precipitation of Iron from Acidic Coal Mine Drainage. *Mine Water and the Environment* **2017**.

220. Flak, D.; Chen, Q.; Mun, B. S.; Liu, Z.; Rękas, M.; Braun, A., In situ ambient pressure XPS observation of surface chemistry and electronic structure of α-Fe2O3 and γ-Fe2O3 nanoparticles. *Applied Surface Science* **2018,** *455*, 1019-1028.

221. Yamashita, T.; Hayes, P., Analysis of XPS spectra of Fe2+ and Fe3+ ions in oxide materials. *Applied Surface Science* **2008,** *254* (8), 2441-2449.

222. Zango, Z. U.; Jumbri, K.; Sambudi, N. S.; Hanif Abu Bakar, N. H.; Fathihah Abdullah, N. A.; Basheer, C.; Saad, B., Removal of anthracene in water by MIL-88(Fe), NH2-MIL-88(Fe), and mixed-MIL-88(Fe) metal–organic frameworks. *RSC Advances* **2019,** *9* (71), 41490-41501.

223. Sui, H.; Li, L.; Zhu, X.; Chen, D.; Wu, G., Modeling the adsorption of PAH mixture in silica nanopores by molecular dynamic simulation combined with machine learning. *Chemosphere* **2016,** *144*, 1950-1959.

224. Hornback, J. M., *Organic Chemistry*. Cengage Learning: 2005.

225. Yoshioka, T.; Ota, M.; Okuwaki, A., Conversion of a Used Poly(ethylene terephthalate) Bottle into Oxalic Acid and Terephthalic Acid by Oxygen Oxidation in Alkaline Solutions at Elevated Temperatures. *Industrial & Engineering Chemistry Research* **2003,** *42* (4), 675-679.

226. Wang, H.; Kojtari, A.; Xu, X.; Ji, H.-F., Self-Assembled Microwires of Terephthalic Acid and Melamine. *Crystals* **2017,** *7* (8).

227. Singh, S.; Sharma, S.; Umar, A.; Mehta, S. K.; Bhatti, M. S.; Kansal, S. K., Recycling of Waste Poly(ethylene terephthalate) Bottles by Alkaline Hydrolysis and Recovery of Pure Nanospindle-Shaped Terephthalic Acid. *J Nanosci Nanotechnol* **2018,** *18* (8), 5804-5809.

228. Ravichandran, S. A.; Rajan, V. P.; Aravind, P. V.; Seenivasan, A.; Prakash, D. G.; Ramakrishnan, K., Characterization of Terephthalic Acid Monomer Recycled from Post-Consumer PET Polymer Bottles. *Macromolecular Symposia* **2016,** *361* (1), 30-33.

229. Tamames-Tabar, C.; Cunha, D.; Imbuluzqueta, E.; Ragon, F.; Serre, C.; Blanco-Prieto, M. J.; Horcajada, P., Cytotoxicity of nanoscaled metal–organic frameworks. *Journal of Materials Chemistry B* **2014,** *2* (3), 262-271.

230. Wang, Y.; Muramatsu, A.; Sugimoto, T., FTIR analysis of well-defined α-Fe2O3 particles. *Colloids and Surfaces A: Physicochemical and Engineering Aspects* **1998,** *134* (3), 281-297.

231. Liu, Z.; He, W.; Zhang, Q.; Shapour, H.; Bakhtari, M. F., Preparation of a GO/MIL-101(Fe) Composite for the Removal of Methyl Orange from Aqueous Solution. *ACS Omega* **2021,** *6* (7), 4597-4608.

232. Hamedi, A.; Trotta, F.; Borhani Zarandi, M.; Zanetti, M.; Caldera, F.; Anceschi, A.; Nateghi, M. R., In Situ Synthesis of MIL-100(Fe) at the Surface of Fe3O4@AC as Highly

Efficient Dye Adsorbing Nanocomposite. *International Journal of Molecular Sciences* **2019,** *20* (22).

233. Carson, F.; Su, J.; Platero-Prats, A. E.; Wan, W.; Yun, Y.; Samain, L.; Zou, X., Framework Isomerism in Vanadium Metal–Organic Frameworks: MIL-88B(V) and MIL-101(V). *Crystal Growth & Design* **2013,** *13* (11), 5036-5044.

234. Zorainy, M. Y.; Gar Alalm, M.; Kaliaguine, S.; Boffito, D. C., Revisiting the MIL-101 metal–organic framework: design, synthesis, modifications, advances, and recent applications. *Journal of Materials Chemistry A* **2021,** *9* (39), 22159-22217.

235. Wu, W.; Decker, G. E.; Weaver, A. E.; Arnoff, A. I.; Bloch, E. D.; Rosenthal, J., Facile and Rapid Room-Temperature Electrosynthesis and Controlled Surface Growth of Fe-MIL-101 and Fe-MIL-101-NH2. *ACS Central Science* **2021,** *7* (8), 1427-1433.

236. Otun, K. O., Temperature-controlled activation and characterization of iron-based metal-organic frameworks. *Inorganica Chimica Acta* **2020,** *507*, 119563.

237. Férey, G.; Mellot-Draznieks, C.; Serre, C.; Millange, F.; Dutour, J.; Surblé, S.; Margiolaki, I., A Chromium Terephthalate-Based Solid with Unusually Large Pore Volumes and Surface Area. *Science* **2005,** *309* (5743), 2040-2042.

238. Karimi Alavijeh, R.; Akhbari, K., Biocompatible MIL-101(Fe) as a Smart Carrier with High Loading Potential and Sustained Release of Curcumin. *Inorganic Chemistry* **2020,** *59* (6), 3570-3578.

239. Latroche, M.; Surblé, S.; Serre, C.; Mellot-Draznieks, C.; Llewellyn, P. L.; Lee, J.-H.; Chang, J.-S.; Jhung, S. H.; Férey, G., Hydrogen Storage in the Giant-Pore Metal–Organic Frameworks MIL-100 and MIL-101. *Angewandte Chemie International Edition* **2006,** *45* (48), 8227-8231.

240. Li, H.; Wang, K.; Sun, Y.; Lollar, C. T.; Li, J.; Zhou, H.-C., Recent advances in gas storage and separation using metal–organic frameworks. *Materials Today* **2018,** *21* (2), 108-121.

241. MacGillivray, L. R., *Metal-organic frameworks: design and application*. John Wiley & Sons: 2010.

242. Musyoka, N. M.; Ren, J.; Annamalai, P.; Langmi, H. W.; North, B. C.; Mathe, M. K.; Cesar, D., Synthesis of a hybrid MIL-101(Cr)/ZTC composite for hydrogen storage applications. 2016.

243. Lupu, D.; Ardelean, O.; Blanita, G.; Borodi, G.; Lazar, M. D.; Biris, A. R.; Ioan, C.; Mihet, M.; Misan, I.; Popeneciu, G., Synthesis and hydrogen adsorption properties of a new

iron based porous metal-organic framework. *International Journal of Hydrogen Energy* **2011,** *36* (5), 3586-3592.

244. Rallapalli, P. B. S.; Raj, M. C.; Senthilkumar, S.; Somani, R. S.; Bajaj, H. C., HF-free synthesis of MIL-101(Cr) and its hydrogen adsorption studies. *Environmental Progress & Sustainable Energy* **2016,** *35* (2), 461-468.

245. Kazemi, S.; Safarifard, V., Carbon dioxide capture in MOFs: The effect of ligand functionalization. *Polyhedron* **2018,** *154*, 236-251.

246. Kong, X.-J.; Li, J.-R., An Overview of Metal–Organic Frameworks for Green Chemical Engineering. *Engineering* **2021,** *7* (8), 1115-1139.

247. Li, H.; Li, L.; Lin, R.-B.; Zhou, W.; Zhang, Z.; Xiang, S.; Chen, B., Porous metal-organic frameworks for gas storage and separation: Status and challenges. *EnergyChem* **2019,** *1* (1), 100006.

248. Bilal, M.; Adeel, M.; Rasheed, T.; Iqbal, H. M. N., Multifunctional metal–organic frameworks-based biocatalytic platforms: recent developments and future prospects. *Journal of Materials Research and Technology* **2019,** *8* (2), 2359-2371.

249. Liao, X.; Wang, F.; Wang, F.; Cai, Y.; Yao, Y.; Teng, B.-T.; Hao, Q.; Shuxiang, L., Synthesis of (100) surface oriented MIL-88A-Fe with rod-like structure and its enhanced fenton-like performance for phenol removal. *Applied Catalysis B: Environmental* **2019,** *259*, 118064.

250. Jönsson, J.; Jönsson, J.; Lövgren, L., Precipitation of secondary Fe(III) minerals from acid mine drainage. *Applied Geochemistry - APPL GEOCHEM* **2006,** *21*, 437-445.

251. Karam, L.; Miglio, A.; Specchia, S.; El Hassan, N.; Massiani, P.; Reboul, J., PET waste as organic linker source for the sustainable preparation of MOF-derived methane dry reforming catalysts. *Materials Advances* **2021,** *2* (8), 2750-2758.

252. Nehra, M.; Dilbaghi, N.; Singhal, N. K.; Hassan, A. A.; Kim, K.-H.; Kumar, S., Metal organic frameworks MIL-100(Fe) as an efficient adsorptive material for phosphate management. *Environmental Research* **2019,** *169*, 229-236.

253. Yurduşen, A.; Yürüm, Y., A Controlled Synthesis Strategy To Enhance the CO2 Adsorption Capacity of MIL-88B Type MOF Crystallites by the Crucial Role of Narrow Micropores. *Industrial & Engineering Chemistry Research* **2019,** *58* (31), 14058-14072.

254. Horcajada, P.; Salles, F.; Wuttke, S.; Devic, T.; Heurtaux, D.; Maurin, G.; Vimont, A.; Daturi, M.; David, O.; Magnier, E.; Stock, N.; Filinchuk, Y.; Popov, D.; Riekel, C.; Férey, G.; Serre, C., *J. Am. Chem. Soc.* **2011,** *133*, 17839.

255. Taylor-Pashow, K. M. L.; Rocca, J. D.; Xie, Z.; Tran, S.; Lin, W., *J. Am. Chem. Soc.* **2009,** *131*, 14261.

256. Xiao, Y.; Guo, X.; Huang, H.; Yang, Q.; Huang, A.; Zhong, C., Synthesis of MIL-88B(Fe)/Matrimid mixed-matrix membranes with high hydrogen permselectivity. *RSC Advances* **2015,** *5* (10), 7253-7259.

257. García-Holley, P.; Schweitzer, B.; Islamoglu, T.; Liu, Y.; Lin, L.; Rodriguez, S.; Weston, M. H.; Hupp, J. T.; Gómez-Gualdrón, D. A.; Yildirim, T.; Farha, O. K., Benchmark Study of Hydrogen Storage in Metal–Organic Frameworks under Temperature and Pressure Swing Conditions. *ACS Energy Letters* **2018,** *3* (3), 748-754.

258. Zeleňák, V.; Saldan, I., Factors Affecting Hydrogen Adsorption in Metal-Organic Frameworks: A Short Review. *Nanomaterials (Basel)* **2021,** *11* (7).

Supplementary data

Appendix I- Fe precipitates

Table S1: ICP-OES measured elemental concentrations from raw AMD and after the extraction of Fe using NaOH with and without the use of an oxidant (H_2O_2)

Sample description	elements						
	Fe (mg/L)	**Al**	**Si**	**Mn**	**Mg**	**Ca**	**Na**
Raw AMD	1251	259	76	56	236	314	29
AMD With H_2O_2	26	266	25	52	224	318	1784
AMD Without H_2O_2	27	275	26	49	237	335	1783

XPS

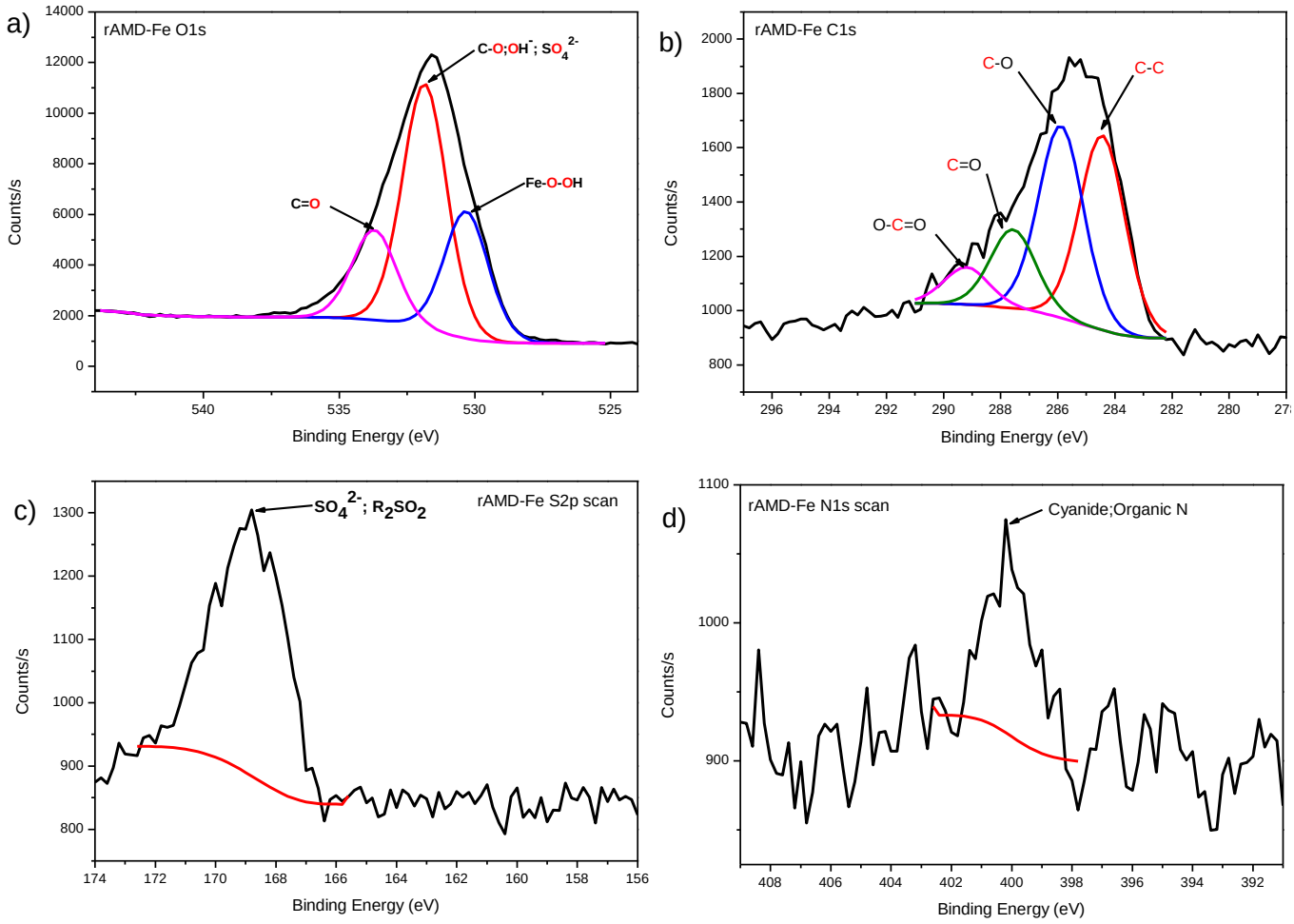

Figure S1: a) O1s scan b) C1s scan c) S2p scan and d) N1s scan for rAMD-Fe.

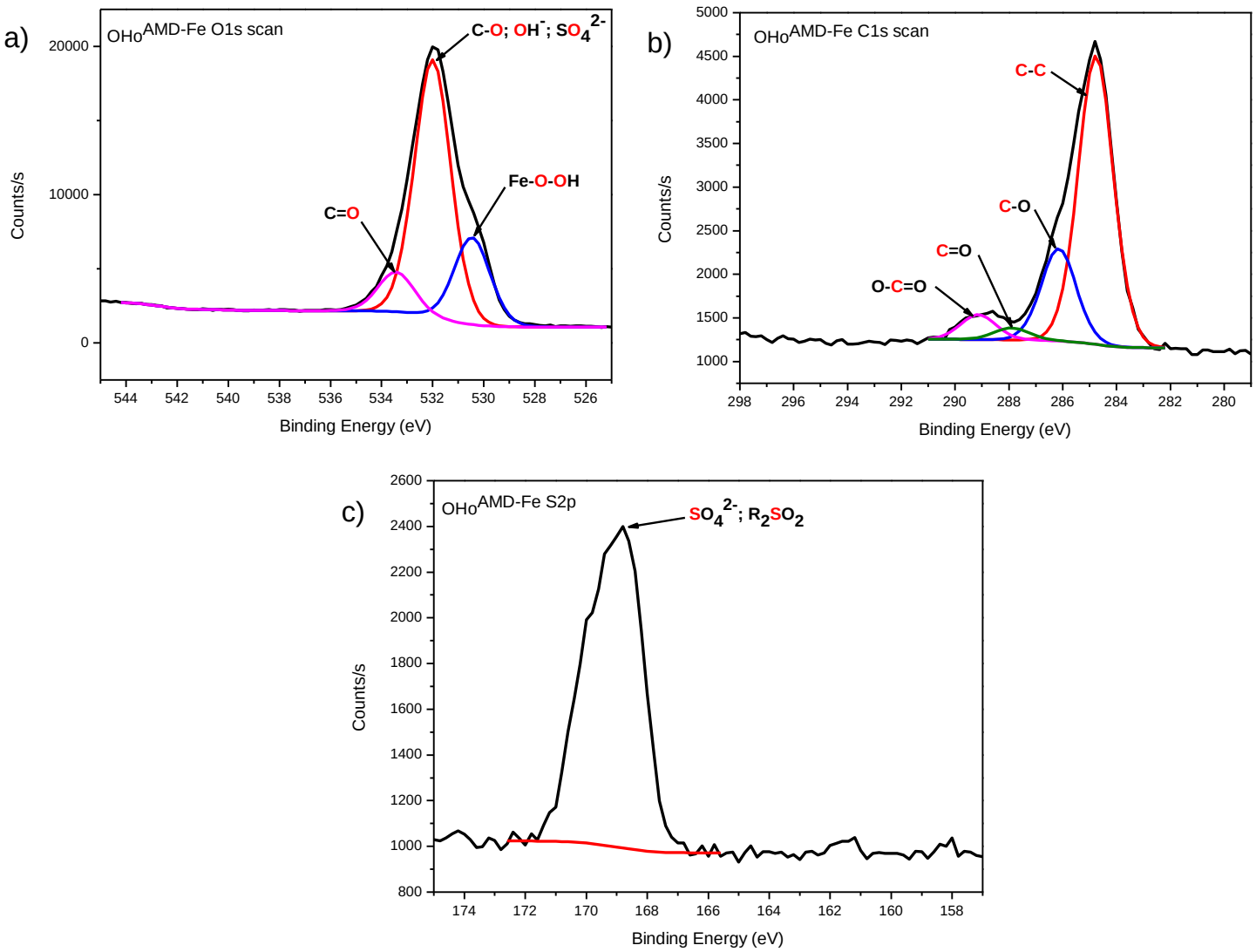

Figure S2: a) O1s scan b) C1s scan and c) S2p scan for $_{OHo}$AMD-Fe precipitate.

Appendix II-MIL-101

BET SA and PV

Table S2: Summary table for BET surface areas and pore volumes obtained for MIL-101 samples.

MOF sample	BET Surface area (m^2/g)	Pore Volume (cm^3/g)
8. MIL-101(Cl)pet	501	0.1904
9. MIL-101-$_{OHo}$AMD-Fe(Cl)$_{pet}$	52.5	0.0623
10. MIL-101-$_{OHo}$AMD-Fe(NO_3)$_{pet}$	565	0.3292

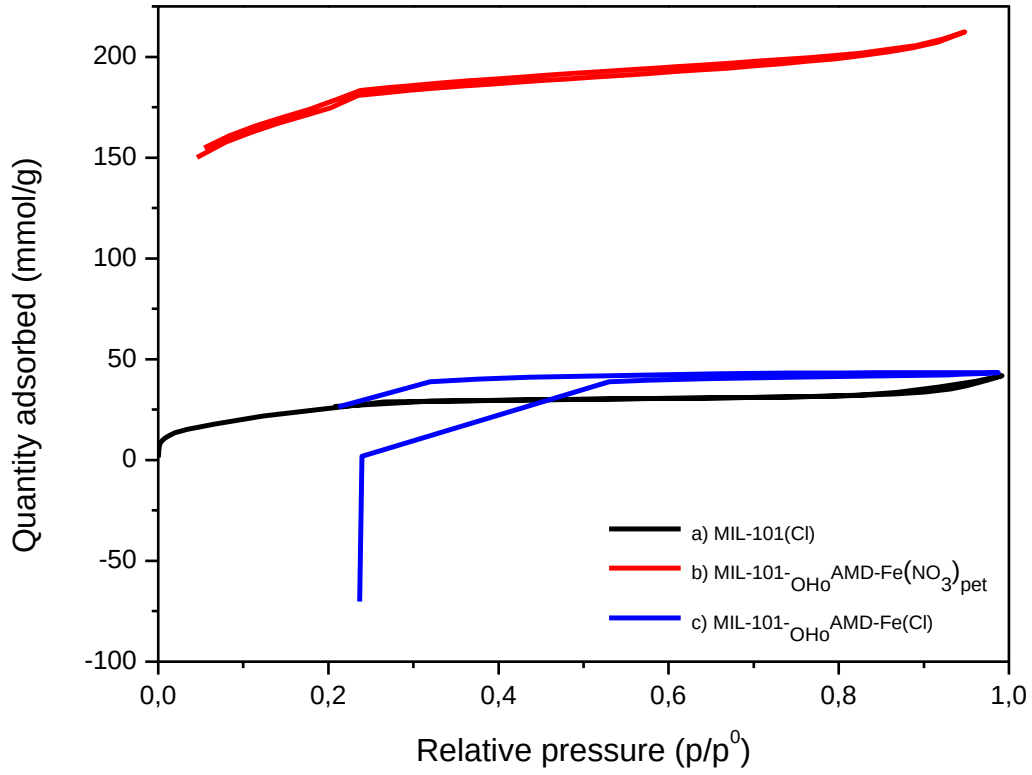

Figure S3: Nitrogen adsorption/desorption isotherms for Fe-MIL-101 materials.

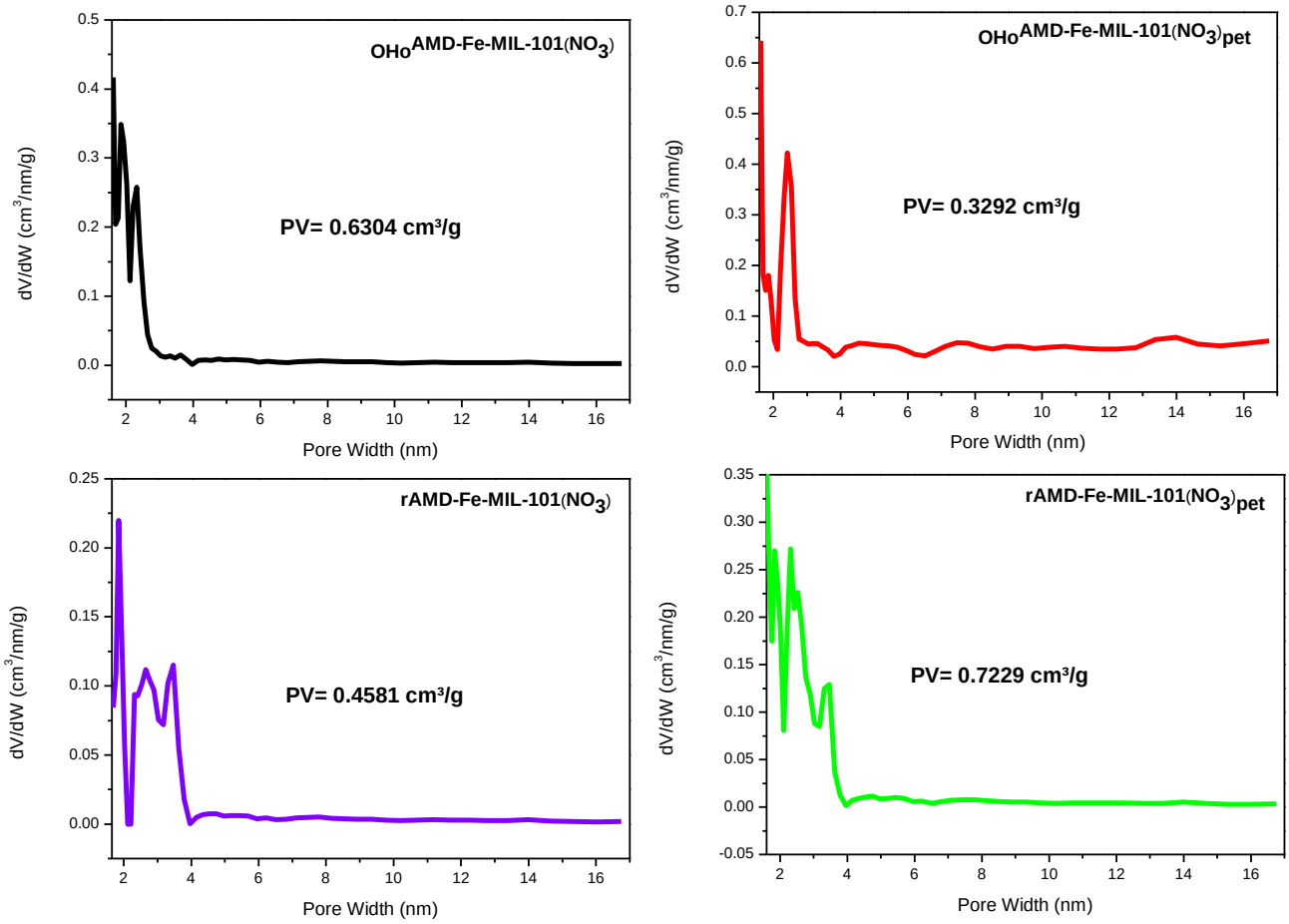

Figure S4: Pore size distribution (PSD) for Fe-MIL-101 materials.

SEM

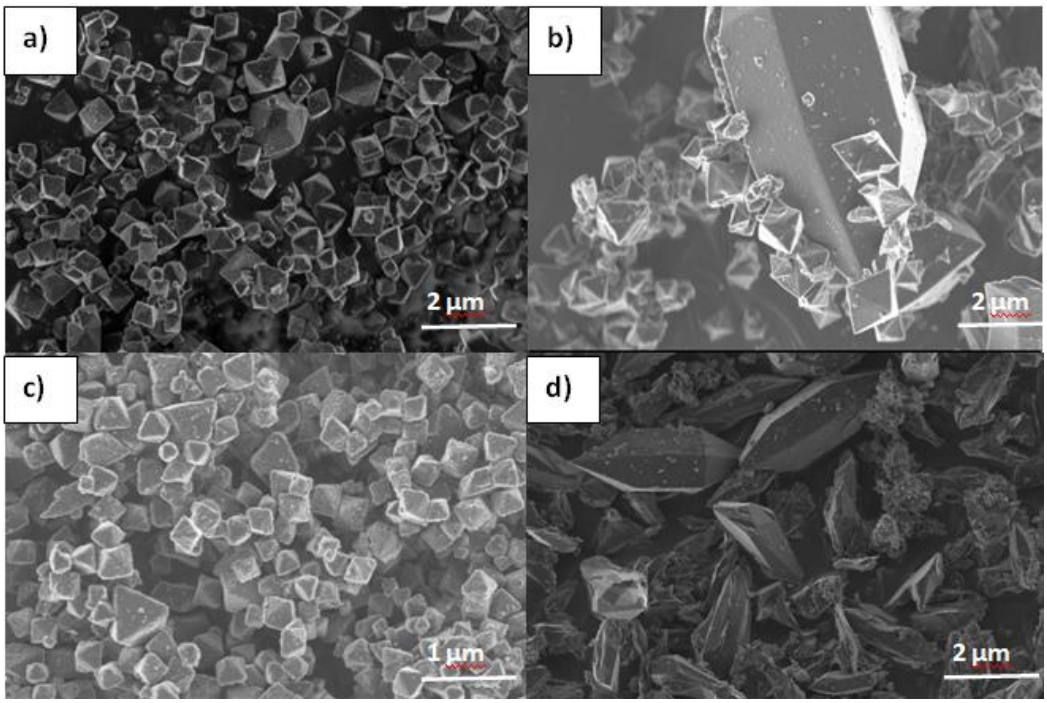

Figure S5: SEM images for a) Fe-MIL-101(Cl) b) OHoAMD-Fe-MIL-101(Cl)$_{pet}$ c) rAMD-Fe-MIL-101(Cl) and d) rAMD-Fe-MIL-101(Cl)$_{pet}$.

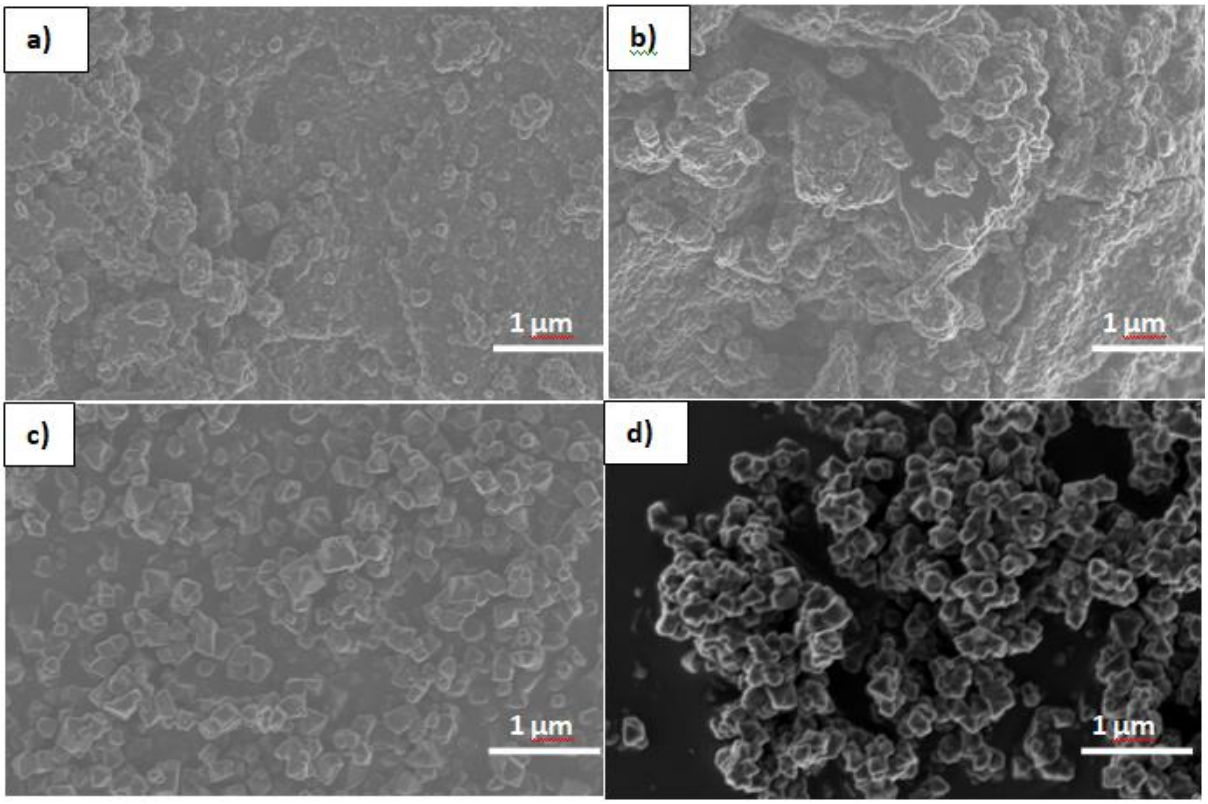

Figure S6: SEM images for a) Fe-MIL-101(NO_3) b) Fe-MIL-101(NO_3)$_{pet}$ c) rAMD-Fe-MIL-101 (NO_3) d) $_{OHo}$AMD-Fe-MIL-101(NO_3).

Appendix III- MIL-88B

BET and PV

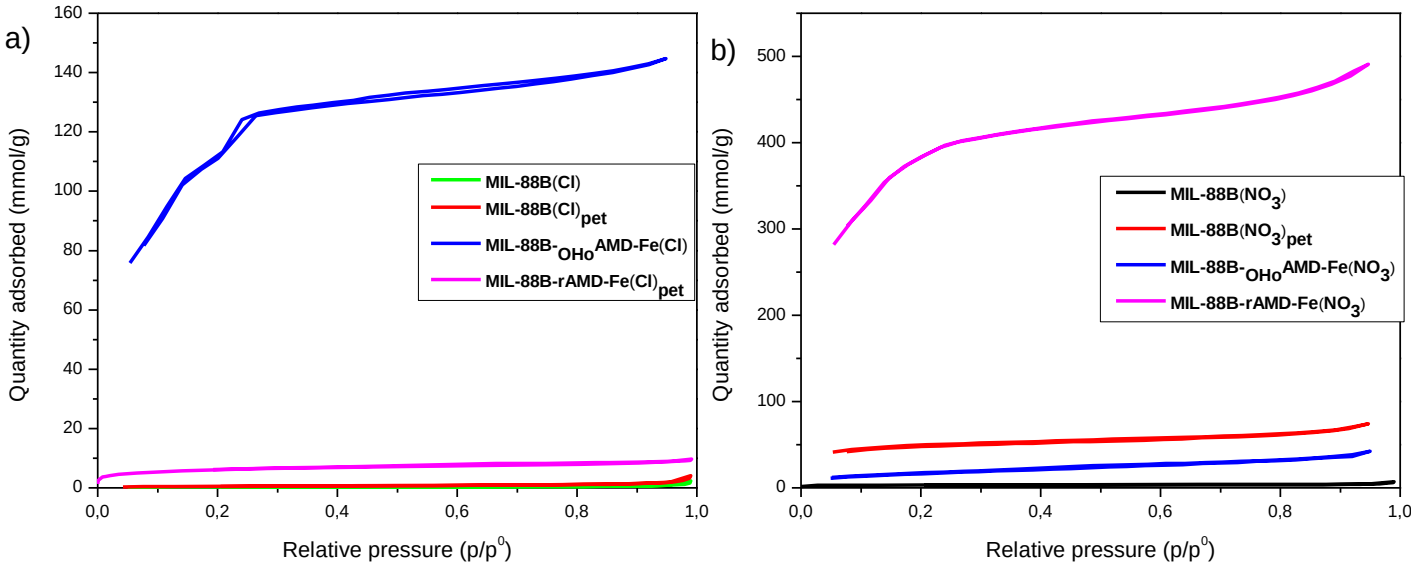

Figure S7: Nitrogen adsorption/desorption isotherms for Fe-MIL-88B materials.

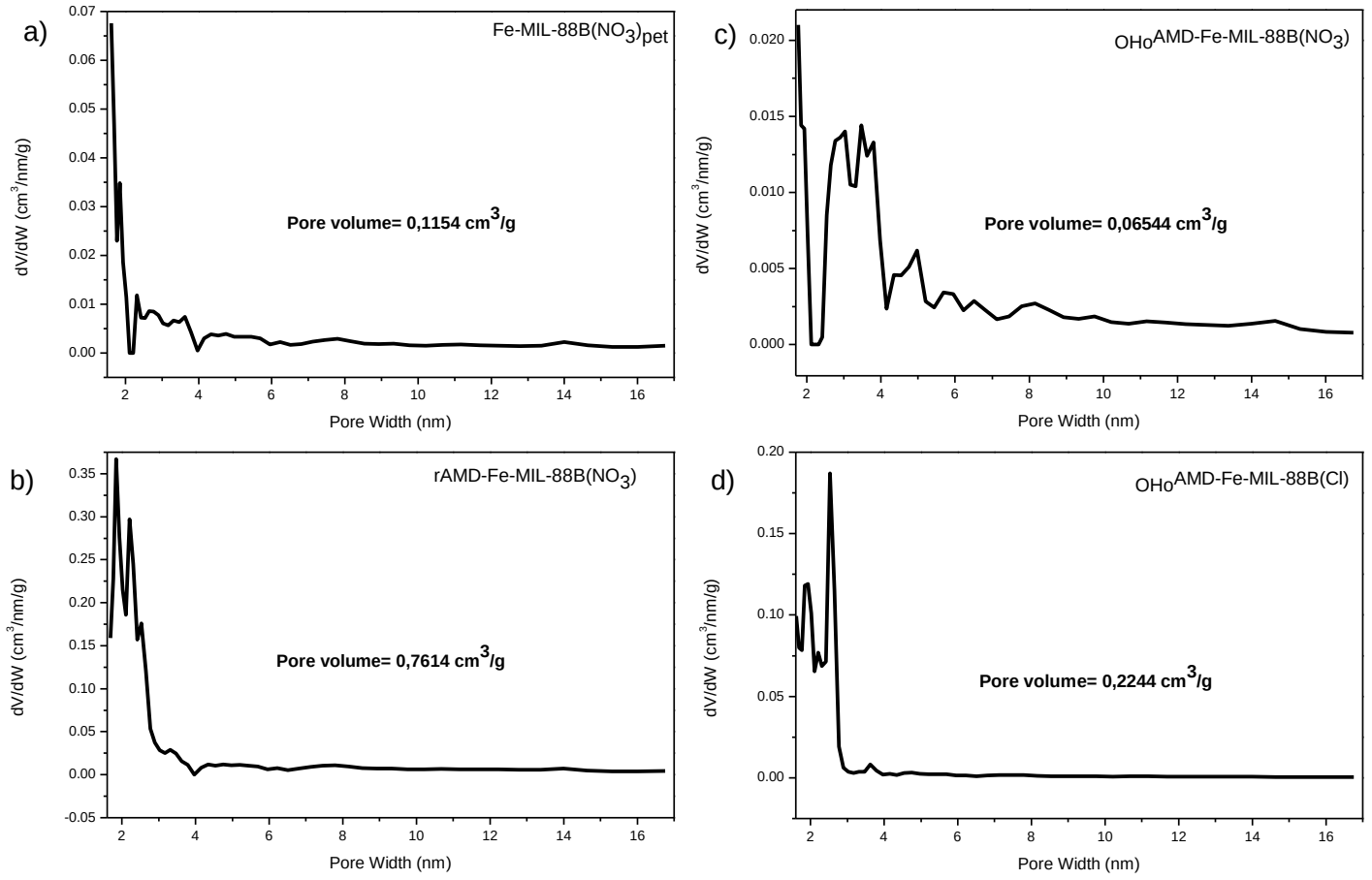

Figure S8: Pore size distribution (PSD) for Fe-MIL-88B materials.

SEM

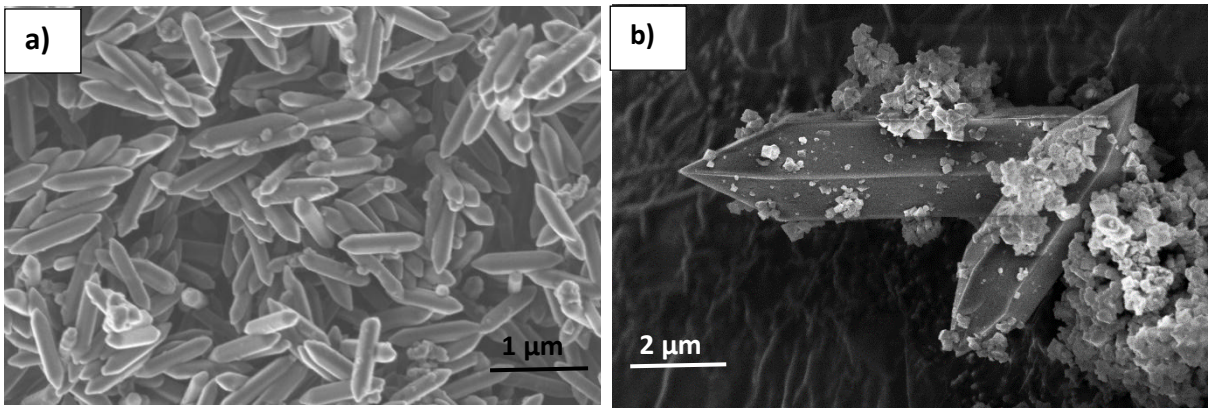

Figure S9: SEM images for a) Fe-MIL-88B(Cl)$_{pet}$ and b) $_{OHo}$AMD-Fe-MIL-88B(Cl).

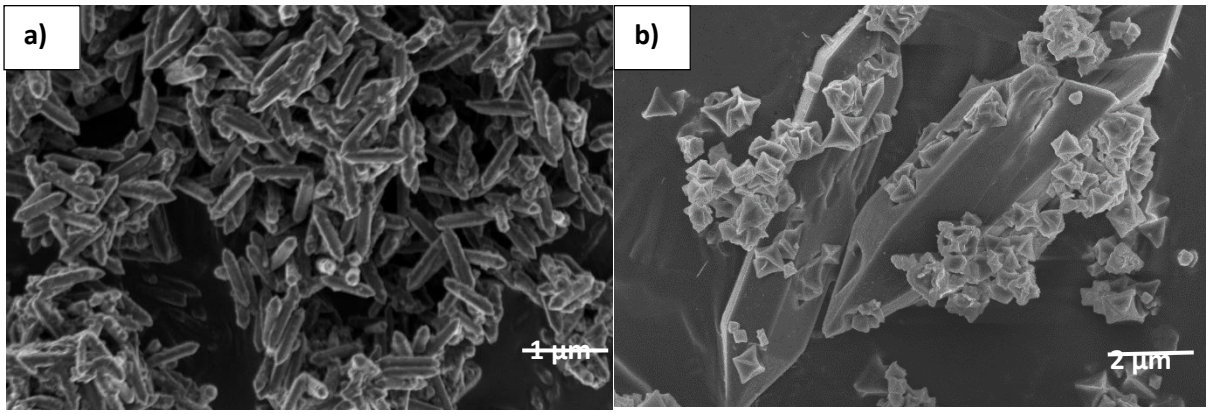

Figure S10: SEM images for a) Fe-MIL-88B(NO_3)$_{pet}$ and b) rAMD-Fe-MIL-88B (NO_3)$_{pet}$.